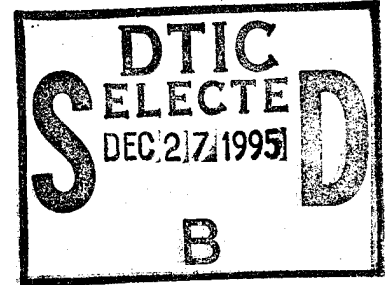


PB85-115368

Prediction of Crack
Extension Direction in
Unidirectional Composites

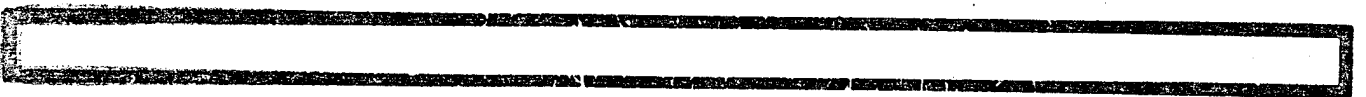
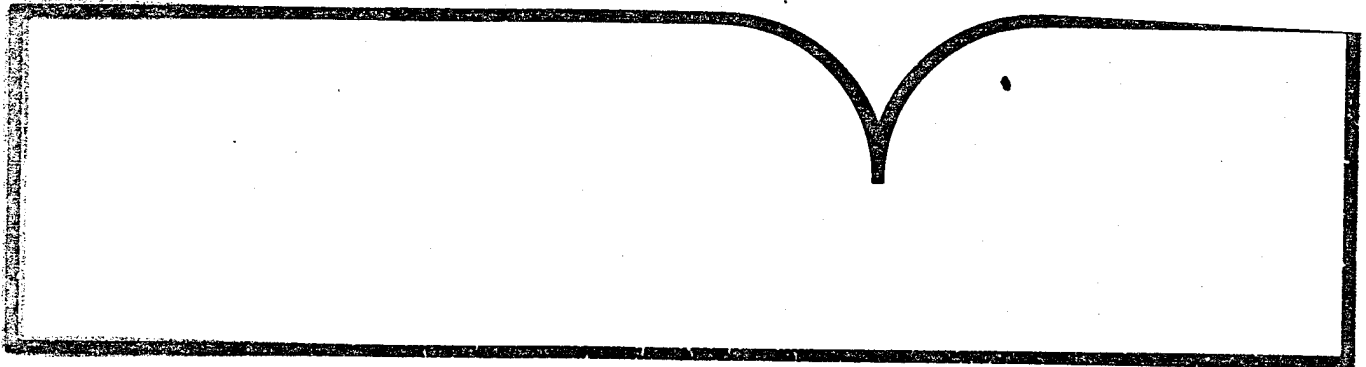
Virginia Polytechnic Inst. and State Univ.
Blacksburg

Prepared for
Hercules, Inc., Magna, UT

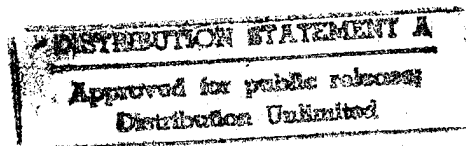


Aug 84

19951218 037



U.S. Department of Commerce
National Technical Information Service



DTIC QUALITY INSPECTED

*MSG DI4 DROLS PROCESSING-LAST INPUT IGNORED

-- 1 OF 1

DTIC DOES NOT HAVE THIS ITEM

- 1 - AD NUMBER: D439297
- 5 - CORPORATE AUTHOR: VIRGINIA POLYTECHNIC INST AND STATE UNIV
BLACKSBURG DEPT OF ENGINEERING SCIENCE AND MECHANICS
- 6 - UNCLASSIFIED TITLE: PREDICTION OF CRACK EXTENSION DIRECTION IN
UNIDIRECTIONAL COMPOSITES,
- 10 - PERSONAL AUTHORS: GREGORY, M. A. ; HERAKOVICH, C. T. ;
- 11 - REPORT DATE: AUG , 1984
- 12 - PAGINATION: 118P
- 14 - REPORT NUMBER: CCMS-84-11, VPI-E-84-27
- 20 - REPORT CLASSIFICATION: UNCLASSIFIED
- 22 - LIMITATIONS (ALPHA): APPROVED FOR PUBLIC RELEASE; DISTRIBUTION
UNLIMITED. ~~AVAILABILITY NATIONAL TECHNICAL INFORMATION SERVICE,
SPRINGFIELD, VA 22161-4000~~
- 33 - LIMITATION CODES: 1 **2**

--*****

END OF DISPLAY LIST

<<ENTER NEXT COMMAND>>

FB85-115368

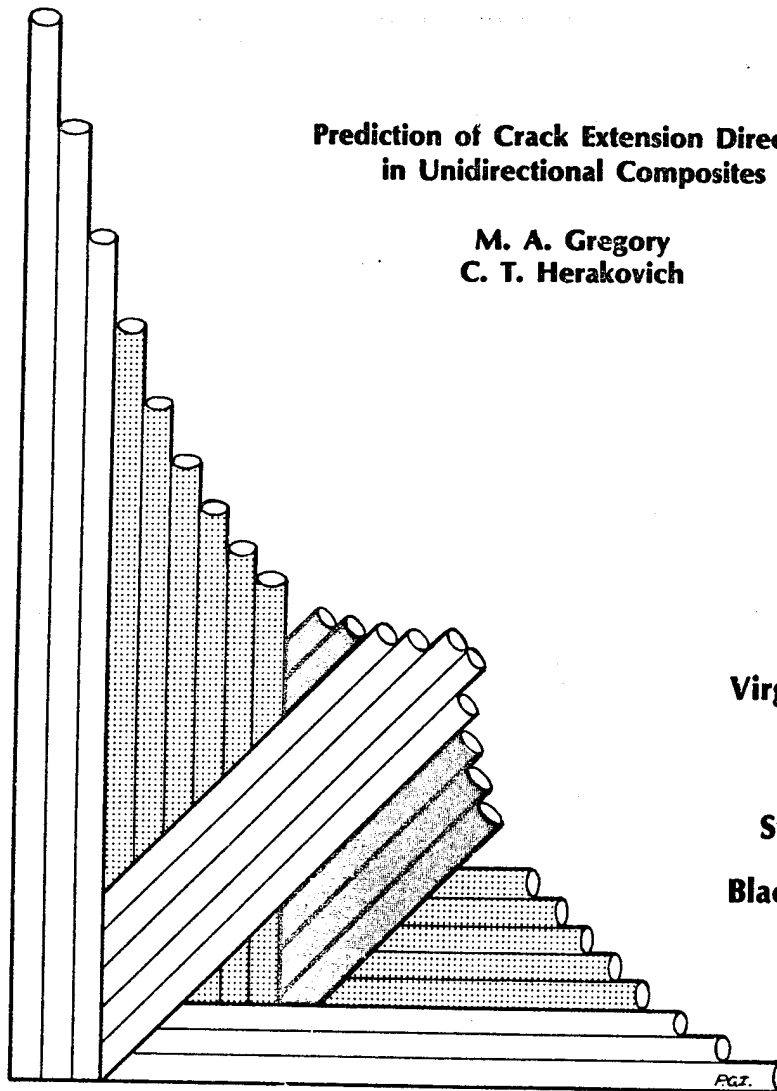
CCMS-84-11

VPI-E-84-27

VIRGINIA TECH
**CENTER FOR
COMPOSITE MATERIALS
AND STRUCTURES**

**Prediction of Crack Extension Direction
in Unidirectional Composites**

**M. A. Gregory
C. T. Herakovich**



**Virginia Polytechnic
Institute
and
State University
Blacksburg, Virginia
24061**

REPRODUCED BY
NATIONAL TECHNICAL
INFORMATION SERVICE
U.S. DEPARTMENT OF COMMERCE
SPRINGFIELD, VA. 22161

BIBLIOGRAPHIC DATA SHEET		1. Report No. CCMS-84-11	2. VPI-E-84-27	3. Recipient's Accession No. P885 115368
4. Title and Subtitle PREDICTION OF CRACK EXTENSION DIRECTION IN UNIDIRECTIONAL COMPOSITES			5. Report Date August, 1984	6.
7. Author(s) M. A. Gregory and C. T. Herakovich			8. Performing Organization Rept. No. VPI-E-84-27	
9. Performing Organization Name and Address Virginia Polytechnic Institute and State University Engineering Science and Mechanics Department Blacksburg, Virginia 24061			10. Project/Task/Work Unit No.	
			11. Contract/Grant No.	
12. Sponsoring Organization Name and Address Hercules Incorporated Magna, UT 84044			13. Type of Report & Period Covered	
			14.	
15. Supplementary Notes				
16. Abstracts <p>The purpose of this study was to gain a better understanding of the parameters affecting crack growth direction in unidirectional composite materials. To achieve this, the effect of anisotropy and biaxial loading on the direction of crack growth in unidirectional off-axis composite materials were investigated. Specific emphasis was placed on defining the crack tip stress field and finding a consistent criterion for predicting the direction of crack growth.</p> <p>Two models are presented to predict the crack tip stress field, an anisotropic elasticity solution and a singular isoparametric finite element formulation. After defining the crack tip stress field, three crack extension direction criteria, the normal stress ratio, the tensor polynomial and the strain energy density criterion, were applied to predict the direction of crack extension.</p> <p>The theoretically predicted crack extension directions were then compared with experimental results. After comparison, it was determined that only the normal stress ratio criterion correctly predicts the direction of crack extension.</p>				
17. Key Words and Document Analysis. 17a. Descriptors <p>composites, fracture, singular finite elements, anisotropic elasticity, crack direction, failure criteria</p>				
17b. Identifiers/Open-Ended Terms				
17c. COSATI Field/Group				
18. Availability Statement Distribution Unlimited			19. Security Class (This Report) UNCLASSIFIED	21. No. of Pages 118
			20. Security Class (This Page)	22. Price

College of Engineering
Virginia Polytechnic Institute and State University
Blacksburg, VA 24061

CCMS-84-11
VPI-E-84-27

August, 1984

Prediction of Crack Extension Direction
in Unidirectional Composites

M. A. Gregory¹

C. T. Herakovich²

Department of Engineering Science & Mechanics

Prepared for: Hercules Incorporated
Magna, Utah 84044

¹Graduate Student

²Professor of Engineering Science & Mechanics

Accession For	
NTIS GRA&I	<input checked="" type="checkbox"/>
DTIC TAB	<input type="checkbox"/>
Unannounced	<input type="checkbox"/>
Justification	
<i>Printout enclosed</i>	
<i>DTICAF memo</i>	
BY <i>27 Nov 85</i>	
Distribution/	
Availability Codes	
Dist	Avail and/or Special
<i>A-1</i>	

ABSTRACT

The purpose of this study was to gain a better understanding of the parameters affecting crack growth direction in unidirectional composite materials. To achieve this, the effect of anisotropy and biaxial loading on the direction of crack growth in unidirectional off-axis composite materials were investigated. Specific emphasis was placed on defining the crack tip stress field and finding a consistent criterion for predicting the direction of crack growth.

Two models are presented to predict the crack tip stress field, an anisotropic elasticity solution and a singular isoparametric finite element formulation. After defining the crack tip stress field, three crack extension direction criteria, the normal stress ratio, the tensor polynomial and the strain energy density criterion, were applied to predict the direction of crack extension.

The theoretically predicted crack extension directions were then compared with experimental results. After comparison, it was determined that only the normal stress ratio criterion correctly predicts the direction of crack extension.

ACKNOWLEDGEMENTS

The authors wish to acknowledge that this research was supported by Hercules Incorporated. In addition, the author wishes to thank Professors M. W. Hyer, J. N. Reddy and C. W. Smith for their helpful discussions.

The authors are also grateful to Ms. Connie Callison for the time and effort she spent in typing this manuscript.

TABLE OF CONTENTS

	Page
ACKNOWLEDGEMENTS.....	iii
LIST OF TABLES.....	vi
LIST OF FIGURES.....	vii
<u>CHAPTER</u>	
1. INTRODUCTION.....	1
1.1 Motivation and Statement of Purpose.....	1
1.2 Literature Review.....	3
2. THEORETICAL CONSIDERATIONS.....	6
2.1 Crack Growth Direction Criteria.....	6
2.1.1 Tensor Polynomial Failure Criterion.....	6
2.1.2 Strain Energy Density Criterion.....	7
2.1.3 Normal Stress Ratio Criterion.....	11
2.2 Crack Tip Stress Field Models.....	12
2.2.1 Anisotropic Elasticity Solution.....	12
2.2.2 Singular Finite Element Formulation.....	20
3. CRACK TIP STRESS ANALYSIS.....	24
3.1 Application of the Anisotropic Elasticity Solution.....	24
3.2 Application of Singular Isoparametric Finite Element....	28
3.3 Verification of the Finite Element Model.....	34
4. OFF-AXIS AND UNIDIRECTIONAL TENSILE COUPONS.....	45
4.1 Unidirectional 30° Off-Axis Tensile Coupon.....	45
4.2 Influence of r_0 on the Predicted Direction of Crack Growth.....	47
4.3 Unidirectional 15° Off-Axis Coupons.....	52
4.4 Unidirectional Lamina Subjected to Mixed-Mode Loadings..	56
5. CONCLUSIONS AND RECOMMENDATIONS.....	62
REFERENCES.....	65
<u>APPENDIX</u>	
A Mathematical Expressions for F_i and F_{ij}	67
B Generation of Singularities in Isoparametric Elements...	68

C	Distribution of Stress Fields Through the Element.....	72
D	Additional Information on Problems Analyzed.....	94
E	Material Properties.....	113
F	Influence of the λ/a Ratio on Finite Element Con- vergence.....	114

LIST OF TABLES

Table	Page
3.0 Interpolation Functions and Numerical Integration Data.....	33
4.0 Comparison of Anisotropic Elasticity to Finite Element Results for Direction of Crack Extension in 30° Off-Axis Tensile Coupons.....	51

LIST OF FIGURES

Figure	Page
1.0 Failure Modes of Angle-Ply Laminates.....	2
2.0 Crack Tip Coordinate System.....	8
2.1 Graphical Application of the Tensor Polynomial Criterion.....	9
2.2 Normal Stress Ratio Parameters.....	13
2.3 Infinite Center Cracked Plate with Far Field Stresses.....	15
2.4 Conformal Mapping of Crack into a Unit Circle.....	19
2.5 Conventional and Singular Isoparametric Triangular Elements...	21
3.0 Infinite Center Cracked Plate Under Biaxial Loading.....	25
3.1 Transformation and Superposition of Far Field Stresses.....	27
3.2 Master Finite Element Configuration.....	29
3.3 Quarter Symmetry Mesh of Center Cracked Plate.....	31
3.4 Exploded View of Crack Tip Elements.....	32
3.5 Distribution of σ_x Near the Crack Tip in a Center Cracked Steel Plate.....	35
3.6 Distribution of σ_y Near the Crack Tip in a Center Cracked Steel Plate.....	36
3.7 Distribution of τ_{xy} Near the Crack Tip in a Center Cracked Steel Plate.....	37
3.8 Distribution of σ_x Near the Crack Tip in a Center Cracked Graphite/Epoxy Plate ($\theta = 0^\circ$).....	39
3.9 Distribution of σ_y Near the Crack Tip in a Center Cracked Graphite/Epoxy Plate ($\theta = 0^\circ$).....	40
3.10 Distribution of τ_{xy} Near the Crack Tip in a Center Cracked Graphite/Epoxy Plate ($\theta = 0^\circ$).....	41

3.11	Distribution of σ_x Near the Crack Tip in a Center Cracked Graphite/Epoxy Plate ($\theta = 90^\circ$).....	42
3.12	Distribution of σ_y Near the Crack Tip in a Center Cracked Graphite/Epoxy Plate ($\theta = 90^\circ$).....	43
3.13	Distribution of τ_{xy} Near the Crack Tip in a Center Cracked Graphite/Epoxy Plate ($\theta = 90^\circ$).....	44
4.0	Center Cracked 30° Off-Axis Coupon.....	46
4.1	Normal Stress Ratio vs. ϕ for 30° Off-Axis Graphite/Epoxy Coupon.....	48
4.2	Tensor Polynomial vs. ϕ for 30° Off-Axis Graphite/Epoxy Coupon.....	49
4.3	Strain Energy Density vs. ϕ for 30° Off-Axis Graphite/Epoxy Coupon.....	50
4.4	Influence of r_0 on the Crack Growth Direction Criteria.....	53
4.5	Influence of r_0 on the Distribution of the Tensor Polynomial.....	54
4.6	Center Cracked 15° Off-Axis Coupon Configurations.....	55
4.7	Normal Stress Ratio vs. ϕ for 15° Off-Axis Graphite/Epoxy Coupon ($\alpha = 0^\circ$).....	57
4.8	Normal Stress Ratio vs. ϕ for 15° Off-Axis Graphite/Epoxy Coupon ($\alpha = 15^\circ$).....	58
4.9	Center Cracked Mixed-Mode Coupon.....	60
4.10	Predicted Crack Growth Direction as a Function of Biaxial Load.....	61
B.1	Node Locations in Conventional and Singular Isoparametric Triangular Elements.....	69
C.1	σ_x vs. ϕ at Gauss Point 1 for a Center Cracked Graphite/Epoxy Plate.....	73
C.2	σ_y vs. ϕ at Gauss Point 1 for a Center Cracked Graphite/Epoxy Plate.....	74

C.3	τ_{xy} vs. ϕ at Gauss Point 1 for a Center Cracked Graphite/Epoxy Plate.....	75
C.4	σ_x vs. ϕ at Gauss Point 2 for a Center Cracked Graphite/Epoxy Plate.....	76
C.5	σ_y vs. ϕ at Gauss Point 2 for a Center Cracked Graphite/Epoxy Plate.....	77
C.6	τ_{xy} vs. ϕ at Gauss Point 2 for a Center Cracked Graphite/Epoxy Plate.....	78
C.7	σ_x vs. ϕ at Gauss Point 3 for a Center Cracked Graphite/Epoxy Plate.....	79
C.8	σ_y vs. ϕ at Gauss Point 3 for a Center Cracked Graphite/Epoxy Plate.....	80
C.9	τ_{xy} vs. ϕ at Gauss Point 3 for a Center Cracked Graphite/Epoxy Plate.....	81
C.10	σ_x vs. ϕ at Gauss Point 4 for a Center Cracked Graphite/Epoxy Plate.....	82
C.11	σ_y vs. ϕ at Gauss Point 4 for a Center Cracked Graphite/Epoxy Plate.....	83
C.12	τ_{xy} vs. ϕ at Gauss Point 4 for a Center Cracked Graphite/Epoxy Plate.....	84
C.13	σ_x vs. ϕ at Gauss Point 5 for a Center Cracked Graphite/Epoxy Plate.....	85

C.14	σ_y vs. ϕ at Gauss Point 5 for a Center Cracked Graphite/Epoxy Plate.....	86
C.15	τ_{xy} vs. ϕ at Gauss Point 5 for a Center Cracked Graphite/Epoxy Plate.....	87
C.16	σ_x vs. ϕ at Gauss Point 6 for a Center Cracked Graphite/Epoxy Plate.....	88
C.17	σ_y vs. ϕ at Gauss Point 6 for a Center Cracked Graphite/Epoxy Plate.....	89
C.18	τ_{xy} vs. ϕ at Gauss Point 6 for a Center Cracked Graphite/Epoxy Plate.....	90
C.19	σ_x vs. ϕ at Gauss Point 7 for a Center Cracked Graphite/Epoxy Plate.....	91
C.20	σ_y vs. ϕ at Gauss Point 7 for a Center Cracked Graphite/Epoxy Plate.....	92
C.21	τ_{xy} vs. ϕ at Gauss Point 7 for a Center Cracked Graphite/Epoxy Plate.....	93
D.1	Influence of r_0 on the Distribution of σ_x in a Center Cracked Graphite/Epoxy Plate ($\theta = 120^\circ$).....	95
D.2	Influence of r_0 on the Distribution of σ_y in a Center Cracked Graphite/Epoxy Plate ($\theta = 120^\circ$).....	96
D.3	Influence of r_0 on the Distribution of τ_{xy} in a Center Cracked Graphite/Epoxy Plate ($\theta = 120^\circ$).....	97
D.4	$\sigma_{\phi\phi}$ vs. ϕ for a Center Cracked 30° Graphite/Epoxy Plate.....	98

D.5	$T_{\phi\phi}$ vs. ϕ for a Center Cracked 30° Graphite/Epoxy Plate.....	99
D.6	Normal Stress Ratio vs. ϕ for a Center Cracked 30° Graphite/Epoxy Plate Under Pure Shear.....	100
D.7	Tensor Polynomial vs. ϕ for a Center Cracked 30° Graphite/Epoxy Plate Under Pure Shear.....	101
D.8	Strain Energy Density vs. ϕ for a Center Cracked 30° Graphite/Epoxy Plate Under Pure Shear.....	102
D.9	$\sigma_{\phi\phi}$ vs. ϕ for a Center Cracked 15° Graphite/Epoxy Plate.....	103
D.10	$T_{\phi\phi}$ vs. ϕ for a Center Cracked 15° Graphite/Epoxy Plate.....	104
D.11	Normal Stress Ratio vs. ϕ for a Center Cracked 15° Graphite/Epoxy Plate.....	105
D.12	Tensor Polynomial vs. ϕ for a Center Cracked 15° Graphite/Epoxy Plate.....	106
D.13	Strain Energy Density vs. ϕ for a Center Cracked 15° Graphite/Epoxy Plate.....	107
D.14	$\sigma_{\phi\phi}$ vs. ϕ for a Center Cracked Graphite/Epoxy Plate ($\alpha = 0^\circ$ and $\theta = 0^\circ$).....	108
D.15	$T_{\phi\phi}$ vs. ϕ for a Center Cracked Graphite/Epoxy Plate ($\alpha = 0^\circ$ and $\theta = 0^\circ$).....	109
D.16	Normal Stress Ratio vs. ϕ for a Center Cracked Graphite/Epoxy Plate ($\alpha = 0^\circ$ and $\theta = 0^\circ$).....	110
D.17	Tensor Polynomial vs. ϕ for a Center Cracked Graphite/Epoxy Plate ($\alpha = 0^\circ$ and $\theta = 0^\circ$).....	111
D.18	Strain Energy Density vs. ϕ for a Center Cracked Graphite/Epoxy Plate ($\alpha = 0^\circ$ and $\theta = 0^\circ$).....	112
F.1	Finite Element Mesh of Center Cracked Plate (Full Plate).....	115
F.2	σ_x vs. ϕ at Gauss Point 1 for a Center Cracked Graphite/Epoxy Plate.....	116
F.3	σ_y vs. ϕ at Gauss Point 1 for a Center Cracked Graphite/Epoxy Plate.....	117
F.4	τ_{xy} vs. ϕ at Gauss Point 1 for a Center Cracked Graphite/Epoxy Plate.....	118

Chapter 1

INTRODUCTION

In the last twenty years, a desire for structural materials with greater strength to weight ratios has led to the development of fiber reinforced composites. Early on, composites were used in applications that were not structurally critical. For those applications, characterization of the mechanical properties of the material was often all that was necessary before application. Now, when composites are used for main load carrying components in structures, an understanding of the failure modes of the composite is necessary. Of particular interest is the fracture response of composites, i.e., the influence of initial flaws and flaws which develop during service, on the structural integrity of the component.

1.1 Motivation and Statement of Purpose

A fundamental problem in predicting the failure of laminated composite materials is an understanding of the direction of crack growth in the individual laminae. The importance of the direction of crack growth on the failure mode of the laminate, is shown in Fig. 1.0 [1]. Clustered $[(\theta)_2/(-\theta)_2]_S$ graphite-epoxy laminates failed in a pure matrix mode (delamination and either intralaminar matrix cracking or fiber matrix debonding). In contrast, the alternating $[(+\theta/-\theta)_2]_S$ laminates exhibited fiber breakage in half of the plies and either matrix cracking or fiber matrix debonding in the others; there was no delamination in the alternating laminates. The mode of failure has a significant effect on the strength of the laminate. The strength of the 10° and 30° alter-

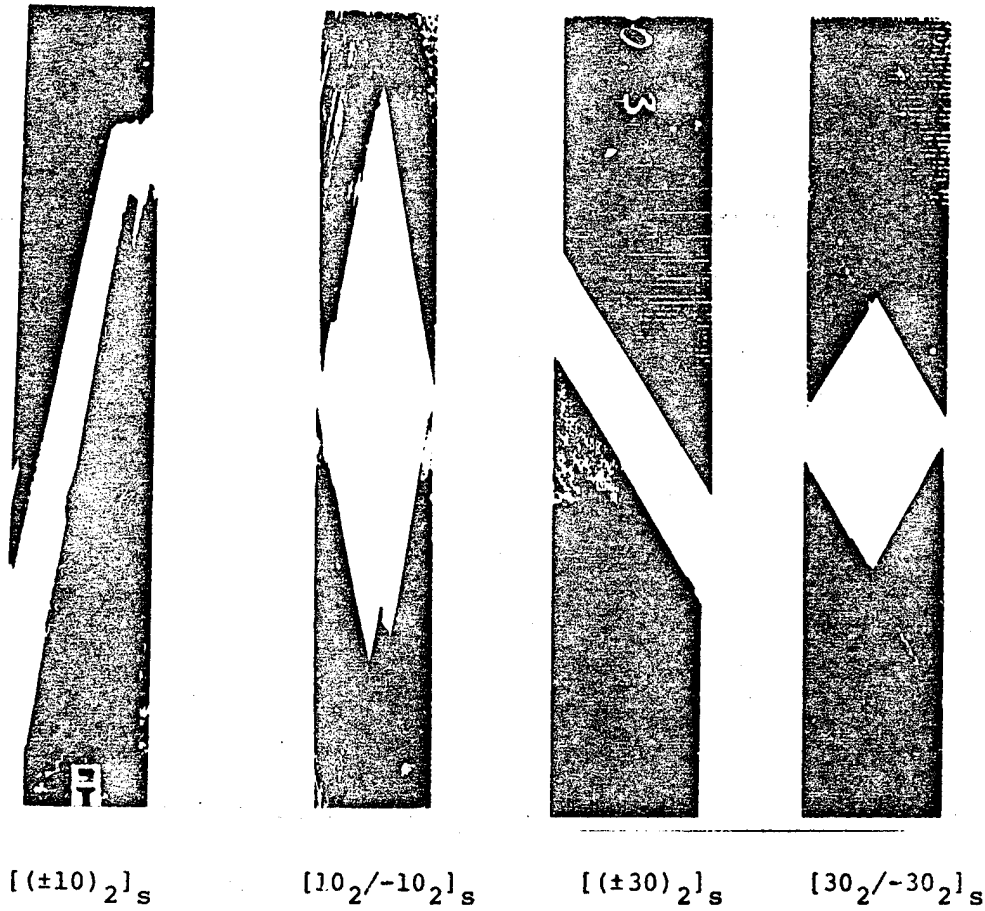


Fig. 1.0 Failure Modes of Angle-Ply Laminates.

nating laminates was 30 and 50 percent greater, respectively, than the strength of the clustered laminates [1]. Hence, understanding the parameters that affect the laminate failure mode, particularly those influencing the direction of crack growth in the lamina, is of critical importance in predicting the fracture response of laminates.

The purpose of this study is to gain a better understanding of the parameters affecting crack growth direction in the lamina. To achieve this, the effect of anisotropy and biaxial loading on the direction of crack growth in unidirectional off-axis composite materials will be investigated. Specific emphasis will be placed on defining the crack tip stress field and finding a consistent criterion for predicting the direction of crack growth.

1.2 Literature Review

Several researchers have addressed fracture of unidirectional composites in the past. Wu [2] and Sih et al. [3] have independently investigated the fracture response of unidirectional glass/epoxy composites. They have shown success in predicting the critical load for mode 1, mode 2, and mixed mode problems, with the restriction that the initial crack be aligned in the fiber direction. Additional work by Wu, some of which applies to the fracture of composite laminates can be found in [4-6], while Sih summarizes much of the current research efforts in composite fracture in [7]. The Wu and Sih theories will be discussed more fully later in this text.

More recently, Goree and Jones [8] examined the fracture behavior of unidirectional boron/aluminum composites. In their analysis, Goree

and Jones treat the material as an inhomogeneous anisotropic body containing broken fibers, undamaged fibers and matrix material. They assume that the fibers carry all of the axial load and that the matrix transfers load from a fiber break to an adjacent unbroken fiber by shear. The initial crack is modeled by an arbitrary number of fiber breaks and the direction of crack extension is predicted by a maximum stress criterion.

These researchers have made significant contributions to understanding the fracture response of unidirectional composites. However, a more general analysis is needed. In the preceding models, numerous assumptions have been made on the orientation of the initial crack, the scope of the analysis (microscopic versus macroscopic), and on the final mode of failure. In order to provide a more general theory, Buczek and Herakovich [9,10] studied the direction of crack growth and the associated energy release rates in a unidirectional off-axis lamina and edge delamination in a $[0/90]_s$ laminate. They treated the lamina as a homogeneous anisotropic material. Using the finite element method to model the crack tip stress field in conjunction with various crack growth criteria, Buczek and Herakovich predicted the direction of crack extension in unidirectional composite tensile coupons. Though the analysis was limited to tensile coupons subjected to uniaxial displacement loading, no restrictions were made on the orientation of the initial crack. Buczek and Herakovich also noted several inconsistencies among the crack growth direction criteria previously presented. As a result, they have hypothesized a model to predict the direction of crack extension in unidirectional composites. For the limited number of cases

analyzed, the direction of crack growth predicted by their new model correlates well with experimental evidence.

Chapter 2

THEORETICAL CONSIDERATIONS

2.1 Crack Growth Direction Criteria

In this section three crack growth direction criteria are presented. Though these criteria can also be used to predict load at failure, the main emphasis in this study is on predicting crack extension direction. The criteria are applied treating the unidirectional composite lamina as a homogeneous anisotropic material. Salient features of these criteria must be the applicability to mixed-mode fracture problems and the ability to account for the anisotropic nature of crack growth resistance in the unidirectional lamina (i.e., accounting for the fact that it is more difficult to break fibers than matrix). Three crack extension criteria addressing these factors have been presented in the literature. They are the Tensor Polynomial Failure Criterion [11], the Strain Energy Density Criterion [12], and the Normal Stress Ratio Criterion [10]. Though the Strain Energy Density Criterion does not specifically account for the anisotropy of strength in composite materials, Sih argues in [3] that the criterion is applicable at least in principle to anisotropic fracture problems.

2.1.1 Tensor Polynomial Failure Criterion

The Tensor Polynomial Criterion is a phenomenological failure theory presented by Tsai and Wu [11]. This theory is based on the existence of a failure surface in stress space of the form:

$$f(\sigma_i) = F_i \sigma_i + F_{ij} \sigma_i \sigma_j \quad (2.1)$$

where F_i and F_{ij} are strength tensors of second and fourth order, and σ_i the contracted form of the stress tensor. Expressions for F_i and F_{ij} , in both the x-y and 1-2 coordinate systems are presented in Appendix A.

When applying the Tensor Polynomial Criterion to fracture problems, the assumed direction of crack extension is the radial direction of maximum $f(\sigma_i)$. The stress components σ_i are those determined by a continuum mechanics based stress analysis and must be evaluated at a finite distance, r_0 , from the crack tip. The crack tip coordinate system is shown in Fig. 2.0.

A graphical application of the Tensor Polynomial Criterion to predict the direction of crack growth is shown by Wu in [2]. This graphical approach is presented in Fig. 2.1. The contour of the stress vector acting on radial planes emanating from the crack tip is represented by S , while the contour of the strength vector on the same planes is represented by F . The predicted direction of crack extension is labeled ϕ_c . It should be noted that the direction of ϕ_c does not necessarily correspond to the direction of maximum S as would be the case for isotropic materials. In anisotropic fracture the crack extension resistance, represented by F , plays an important role in determining ϕ_c and must be accounted for.

2.1.2 Strain Energy Density Criterion

The Strain Energy Density Criterion is phenomenological in nature and is based on variations in the energy stored along the periphery of a

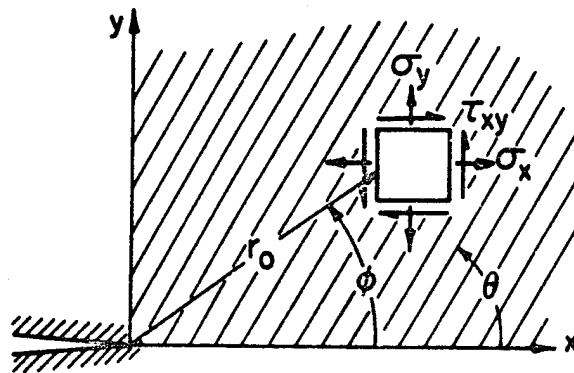
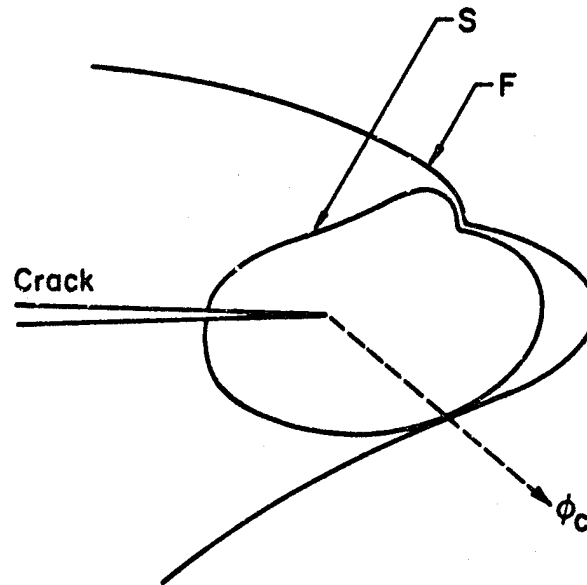


Fig. 2.0 Crack Tip Coordinate System.



where.

F = Contour of Strength Vector

S = Contour of Stress Vector

ϕ_c = Predicted Direction of Crack Extension

Fig. 2.1 Graphical Application of the Tensor Polynomial Criterion.

core region surrounding the crack. Sih presents the criterion in [12] for isotropic fracture and a modified form for application to anisotropic fracture in [3].

Sih defines the strain energy density factor, S , as:

$$\frac{\partial W}{\partial V} = \frac{S}{r} \quad (2.2)$$

where $\frac{\partial W}{\partial V}$ is the strain energy density function and r the distance from the crack tip. Since the strain energy density function can be expressed in terms of the crack tip stresses and strains as:

$$\frac{\partial W}{\partial V} = \frac{1}{2} (\sigma_x \epsilon_x + \sigma_y \epsilon_y + \tau_{xy} \gamma_{xy}) \quad (2.3)$$

an expression for the strain energy density factor, S , can be obtained by substitution. This expression is:

$$S = \frac{r}{2} (\sigma_x \epsilon_x + \sigma_y \epsilon_y + \tau_{xy} \gamma_{xy}) \quad (2.4)$$

The fundamental hypothesis of Sih [3] on unstable crack growth is: Crack initiation takes place in the radial direction corresponding to a minimum value of the strain energy density factor, i.e.,

$$\frac{\partial S}{\partial \phi} = 0 \text{ and } \frac{\partial^2 S}{\partial \phi^2} > 0 \text{ at } \phi = \phi_c \quad (2.5)$$

Sih cautions that for very small values of r a continuum mechanics based crack tip stress analysis is invalid. Hence the strain energy factor should be evaluated at a finite distance, r_0 , from the crack tip, where r_0 is of the same order of magnitude as the crack tip curvature. The crack tip coordinate system for this criterion is similar to that of the Tensor Polynomial as shown in Fig. 2.0.

2.1.3 Normal Stress Ratio Criterion

Buczek and Herakovich [10] have hypothesized the Normal Stress Ratio Criterion as a phenomenological crack growth direction criterion. The model assumes that the direction of crack extension corresponds to the direction of the maximum value of $R(r_0, \phi)$, defined as

$$R(r_0, \phi) = \frac{\sigma_{\phi\phi}}{T_{\phi\phi}} \quad (2.6)$$

In the expression for $R(r_0, \phi)$, $\sigma_{\phi\phi}$ corresponds to the normal stress acting on a radial plane defined by ϕ , at a given distance r_0 from the crack tip, and $T_{\phi\phi}$ is the tensile strength normal to the ϕ plane.

Since the tensile strength of an arbitrary plane is difficult if not impossible to measure, $T_{\phi\phi}$ is defined in a consistent manner with the tests that can be performed. To meet these requirements, a mathematical definition of $T_{\phi\phi}$ must satisfy the following conditions:

- (1) for an isotropic material, $T_{\phi\phi}$ must be independent of ϕ .
- (2) for crack growth parallel to the fibers, $T_{\phi\phi}$ must equal the transverse tensile strength Y_T .

- (3) for crack growth perpendicular to the fibers, $T_{\phi\phi}$ must equal the longitudinal strength χ_T .

A definition satisfying these conditions is:

$$T_{\phi\phi} = \chi_T \sin^2(\beta) + \gamma_T \cos^2(\beta) \quad (2.7)$$

where β is the angle from the plane of interest to the fiber direction. These parameters along with the crack tip coordinate system for the Normal Stress Ratio are shown in Fig. 2.2.

2.2 Crack Tip Stress Field Models

Two theoretical models to predict the crack tip stress field in homogeneous anisotropic materials are presented in this section. The first is an anisotropic elasticity solution for a biaxially loaded center cracked infinite plate. The second is a singular finite element formulation which allows for variable loading and geometries.

2.2.1 Anisotropic Elasticity Solution

The stress analysis of an infinite homogeneous anisotropic plate containing a center crack can be directly related to a homogeneous anisotropic plate with an elliptic hole. By reducing the minor axis dimension to zero and evaluating the stress potential functions in the neighborhood of the crack tip, Lekhnitskii's complex variable solution [13] for an elliptic hole in an anisotropic plate can be applied to anisotropic fracture problems. Wu presents a detailed description of

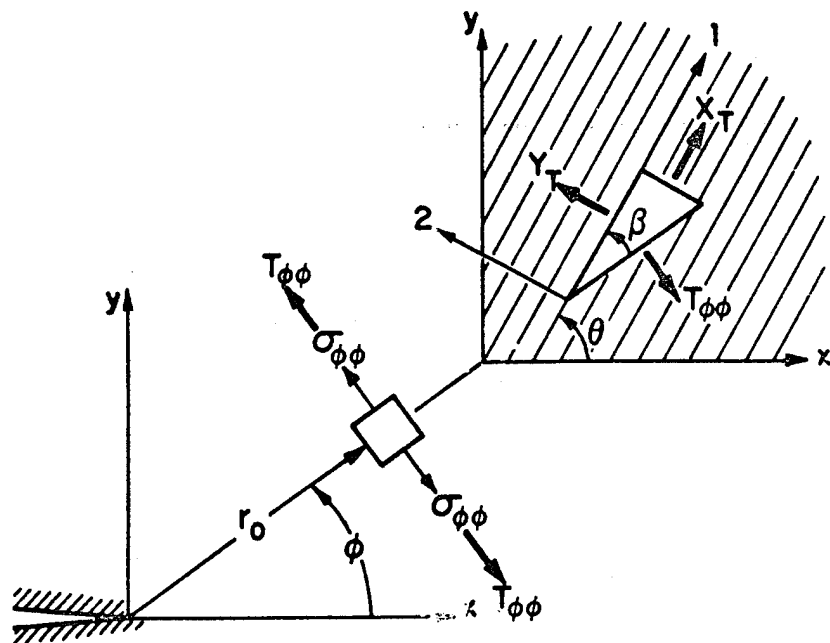


Fig. 2.2 Normal Stress Ratio Parameters.

this application in [14] along with equations describing the crack tip stresses for an infinite homogeneous anisotropic center cracked plate. Figure 2.3 shows the problem under consideration along with the crack tip coordinate system.

The governing partial differential equation for the problem in terms of the Airy's stress function U is:

$$\frac{\partial^4 U}{\partial x^4} - \frac{2A_{26}}{A_{22}} \frac{\partial^4 U}{\partial x^3 \partial y} + \frac{(2A_{12} + A_{66})}{A_{22}} \frac{\partial^4 U}{\partial x^2 \partial y^2} - \frac{2A_{16}}{A_{22}} \frac{\partial^4 U}{\partial x \partial y^3} + \frac{A_{11}}{A_{22}} \frac{\partial^4 U}{\partial y^4} = 0 \quad (2.8)$$

where A_{ij} are components of the compliance tensor for plane stress or plane strain depending on the analysis desired.

Assuming $U = e^x + Sy$, the characteristic equation for (2.8) takes the form:

$$A_{11}S^4 - 2A_{16}S^3 + (2A_{12} + A_{66})S^2 - 2A_{26}S + A_{22} = 0 \quad (2.9)$$

The roots of the characteristic equation, S_1 and S_2 , are complex and are functions of the material properties and the orientation of the crack relative to the material principal direction.

The solution of Eq. 2.8 can be obtained in terms of two holomorphic functions, $\phi_1(z_1)$ and $\phi_2(z_2)$, in the following form:

$$U = z \operatorname{Re}\{F_1(z_1) + F_2(z_2)\} \quad (2.10)$$

where

$$\phi_1(z_1) = \frac{dF_1(z_1)}{dz_1}, \quad \phi_2(z_2) = \frac{dF_2(z_2)}{dz_2} \quad (2.11)$$

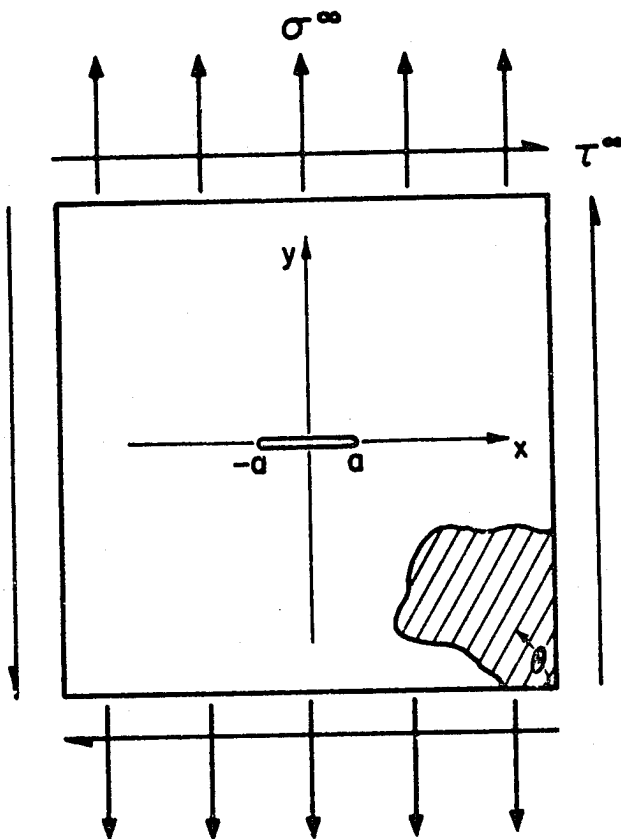


Fig. 2.3 Infinite Center Cracked Plate with Far Field Stresses.

and the complex variables are defined as:

$$z_1 = x + S_1 y, \quad z_2 = x + S_2 y \quad (2.12)$$

The stress and displacement components for an anisotropic body expressed in terms of the complex potentials $\phi_1(z_1)$ and $\phi_2(z_2)$ are:

$$\begin{aligned} \sigma_x &= 2\text{Re} [S_1^2 \phi_1'(z_1) + S_2^2 \phi_2'(z_2)] \\ \sigma_y &= 2\text{Re} [\phi_1'(z_1) + \phi_2'(z_2)] \\ \tau_{xy} &= -2\text{Re} [S_1 \phi_1'(z_1) + S_2 \phi_2'(z_2)] \end{aligned} \quad (2.13)$$

and

$$\begin{aligned} u &= 2\text{Re} [p_1 \phi_1(z_1) + p_2 \phi_2(z_2)] \\ v &= 2\text{Re} [q_1 \phi_1(z_1) + q_2 \phi_2(z_2)] \end{aligned} \quad (2.14)$$

where

$$\begin{aligned} p_1 &= A_{11} S_1^2 + A_{12} - A_{16} S_1 \\ p_2 &= A_{11} S_2^2 + A_{12} - A_{16} S_2 \\ q_1 &= \frac{A_{12} S_1^2 + A_{22} - A_{26} S_1}{S_1} \\ q_2 &= \frac{A_{12} S_2^2 + A_{22} - A_{26} S_2}{S_2} \end{aligned} \quad (2.15)$$

Savin [15] presents complex stress potentials satisfying the boundary conditions for a crack in an infinite plate subjected to tension σ^∞ and shear τ^∞ at infinity as indicated in Fig. 2.3. These complex potential functions are:

$$\begin{aligned}\phi_1(z_1) &= \frac{a(\tau^\infty + S_2\sigma^\infty)}{2(S_1 - S_2)} \zeta_1 \\ \phi_2(z_2) &= \frac{-a(\tau^\infty + S_1\sigma^\infty)}{2(S_1 - S_2)} \zeta_2\end{aligned}\quad (2.16)$$

where

$$\begin{aligned}\zeta_1 &= r\cos\phi + S_1r\sin\phi \\ \zeta_2 &= r\cos\phi + S_2r\sin\phi\end{aligned}\quad (2.17)$$

These functions were obtained through a conformal mapping of the crack into a unit circle and satisfy the boundary conditions:

$$\sigma_y = \tau_{xy} = 0 \quad -a < x < a \quad (2.18)$$

To examine the crack tip stress distribution, these stress potentials are evaluated as the ζ_j approach 1.

$$\lim_{\zeta_1 \rightarrow 1} \phi_1'(z_1) = \frac{(\tau^\infty \sqrt{a} + S_1\sigma^\infty \sqrt{a})}{2(S_1 - S_2)\sqrt{2r}(\cos\phi + S_2\sin\phi)} \quad (2.19)$$

$$\lim_{\zeta_2 \rightarrow 1} \phi_2'(z_2) = \frac{(\tau^\infty \sqrt{a} + S_1\sigma^\infty \sqrt{a})}{2(S_1 - S_2)\sqrt{2r}(\cos\phi + S_2\sin\phi)}$$

The potentials are evaluated as the ζ_j approach 1, because the conformal mapping transforms the region surrounding the crack to the interior of a unit circle whose radius is represented by ζ_j . The transformation of a crack into a unit circle is shown in Fig. 2.4.

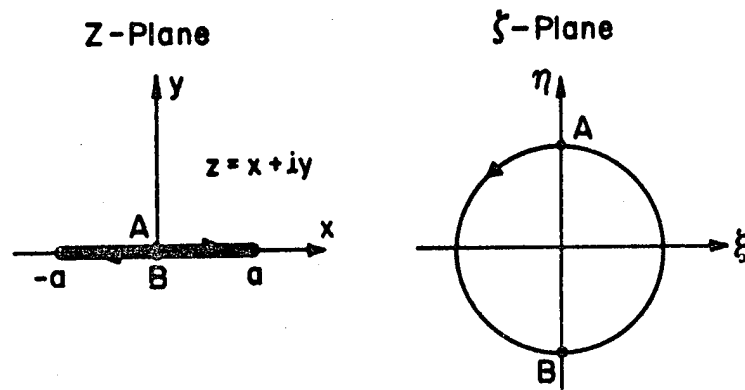
Substitution of (2.19) into (2.13) and (2.14) gives the stress and displacement distribution near the crack tip.

$$\begin{aligned}\sigma_x &= \frac{\sigma^\infty \sqrt{a}}{\sqrt{2r}} \operatorname{Re} \left\{ \frac{S_1 S_2}{(S_1 - S_2)} \left[\frac{S_2}{\psi_2^{1/2}} - \frac{S_1}{\psi_1^{1/2}} \right] \right\} + \frac{\tau^\infty \sqrt{a}}{\sqrt{2r}} \operatorname{Re} \left\{ \frac{1}{(S_1 - S_2)} \left[\frac{S_2^2}{\psi_2^{1/2}} - \frac{S_1^2}{\psi_1^{1/2}} \right] \right\} \\ \sigma_y &= \frac{\sigma^\infty \sqrt{a}}{\sqrt{2r}} \operatorname{Re} \left\{ \frac{1}{(S_1 - S_2)} \left[\frac{S_1}{\psi_2^{1/2}} - \frac{S_2}{\psi_1^{1/2}} \right] \right\} + \frac{\tau^\infty \sqrt{a}}{\sqrt{2r}} \operatorname{Re} \left\{ \frac{1}{(S_1 - S_2)} \left[\frac{1}{\psi_2^{1/2}} - \frac{1}{\psi_1^{1/2}} \right] \right\} \\ \tau_{xy} &= \frac{\sigma^\infty \sqrt{a}}{\sqrt{2r}} \operatorname{Re} \left\{ \frac{S_1 S_2}{(S_1 - S_2)} \left[\frac{1}{\psi_1^{1/2}} - \frac{1}{\psi_2^{1/2}} \right] \right\} + \frac{\tau^\infty \sqrt{a}}{\sqrt{2r}} \operatorname{Re} \left\{ \frac{1}{(S_1 - S_2)} \left[\frac{S_1}{\psi_1^{1/2}} - \frac{S_2}{\psi_2^{1/2}} \right] \right\} \\ u &= \sigma^\infty \sqrt{2ar} \operatorname{Re} \left\{ \frac{1}{(S_1 - S_2)} [S_1 p_2 \psi_2^{1/2} - S_2 p_1 \psi_1^{1/2}] \right\} \\ &\quad + \tau^\infty \sqrt{2ar} \operatorname{Re} \left\{ \frac{1}{(S_1 - S_2)} [p_2 \psi_2^{1/2} - p_1 \psi_1^{1/2}] \right\} \\ v &= \sigma^\infty \sqrt{2ar} \operatorname{Re} \left\{ \frac{1}{(S_1 - S_2)} [S_1 p_2 \psi_2^{1/2} - S_2 p_1 \psi_1^{1/2}] \right\} \\ &\quad + \tau^\infty \sqrt{2ar} \operatorname{Re} \left\{ \frac{1}{(S_1 - S_2)} [q_2 \psi_2^{1/2} - q_1 \psi_1^{1/2}] \right\}\end{aligned}\tag{2.20}$$

where

$$\psi_1 = \cos\phi + S_1 \sin\phi$$

$$\psi_2 = \cos\phi + S_2 \sin\phi$$



Conformal Transformations

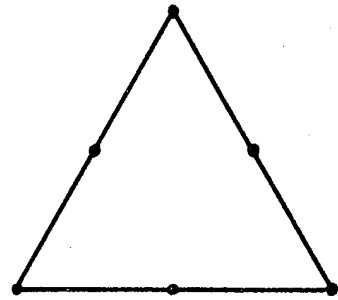
$$z_j = \omega(\zeta_j) = \frac{a}{2} \left(\zeta_j + \frac{1}{\zeta_j} \right) \quad j=1,2$$

Fig. 2.4 Conformal Mapping of Crack into a Unit Circle.

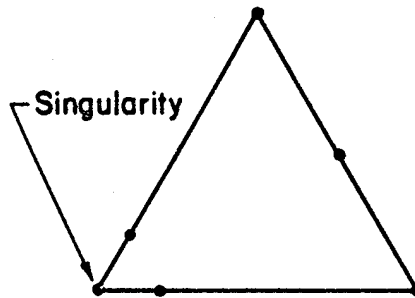
The crack tip stresses exhibit a singularity of $1/\sqrt{r}$ as in the isotropic case. However, the magnitude of the stresses are not simply a function of the stress intensity factors as in the isotropic case; the quantities S_1 and S_2 also affect the magnitude of the stresses. This is an important difference between anisotropic and isotropic fracture mechanics. In anisotropic fracture mechanics, the magnitude of the crack tip stresses are a function not only of the applied load, specimen geometry and crack length, but also the material properties and the orientation of the crack relative to the principal material direction.

2.2.2 Singular Finite Element Formulation

From the anisotropic elasticity solution, it is evident that near the crack tip there exists a singularity in the stress field of order $1/\sqrt{r}$. A finite element with a similar singularity incorporated into the equations describing the stress field over the domain of the element would be advantageous. Barsoum presents such a singular element in [16] (the idea of applying singular isoparametric elements to fracture problems was presented independently by Barsoum [16] and by Henshell and Shaw [18]). The advantage of Barsoum's formulation is that a special crack tip element is not necessary. The $1/\sqrt{r}$ singularity can be generated in quadratic isoparametric elements by positioning the mid-side nodes near the crack at the quarter points. The technique is depicted in Fig. 2.5. (A derivation of the singularity is presented in Appendix B). Freese and Tracey point out in [17] that this singularity is present in both the natural isoparametric triangle and the quadratic triangular element generated by collapsing one side of an eight noded



**Conventional Triangular
Element**



**Singular Triangular
Element**

Fig. 2.5 Conventional and Singular Isoparametric Triangular Elements.

isoparametric quadrilateral element. However, as Barsoum shows in [16], to obtain the $1/\sqrt{r}$ singularity in the collapsed quadrilateral the overlapping nodes must be constrained to have the same displacements. An obvious advantage of the natural isoparametric triangle is that multi-point constraints of overlapping nodes is not required. Another advantage shown by Freese et al. [17], is that the natural isoparametric triangle allows for distorted triangular shapes (e.g., pie-shaped elements) while the collapsed quadrilateral requires the element edges to remain straight.

Though Barsoum [16] only presents applications of the singular isoparametric element in isotropic fracture mechanics, the element does have applications in anisotropic fracture. Since Freese et al. [17] have shown that the natural isoparametric element can represent a radial displacement variation of the form:

$$u_i = A_i + B_i\sqrt{r} + C_i r \quad (2.21)$$

and since the displacements from the anisotropic elasticity solution take the form:

$$u_i = A_i\sqrt{r} \quad (2.22)$$

the natural isoparametric element has as many applications in anisotropic fracture as in isotropic fracture.

A survey of alternative finite element methods in fracture mechanics is given by Hilton and Sih in [19]. The emphasis of their paper is

on calculation of stress intensity factors using finite elements; however, several state-of-the-art finite element formulations for solution of fracture problems are presented.

Chapter 3

CRACK TIP STRESS ANALYSIS

As previously mentioned, one of the objectives of this work is the prediction of crack tip stresses in anisotropic materials without restrictions as to the orientation the crack relative to the principal material direction or the type of loading applied. In this chapter, the application of the anisotropic elasticity solution and the singular isoparametric finite element formulation to the general fracture problem presented in Fig. 3.0 is discussed. Note there are no restrictions as to the orientation of the crack, defined by the angle α , or that of the principal material (fiber) direction defined by θ . Also, complete biaxial loading is allowed; the far field loads can all be specified independently. The only constraint is that the crack is assumed to have a finite height. This disallows the specification of far field loadings that cause crack closure.

3.1 Application of the Anisotropic Elasticity Solution

Valid loadings for the elasticity solution presented in Section (2.2.1) are shown in Fig. 2.3 and consist of a uniform tensile stress σ^∞ and a shear stress τ^∞ . Though the solution allows for independent specification of the material principal direction defined by the angle θ , the crack is assumed to be parallel to the x-axis. This is not as general as the problem defined in Fig. 3.0 which allows for the specification of five independent values $\bar{\sigma}_x$, $\bar{\sigma}_y$, $\bar{\tau}_{xy}$, α and θ . However, by transforming the far field stresses to a crack tip coordinate system and realization that the far field stress parallel to the crack does not

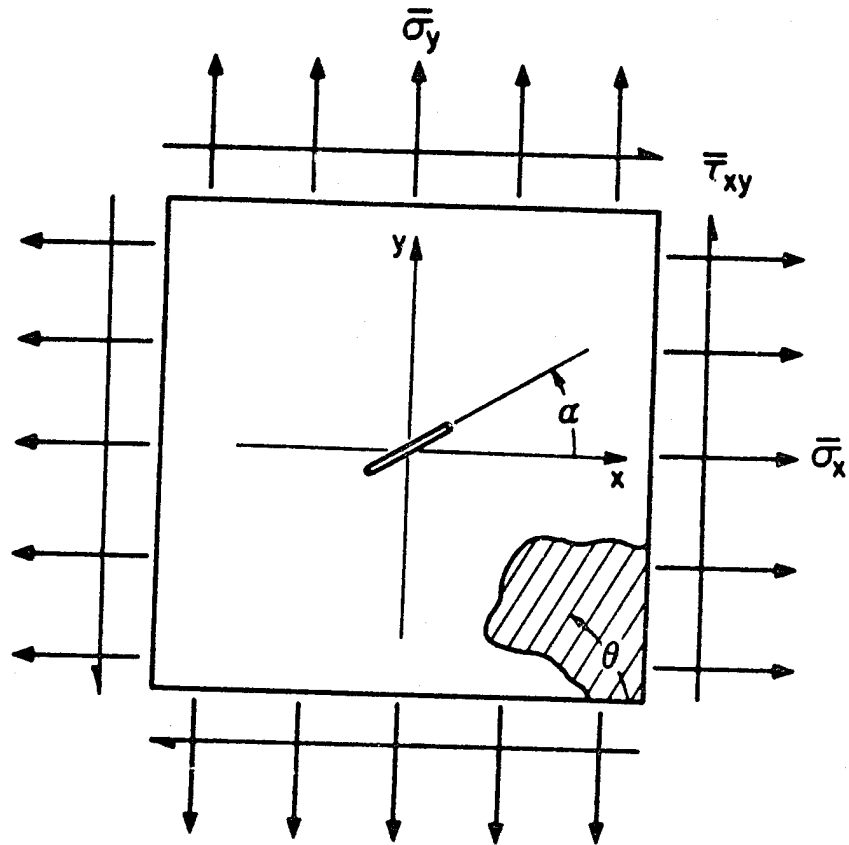


Fig. 3.0 Infinite Center Cracked Plate Under Biaxial Loading.

contribute to the singularity (this fact is discussed in Wu [14]) the elasticity solution can be applied to problems similar to that of Fig. 3.0.

The details of this transformation and superposition are shown in Fig. 3.1. First, the far field stresses of Fig. 3.1a are transformed to a crack tip coordinate system defined by the angle α shown in Fig. 3.1b (the crack tip coordinate system is represented by the axes ξ and η). In the ξ - η coordinate system, the effect of σ_{11}^{∞} and $\tau_{\xi\eta}^{\infty}$ on the crack tip stress field can be evaluated by applying Eq. 2.20. The stresses are separated into singular and non-singular components as shown in Fig. 3.1c. Before Eq. 2.20 can be applied, the components of the compliance tensor, A_{ij} , must also be transformed to the crack tip coordinate system. Since the crack was originally oriented at an angle α and the material principal direction was defined by the angle θ , the compliance tensor must be transformed by the angle $(\theta-\alpha)$. Let β represent the angle $(\theta-\alpha)$.

The use of stress transformation along with the fact that the far field stress parallel to the crack does not contribute to the singularity, allows for the application of specific elasticity solutions to general fracture problems. In the preceding problem, an elasticity solution allowing the specification of two independent values is used to solve a problem requiring the specification of five values.

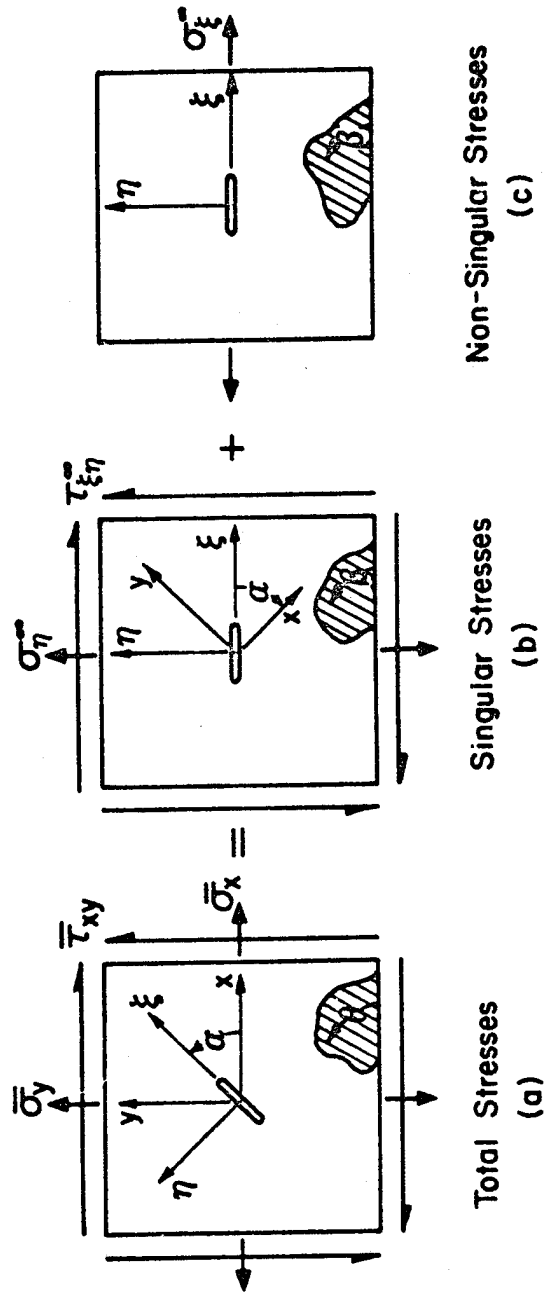


Fig. 3.1 Transformation and Superposition of Far Field Stresses.

3.2 Application of Singular Isoparametric Finite Elements

Since many fracture problems of interest do not satisfy the infinite boundary conditions of the anisotropic elasticity solution, an anisotropic finite element fracture mechanics code was developed. This code, ANFRAC (anisotropic fracture mechanics code), incorporates an isoparametric, quadratic, triangular element and the inherent singularity associated with this element when the mid-side nodes are positioned at quarter points. The advantage of a finite element model is the ability to analyze specific geometries and loading conditions that cannot be addressed with an elasticity solution.

ANFRAC is a linear, two-dimensional, quadratic, isoparametric finite element code. The outline of ANFRAC is similar to that of FEM2D, an isoparametric finite element code presented by Reddy [20]. A description of the quadratic isoparametric triangular element along with practical considerations on the use of isoparametric elements is given in Bathe [21].

The master configuration of this element along with the location of the integration stations is shown in Fig. 3.2. Numerical integration over triangular domains is discussed by Cook [22]. The integration scheme used to calculate the element stiffness matrix is a seven point Gaussian quadrature. The formula for the numerical integration is:

$$\iint f \, dA = \sum_{i=1}^7 w_i f(r,s) \quad (3.1)$$

where

f is the function to be integrated over the triangular area A ,

w_i is the weight associated with the i th sampling point,

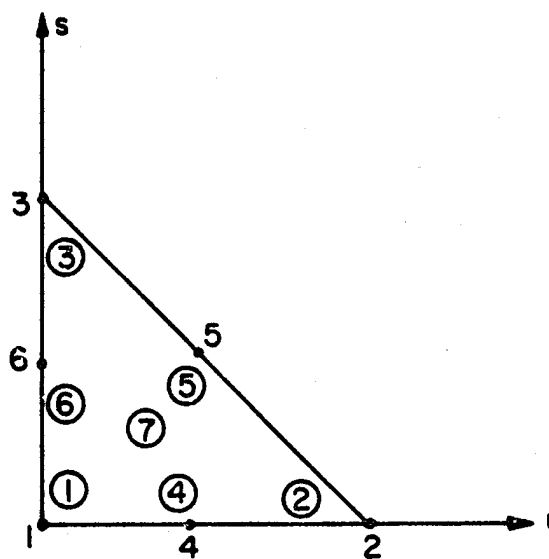


Fig. 3.2 Master Finite Element Configuration.

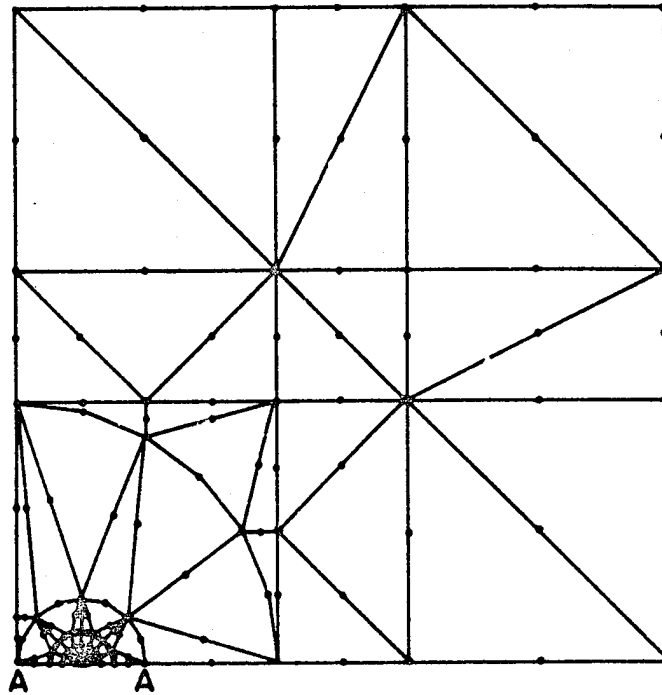
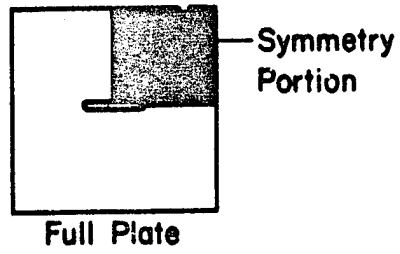
and

$f(r,s)$ is the value of f evaluated at the i th sampling point.

The interpolation functions and weights for the isoparametric quadratic triangular element were taken from Bathe [21] and are given in Table 3.0.

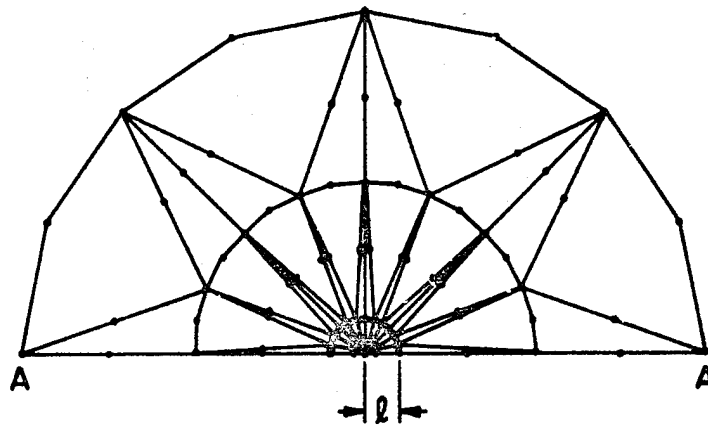
As discussed in Barsoum [23], the ratio of element length to half crack length (designated l/a) significantly influences the crack tip stress field. A similar effect is found in the natural isoparametric element. Freese and Tracey [17] present stress intensity factor results for an isotropic plate with an edge crack using the natural isoparametric triangular element. They have chosen an l/a ratio of 0.1, and present data that is independent of the angle ϕ . With their results in mind, a quarter-symmetry finite element mesh was developed to solve fracture problems involving a center cracked plate. This mesh is shown in Fig. 3.3 and an exploded view of the crack tip elements is given in Fig. 3.4. The l/a ratio of this mesh is 0.1 and the ratio of $2a/w$ is also 0.1. The ratio $2a/w$ is a measure of the infinite nature of the cracked plate. As the ratio of the crack length, $2a$, to the plate width, w , decreases, the infinite boundary conditions of the elasticity solution are closer to being satisfied. A $2a/w$ ratio of 0.1 implies the plate width is an order of magnitude larger than the crack length. For data given in Hertzberg [24], an isotropic plate of this size adequately satisfies the infinite boundary conditions. This appears to be true for anisotropic plates based on data provided by Smith and Mullinix [25].

Since the mesh shown in Fig. 3.3 is a quarter symmetry mesh it can only be used for problems with a crack orientation of 0° and dis-



Note: See Fig. 3.4 for Enlargement of Region A-A

Fig. 3.3 Quarter Symmetry Mesh of Center Cracked Plate.



Note: See Fig. 3.3 for Relative Location of Region A-A.

Fig. 3.4 Exploded View of Crack Tip Elements.

Table 3.0
Interpolation Functions and Numerical Integration Data

Interpolation Functions

$$h_1 = 2r^2 - 3r + 4rs - 3s + 2s^2 + 1$$

$$h_2 = 2r^2 - r$$

$$h_3 = 2s^2 - s$$

$$h_4 = -4r^2 + 4r - 4rs$$

$$h_5 = 4rs$$

$$h_6 = -4s^2 + 4s - 4rs$$

Gauss Point Coordinates and Weights

r - coordinates	s - coordinates	Weights
$r_1 = 0.10128\ 65073\ 235$	$s_1 = r_1$	$w_1 = 0.12593\ 91805\ 448$
$r_2 = 0.79742\ 69853\ 531$	$s_2 = r_1$	$w_2 = w_1$
$r_3 = r_1$	$s_3 = r_2$	$w_3 = w_1$
$r_4 = 0.47014\ 20641\ 051$	$s_4 = r_6$	$w_4 = 0.13239\ 41527\ 885$
$r_5 = r_4$	$s_5 = r_4$	$w_5 = w_4$
$r_6 = 0.05971\ 58717\ 898$	$s_6 = r_4$	$w_6 = w_4$
$r_7 = 0.33333\ 33333\ 333$	$s_7 = r_7$	$w_7 = 0.225$

placement fields symmetric about the x and y axes. Symmetry arguments allow the analysis to be limited to one-quarter of the plate and hence reduce the degrees of freedom of the model. Solving fracture problems that do not allow the use of symmetry arguments requires significantly larger amounts of computer storage or more sophisticated storage and equation solving routines than those used in this investigation.

3.3 Verification of the Finite Element Model

Distributions of the stress components near the crack tip for an infinite center cracked plate subjected to a uniaxial loading of $\bar{\sigma}_y$ equal to 1.0 ksi and a crack orientation of $\alpha = 0^\circ$ are shown in Figs. 3.5 to 3.13. In these figures, the solid lines represent results from the elasticity solution and the finite element results for gauss point 1 (Fig. 3.2) are represented by circles. This point was chosen since it is the nearest integration station to the crack tip and it lies on a radial line through the centroid of the element. Similar plots for the stress distributions at other gauss points are presented in Appendix C.

Figures 3.5 to 3.7 are for a steel plate. For this isotropic problem, the finite element stress results compare very well to the elasticity solution. There is excellent correlation both in magnitude of the stresses and distribution as a function of ϕ .

Figures 3.8 to 3.10 correspond to a plate manufactured from Hercules AS4/3501-6 graphite/epoxy (material properties are given in Appendix E). For this problem, the fiber orientation angle, θ , is equal to zero degrees. Overall, there is correlation in the stress

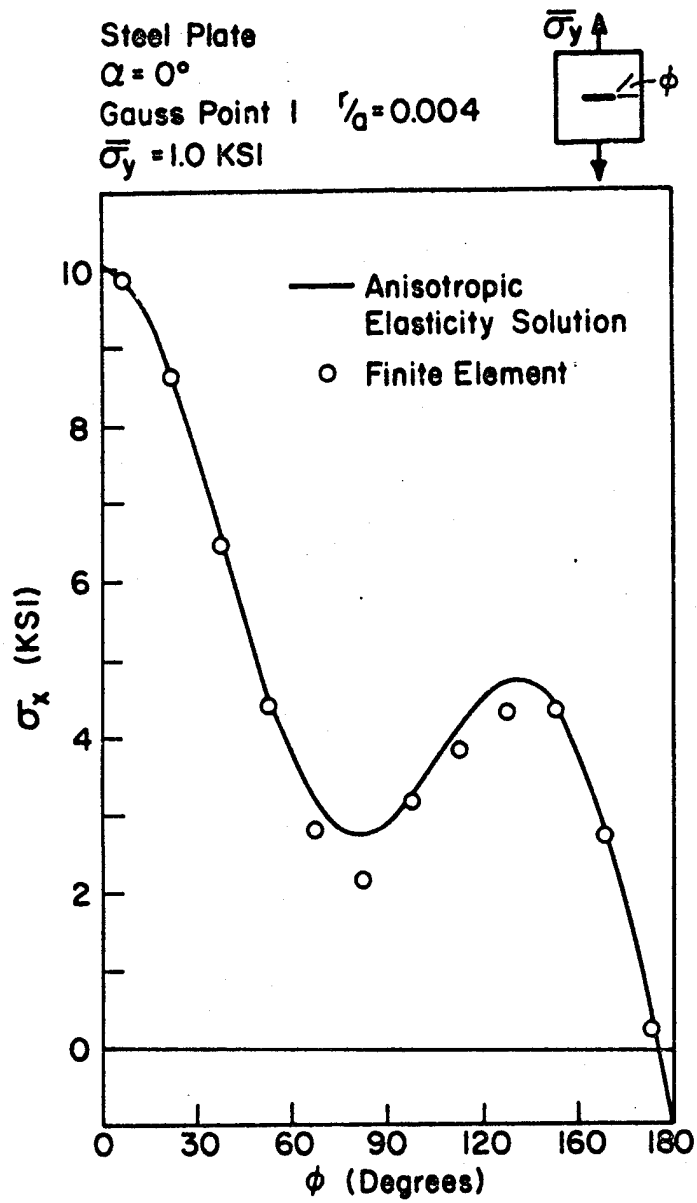


Fig. 3.5 Distribution of σ_x Near the Crack Tip in a Center Cracked Steel Plate.

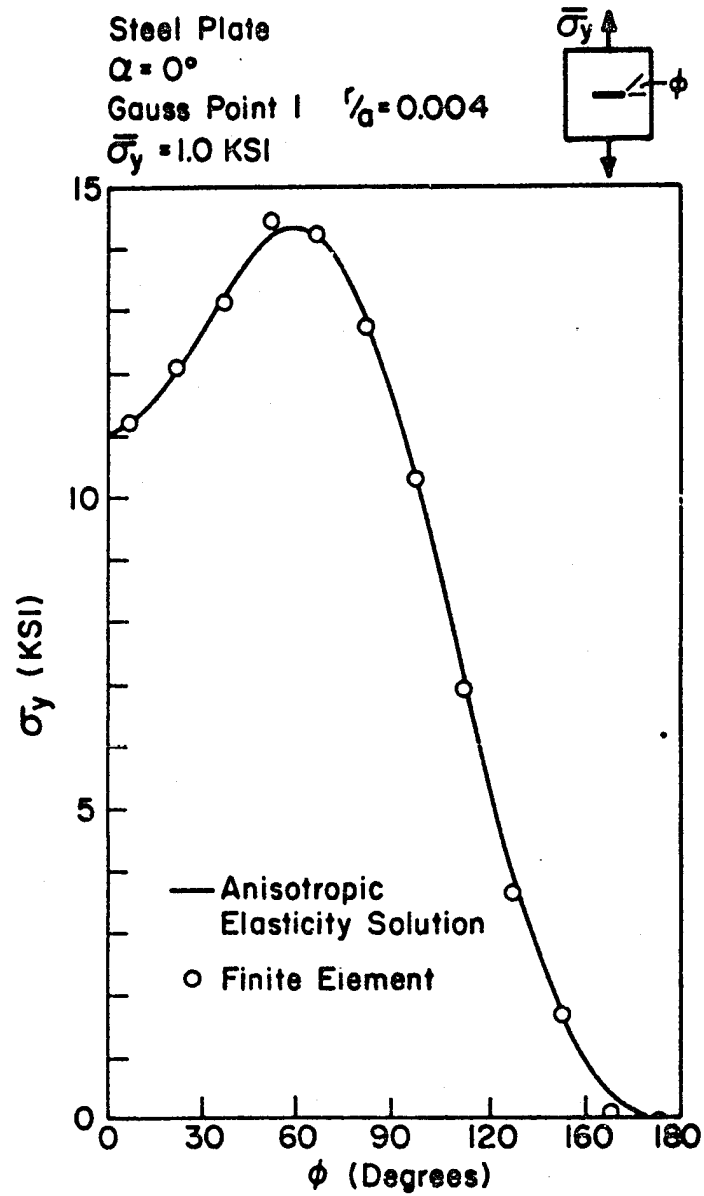


Fig. 3.6 Distribution of σ_y Near the Crack Tip in a Center Cracked Steel Plate.

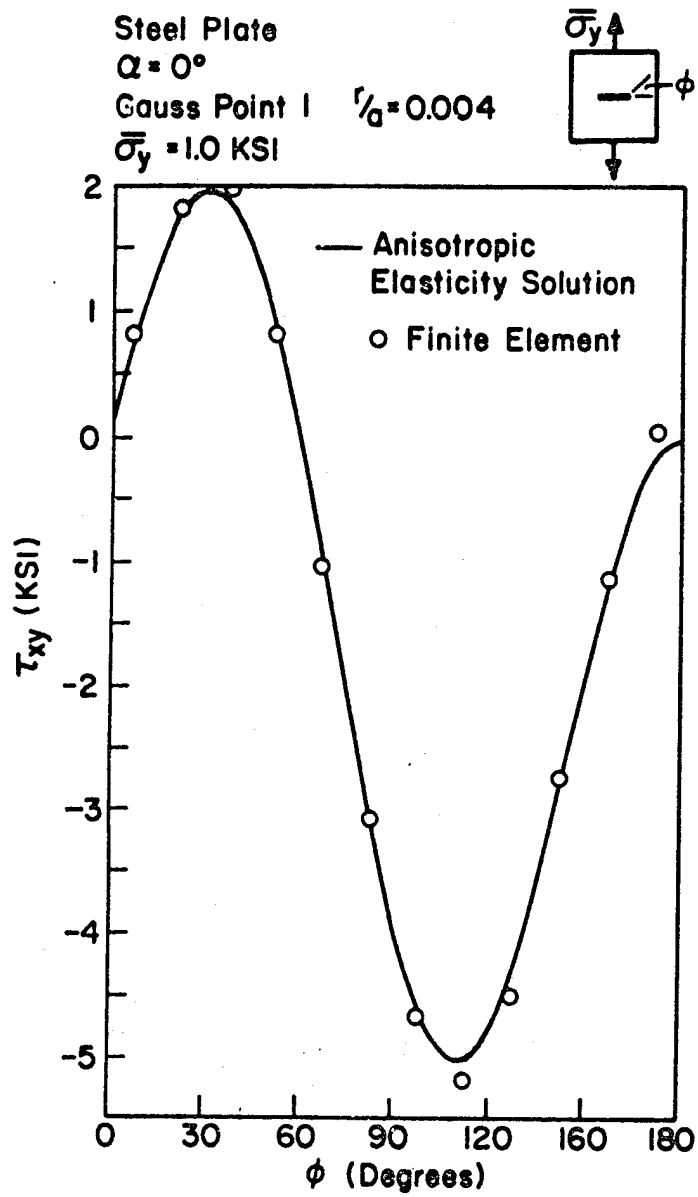


Fig. 3.7 Distribution of τ_{xy} Near the Crack Tip in a Center Cracked Steel Plate.

distribution as a function of ϕ and in the stress magnitudes. However, the finite element prediction of the magnitude of σ_x , shown in Fig. 3.8, does not compare as well as the other stress components. The lack of better agreement for this stress component is due to the high gradient that exists as a function of ϕ . If the l/a ratio were reduced and the concentration of elements increased, the σ_x component predicted by the finite element model should improve. Since the gradients in the stress components for graphite/epoxy are greater than that of steel, there is no reason to expect that a mesh that has converged for an isotropic fracture problem has also converged for a highly orthotropic one.

Similar results are seen in Figs. 3.11 to 3.13 which correspond to a plate manufactured from AS4/3501-6 graphite/epoxy with a fibers orientation angle of 90° . The distribution in stress components as a function of ϕ compares well with the elasticity solution while there is some discrepancy in the magnitude of σ_x . The difference in magnitude is less than that of the $\theta = 0^\circ$ problem. This fact is not surprising since the gradient of σ_x as a function of ϕ is an order of magnitude smaller for the 90° problem.

These results indicate that singular finite elements can be applied to anisotropic fracture problems. However, prior to their application, a detailed study on the convergence of singular isoparametric elements in anisotropic fracture is required. Since stress gradients in anisotropic materials can be significantly larger than those in isotropic materials, the mesh building guidelines of Freese and Tracey [17] are no longer applicable. An example of the importance of the l/a ratio on the prediction of crack tip stresses in anisotropic materials is shown in Appendix F.

AS4/3501-6
 $\alpha = 0^\circ \quad \theta = 0^\circ$
 Gauss Point 1 $r/a = 0.004$
 $\bar{\sigma}_y = 1.0 \text{ KSI}$

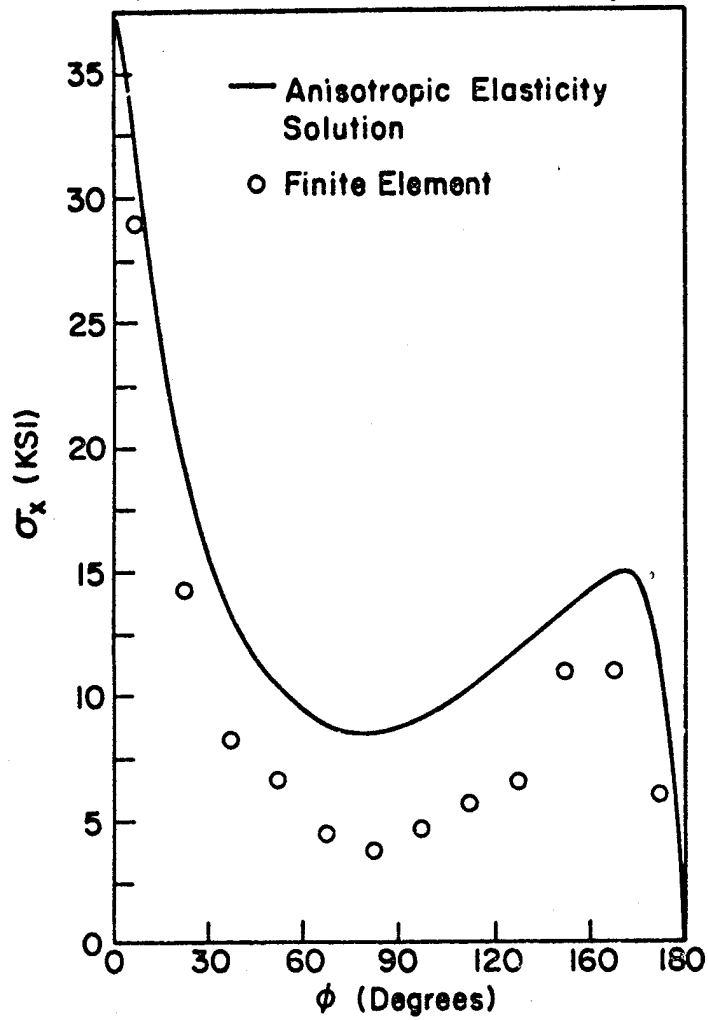
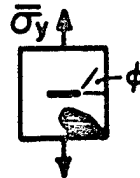


Fig. 3.8 Distribution of σ_x Near the Crack Tip in a Center Cracked Graphite/Epoxy Plate ($\theta = 0^\circ$).

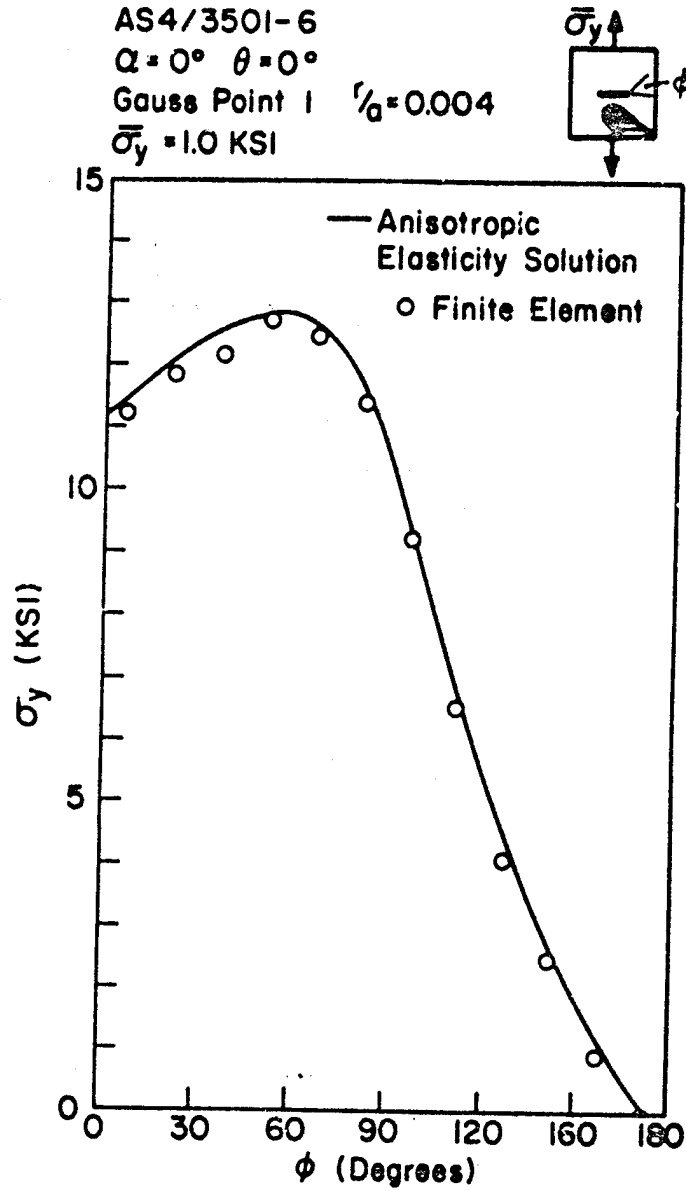


Fig. 3.9 Distribution of σ_y Near the Crack Tip in a Center Cracked Graphite/Epoxy Plate ($\theta = 0^\circ$).

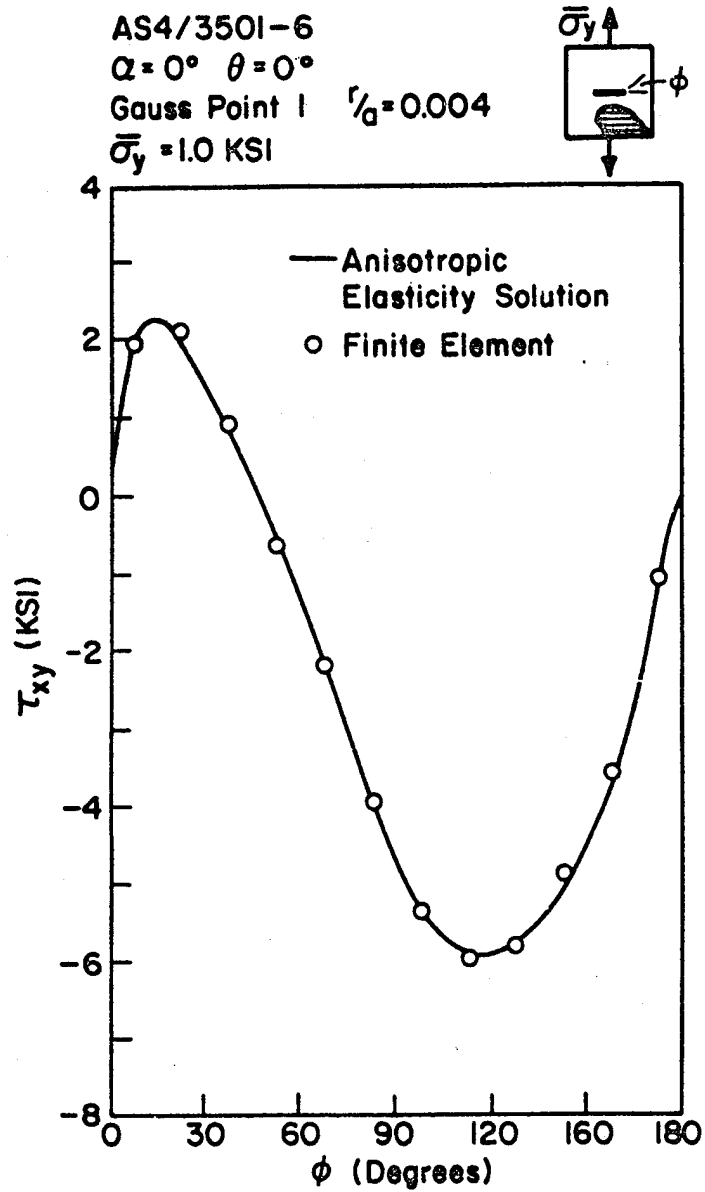


Fig. 3.10 Distribution of τ_{xy} Near the Crack Tip in a Center Cracked Graphite/Epoxy Plate ($\theta = 0^\circ$).

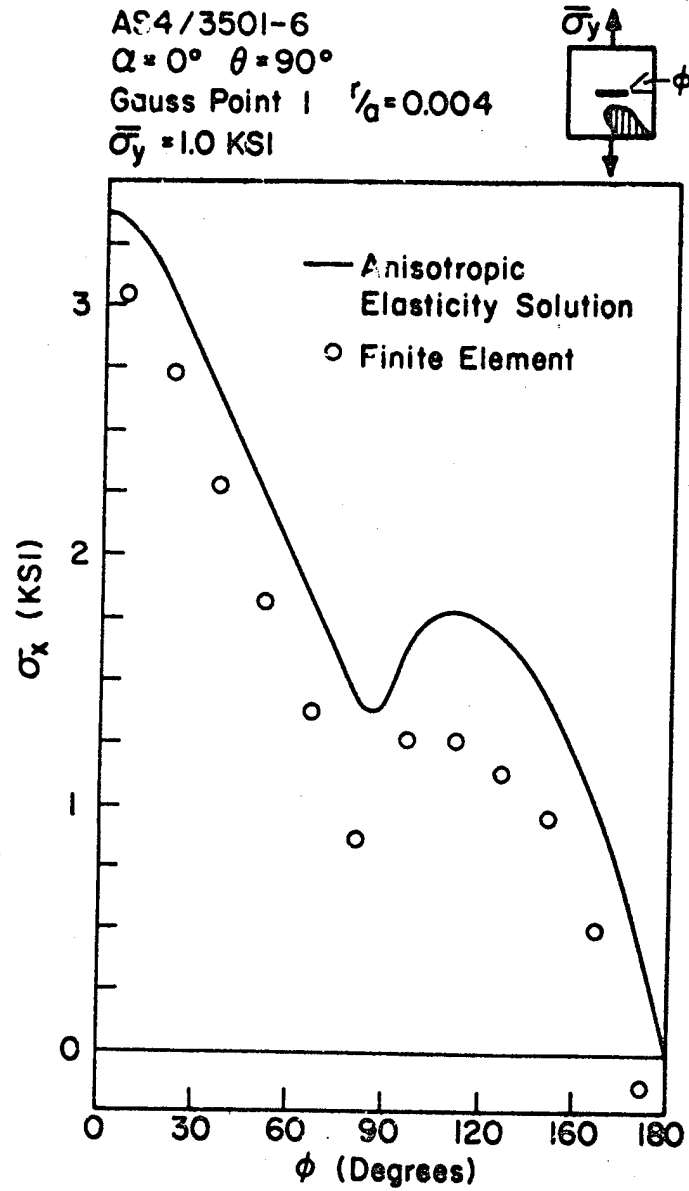


Fig. 3.11 Distribution of σ_x Near the Crack Tip in a Center Cracked Graphite/Epoxy Plate ($\theta = 90^\circ$).

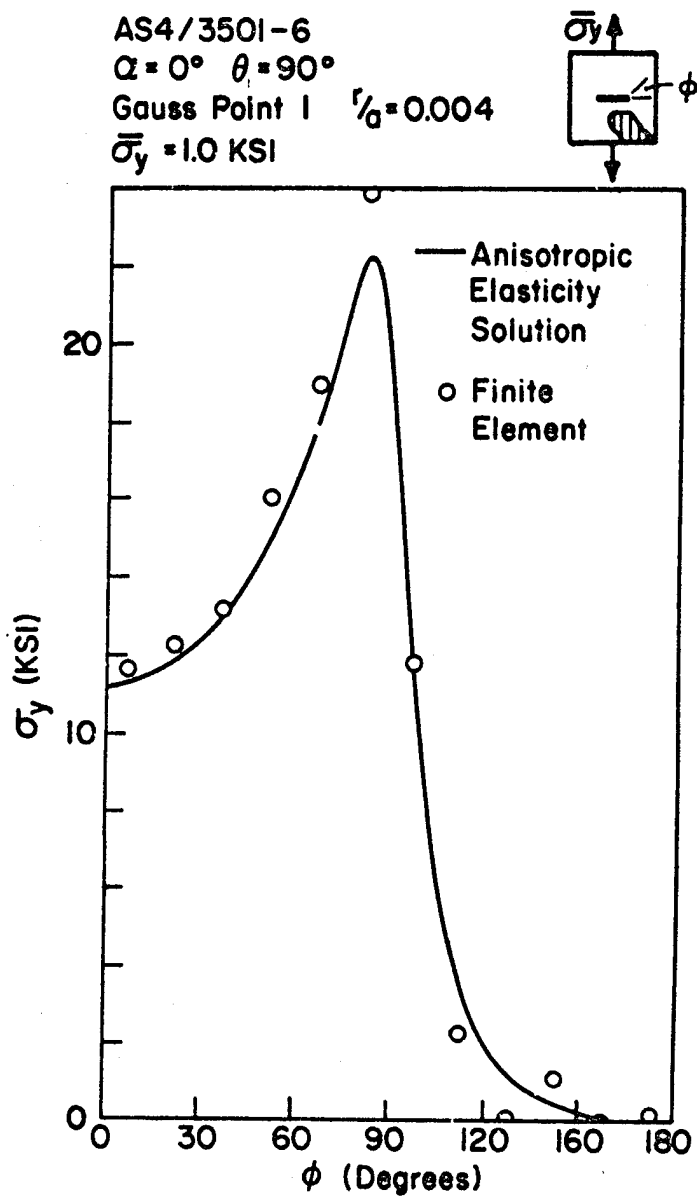


Fig. 3.12 Distribution of σ_y Near the Crack Tip in a Center Cracked Graphite/Epoxy Plate ($\theta = 90^\circ$).

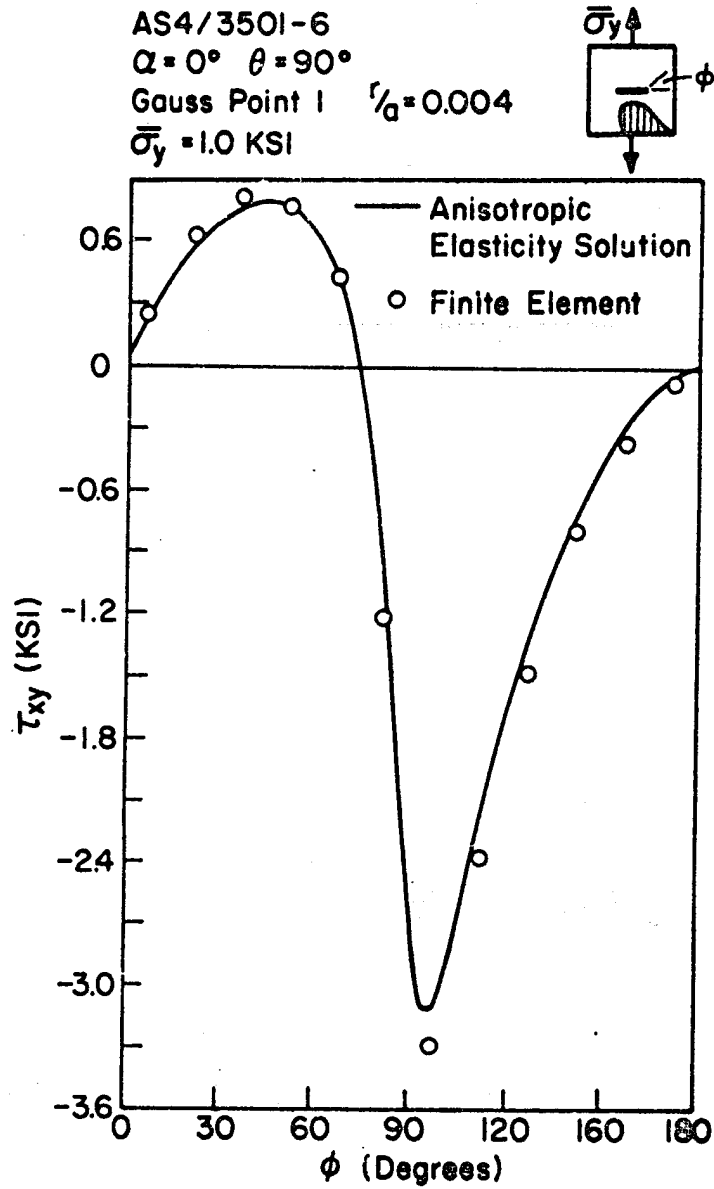


Fig. 3.13 Distribution of τ_{xy} Near the Crack Tip in a Center Cracked Graphite/Epoxy Plate ($\theta = 90^\circ$).

Chapter 4

OFF-AXIS AND UNIDIRECTIONAL TENSILE COUPONS

In this section analytical results are presented for graphite/epoxy tensile coupons containing center cracks. The emphasis of the analysis was to verify the numerical results of Buczek and Herakovich [5] and to develop analytical results which when compared to existing experimental results would test the credibility of the Normal Stress Ratio as a viable crack extension direction criterion. All results were generated using the anisotropic elasticity solution of Section (3.1). Additional results for analyses presented in this chapter can be found in Appendix D.

4.1 Unidirectional 30° Off-Axis Tensile Coupon

Buczek and Herakovich compared several crack extension direction theories with experimental results for a 30° off-axis tensile coupon ($\theta = 120^\circ$) and found surprising results. Of the three crack growth direction criteria described in Section (2.1), only the Normal Stress Ratio agreed with the experimental value of 300°. Since the finite element formulation which they employed was not developed specifically to describe the stress field near a singularity, it was desired to test the theory using a more accurate stress analysis. In an effort to verify their results, the same 30° off-axis tensile coupon was analyzed using the anisotropic elasticity solution.

The geometry of the specimen is shown in Fig. 4.0. The crack tip stresses were evaluated for an applied load $\bar{\sigma}_y = 1.0$ ksi at an r_0 value of 0.005 inches. An r_0 of 0.005 was chosen to match that selected by

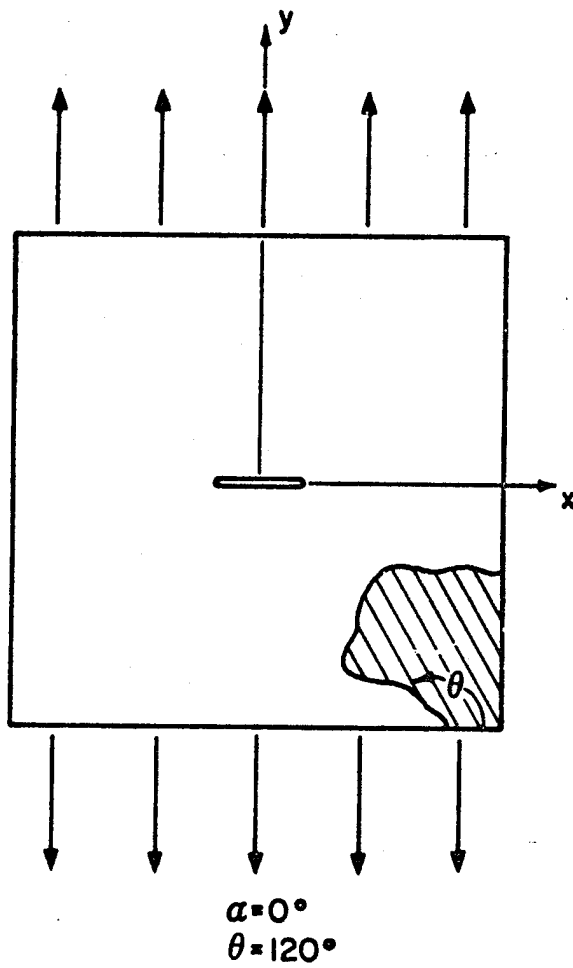


Fig. 4.0 Center Cracked 30° Off-Axis Coupon.

Buczek and Herakovich. The distributions of the crack growth direction criteria as a function of ϕ are shown in Figs. 4.1 through 4.3. A comparison of the predicted crack growth directions using anisotropic elasticity with those predicted by finite elements [5] is given in Table 4.0.

The direction of crack extension predicted by the Normal Stress Ratio is very consistent in both the analytical and finite element solutions, while the direction of crack extension predicted by the Tensor Polynomial and Strain Energy Density is not consistent. The discrepancy in the crack growth direction predicted by the Tensor Polynomial and Strain Energy Density in the two analyses is due to the finite element formulation used by Buczek and Herakovich [5]. Rather than concentrating on approximating the stress field around the crack tip, their formulation emphasizes evaluation of the strain energy released during crack extension.

It is important to note that the conclusions drawn by Buczek and Herakovich concerning the inconsistencies of the Tensor Polynomial and Strain Energy Density Criterion in predicting the direction of crack extension are supported by the anisotropic elasticity solution. The difference in the value of ϕ_c predicted by the two methods is due to the improved accuracy of the anisotropic elasticity solution relative to the conventional finite element formulation.

4.2 Influence of r_0 on the Predicted Direction of Crack Growth

Investigation as to the influence of r_0 on the crack growth direction criteria yields interesting results. The direction of crack

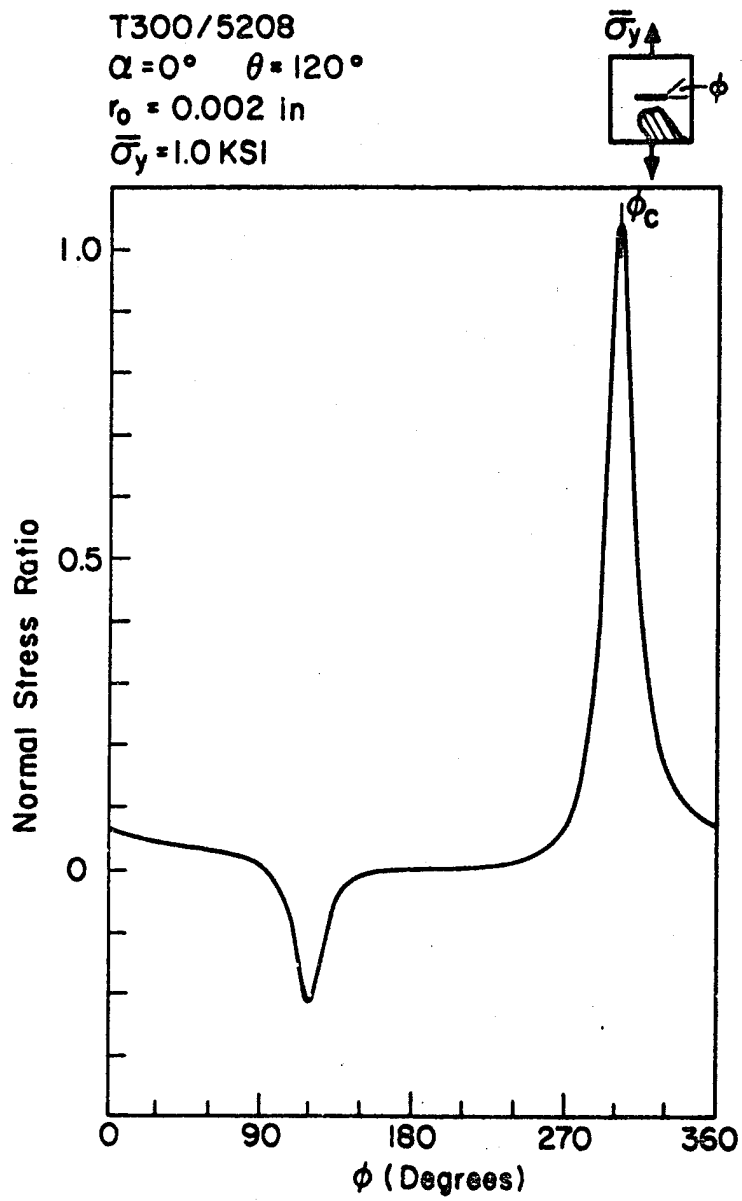


Fig. 4.1 Normal Stress Ratio vs. ϕ for 30° Off-Axis Graphite/Epoxy Coupon.

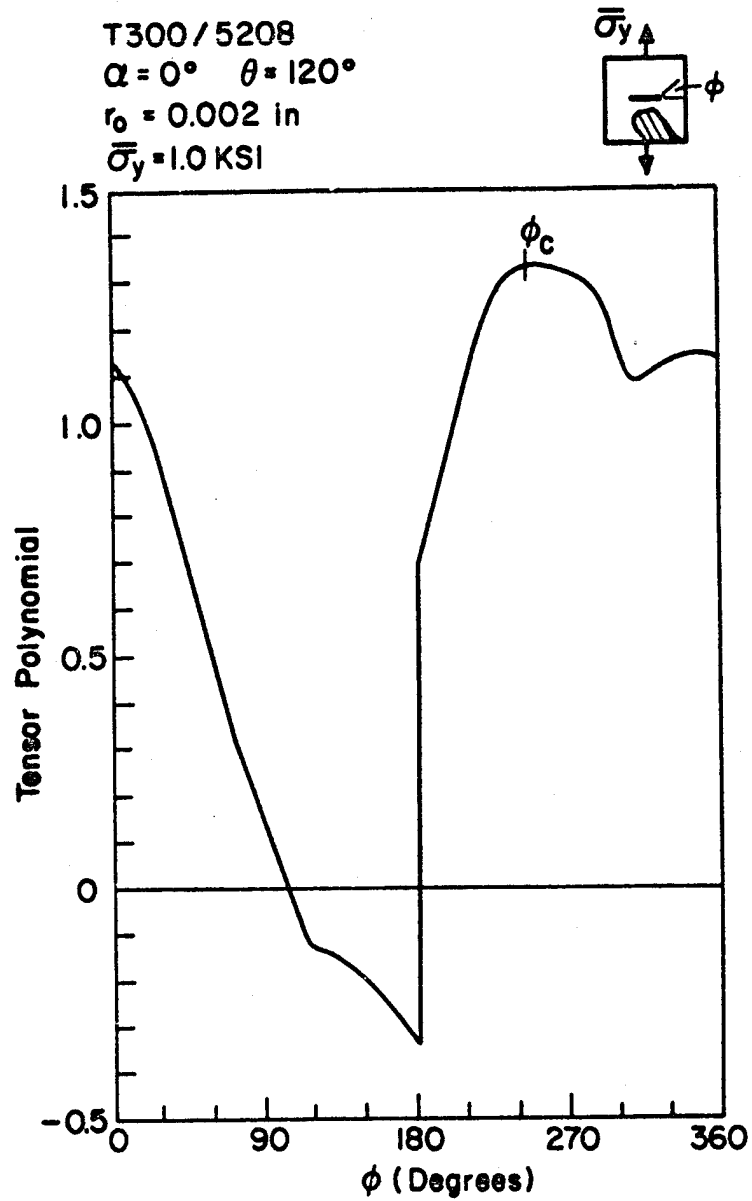


Fig. 4.2 Tensor Polynomial vs. ϕ for 30° Off-Axis Graphite/Epoxy Coupon.

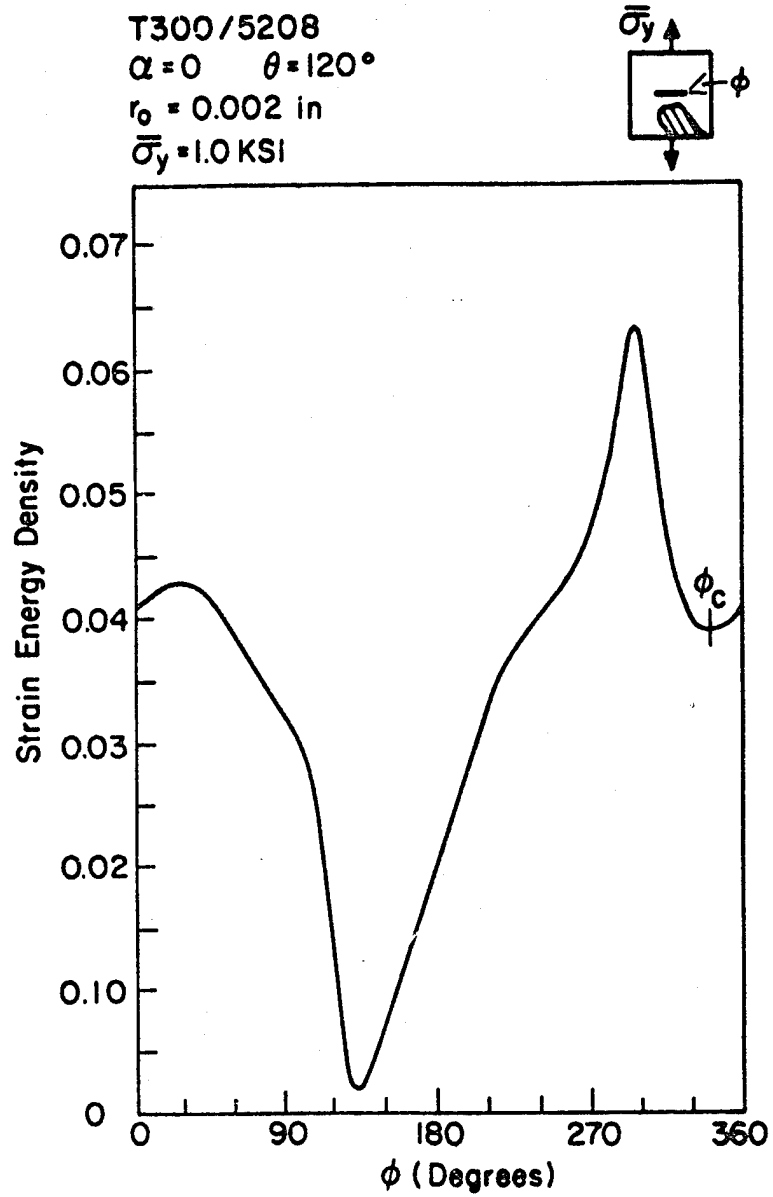
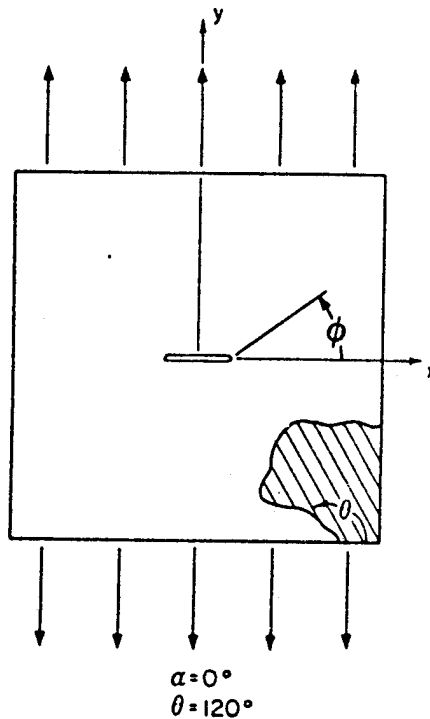


Fig. 4.3 Strain Energy Density vs. ϕ for 30° Off-Axis Graphite/Epoxy Coupon.

Table 4.0

Comparison of Anisotropic Elasticity to Finite Element Results for
Direction of Crack Extension in 30° Off-Axis Tensile Coupons

Crack Extension Criterion	Anisotropic Elasticity	Finite Element [9]
Normal Stress Ratio	301°	300°
Tensor Polynomial	248°	90°
Strain Energy Density	340°	360°



extension predicted by the Normal Stress Ratio and Strain Energy Density Criteria is independent of the value of r_0 , but this is not the case for the Tensor Polynomial. These facts are shown dramatically in Fig.

4.4. From this figure, it is apparent that a small change in the value of r_0 can affect the value of ϕ_c as predicted by the Tensor Polynomial by as much as 40° . As seen in Fig. 4.5, the change in the distribution of the Tensor Polynomial as a function of ϕ for an order of magnitude change in r_0 is significant. For an r_0 of $5.0E-03$ ", the Tensor Polynomial predicts the direction of crack growth to be 248° , while for an r_0 of $5.0E-04$ ", the predicted direction is 253° .

4.3 Unidirectional 15° Off-Axis Coupons

In an attempt to further verify the consistency of the Normal Stress Ratio Criterion, the experimental configurations of Herakovich et al. [26] were also analyzed. The geometries of the specimens analyzed are shown in Fig. 4.6. The experimental observations for the direction of crack extension were made with AS4/3501-6 graphite/epoxy. The analysis consisted of comparing the predicted direction of crack extension in an infinite plate ($\theta = 105^\circ$) with an applied load of $\bar{\sigma}_y = 1.0$ ksi and an r_0 of 0.002 inches with the experimentally observed crack extension direction. An r_0 of 0.002 inches corresponds with the location of gauss point 1 in the singular isoparametric finite element solution.

The first specimen analyzed has a crack orientation angle, α , of 0° . The direction of crack growth predicted by the Normal Stress Ratio for this sample is 286° . This corresponds very well with the experimental value of 285° (parallel with the fibers) observed by Herakovich et

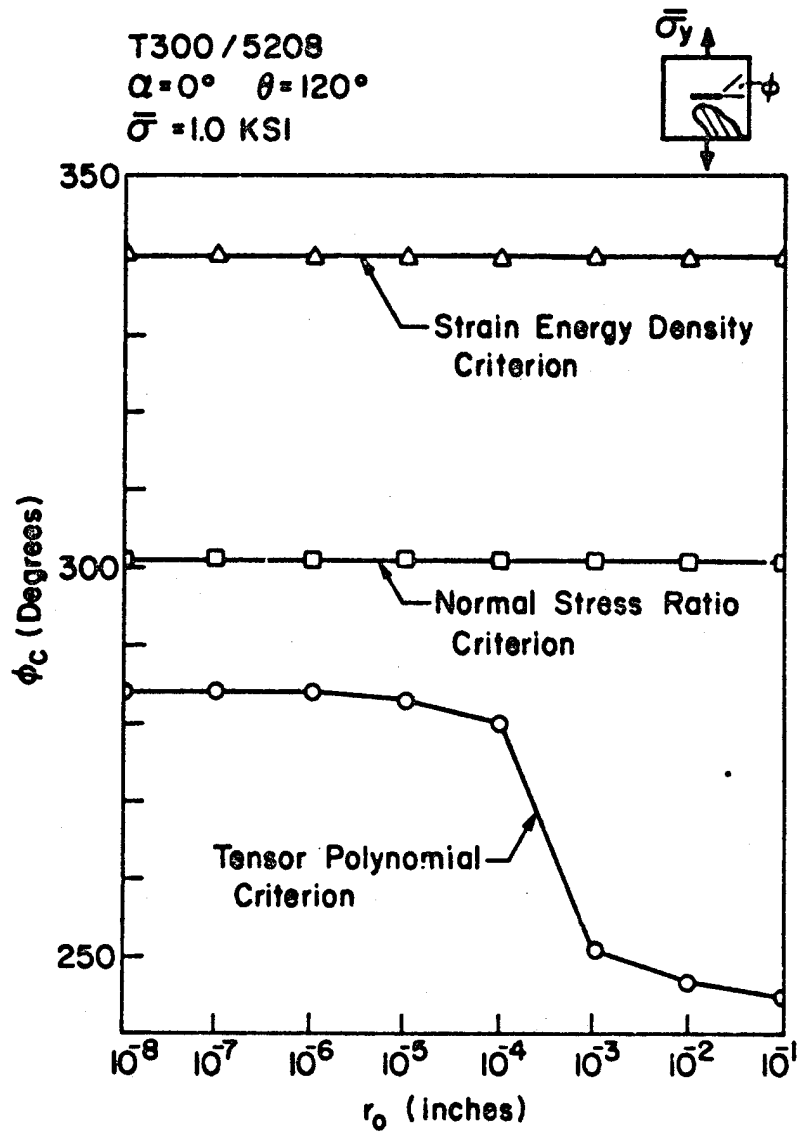


Fig. 4.4 Influence of r_0 on the Crack Growth Direction Criteria.

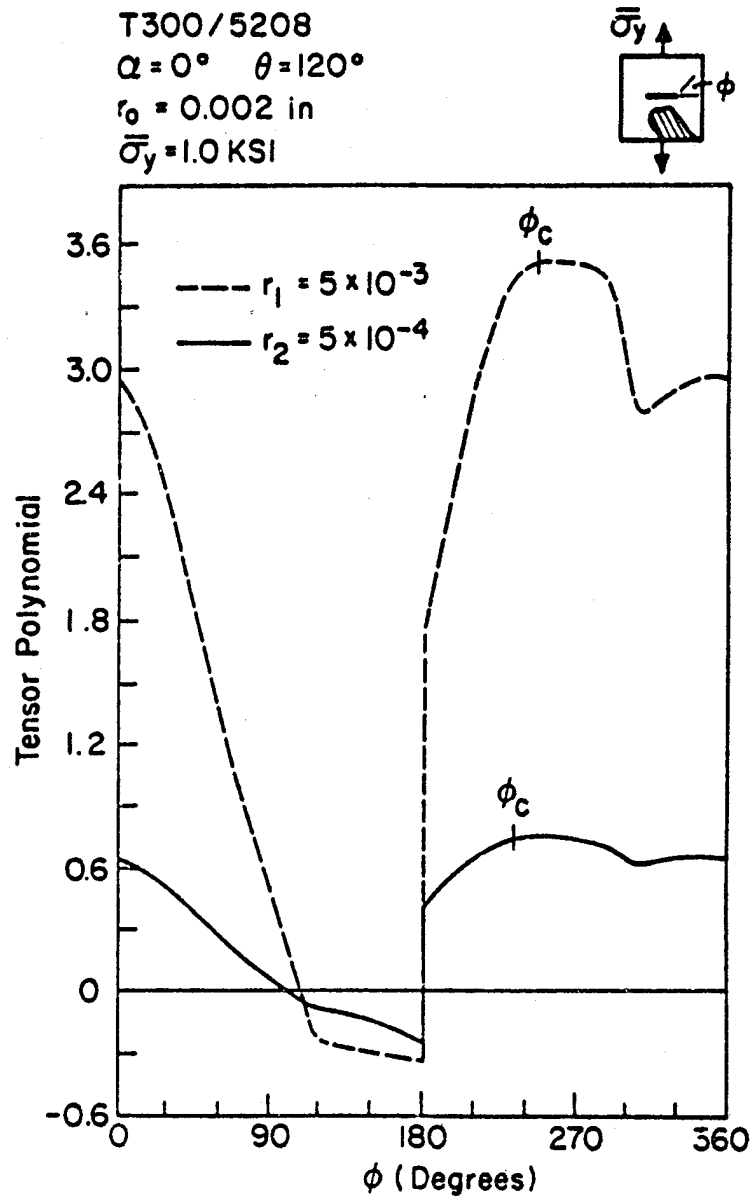


Fig. 4.5 Influence of r_0 on the Distribution of the Tensor Polynomial.

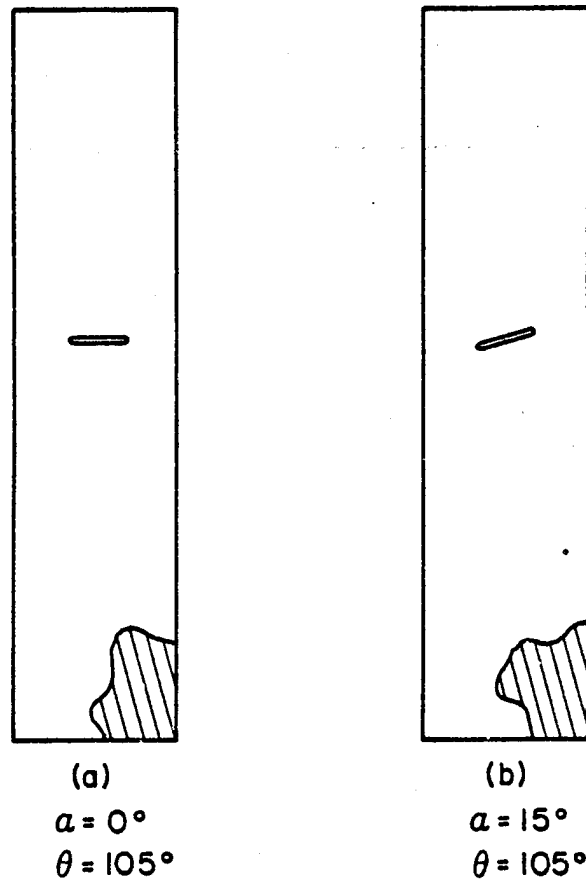


Fig. 4.6 Center Cracked 15° Off-Axis Coupon Configurations.

al. [26]. The distribution of the Normal Stress Ratio as a function of ϕ for this problem is shown in Fig. 4.7.

For the second specimen, the crack was aligned perpendicular to the fibers ($\alpha = 15^\circ$). The distribution of the Normal Stress Ratio as a function of ϕ for this problem is shown in Fig. 4.8. The Normal Stress Ratio predicts the direction of crack extension to be 271° , while the experimental results of Herakovich et al. [26] showed crack extension to occur at 270° . Again there is good correlation between the analytical model and the experimental results.

Analysis of Figs. 4.7 and 4.8 yields interesting results. For both problems, the theoretical prediction of ϕ_c differs slightly from the experimentally observed value. However, for both cases there is a strong peak in the distribution of the Normal Stress Ratio as a function of ϕ in the actual direction of crack growth. This fact is very important. The Normal Stress Ratio may not have the accuracy to predict the direction of crack extension correctly to within one degree. However, when observed graphically, the Normal Stress Ratio represents the direction of crack extension exceptionally well.

4.4 Unidirectional Lamina Subjected to Mixed-Mode Loadings

In order to study crack growth in fibrous composites under more general loading conditions, and to assist the experimentalist in verification of the Normal Stress Ratio Criterion, unidirectional lamina were analyzed for various mixed-mode loadings and the predicted values of ϕ_c determined. Studies of this nature can be very beneficial. In addition to providing theoretical predictions for the direction of crack

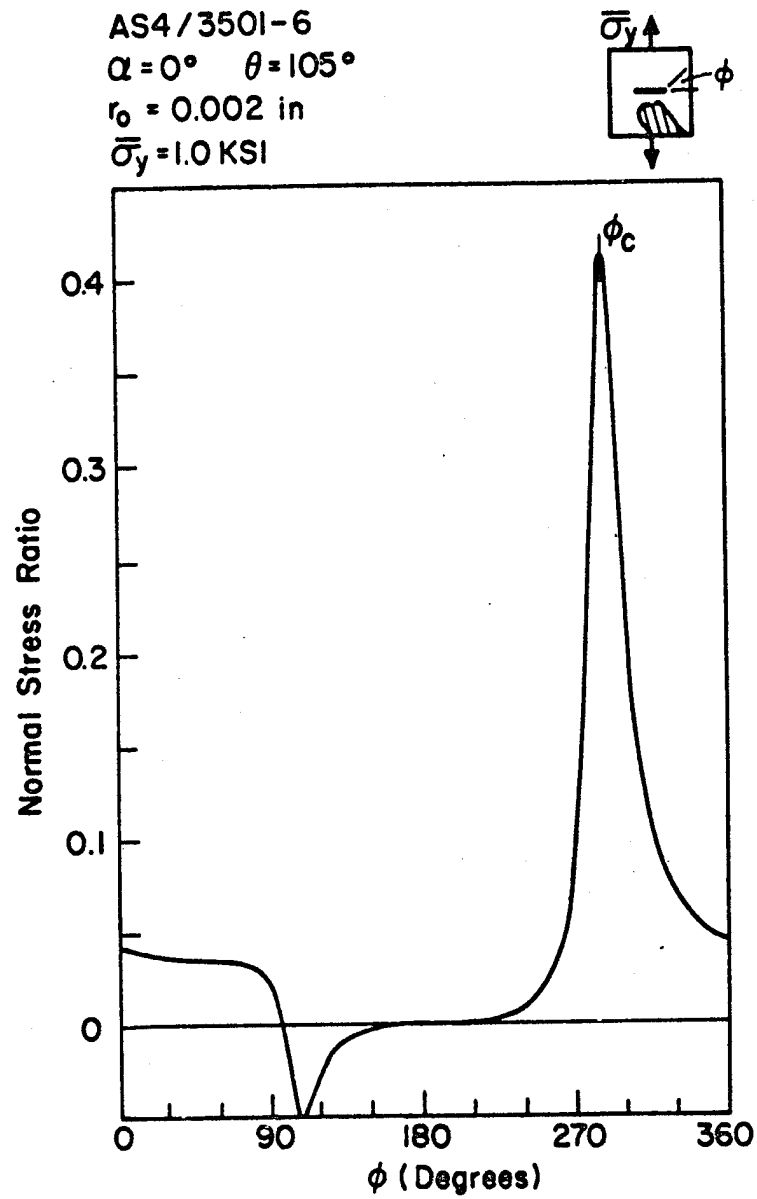


Fig. 4.7 Normal Stress Ratio vs. ϕ for 15° Off-Axis Graphite/epoxy Coupon ($\alpha = 0^\circ$).

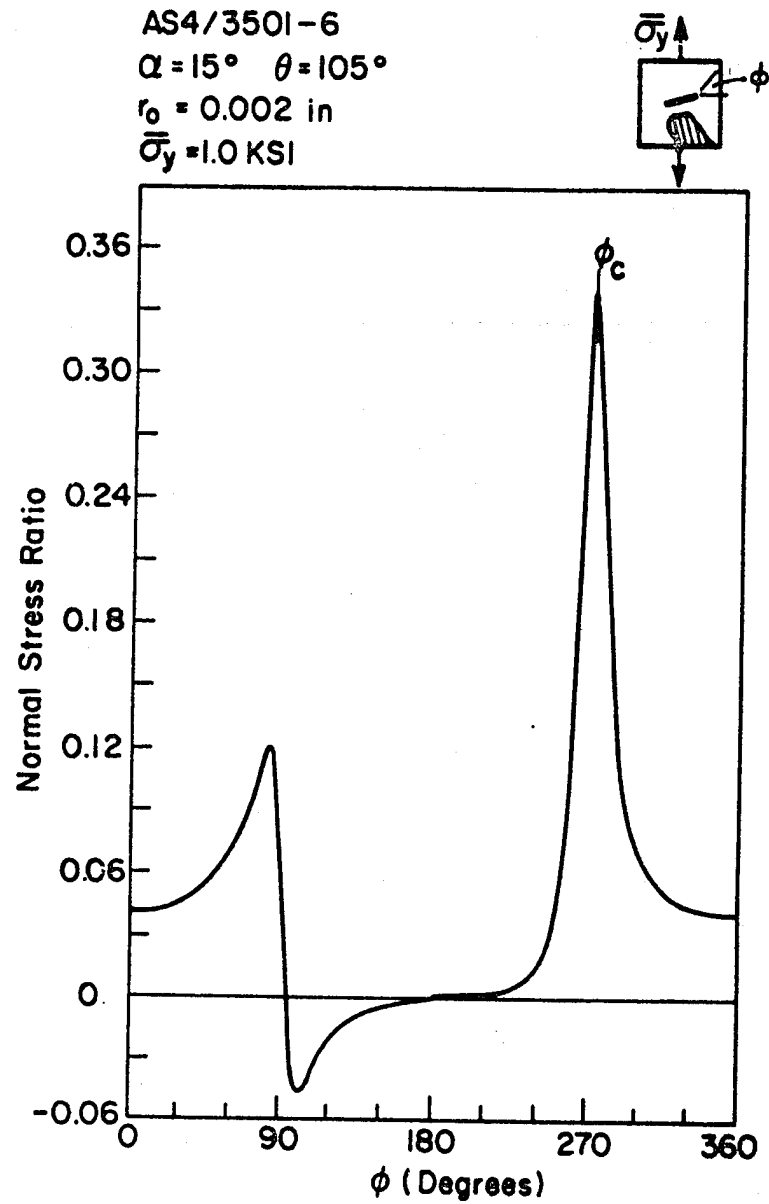


Fig. 4.8 Normal Stress Ratio vs. ϕ for 15° Off-Axis Graphite/Epoxy Coupon ($\alpha = 15^\circ$).

extension under mixed-mode loading, they serve as a guide to the experimentalist. With knowledge of the predicted response in hand, one can then choose the most appropriate laboratory experiments necessary to critically test the hypothesis, without running a plethora of tests.

The geometry and loading of the specimens analyzed is shown in Fig. 4.9. The fiber orientation angle, θ , is 0° , the crack orientation, α , is 0° and r_0 was chosen to be 0.002 inches. Mixed-mode analysis requires the definition of a parameter, λ , which is the ratio of $\bar{\sigma}_y$ to $\bar{\tau}_{xy}$. Mode I loading corresponds to $\lambda = \infty$, while mode II is defined as $\lambda = 0$. Figure 4.10 shows the predicted direction of crack growth, ϕ_c for pure mode II and various degrees of mixed-mode loading.

By analyzing Fig. 4.10 a great deal of information can be gained about the mixed mode response of 0° graphite/epoxy material. The direction of crack extension is strongly dependent on λ for small value of λ (i.e., < 2.0). For $\lambda > 2.0$ the predicted direction of crack growth is independent of λ . For pure mode II loading, the predicted crack extension direction is 348° . In contrast, a mixed-mode loading of $\lambda = 1$ generates crack extension at 358° , while pure mode I generates crack growth at 0° . From these results, an ideal laboratory test to verify the Normal Stress Ratio would be pure mode II loading. The predicted direction of crack extension for this loading, 348° , clearly implies fiber breakage. A very poor test would be any mixed-mode test that was not predominantly mode II because the direction of crack extension appears to be dominated by the mode I response when $\lambda > 2.0$.

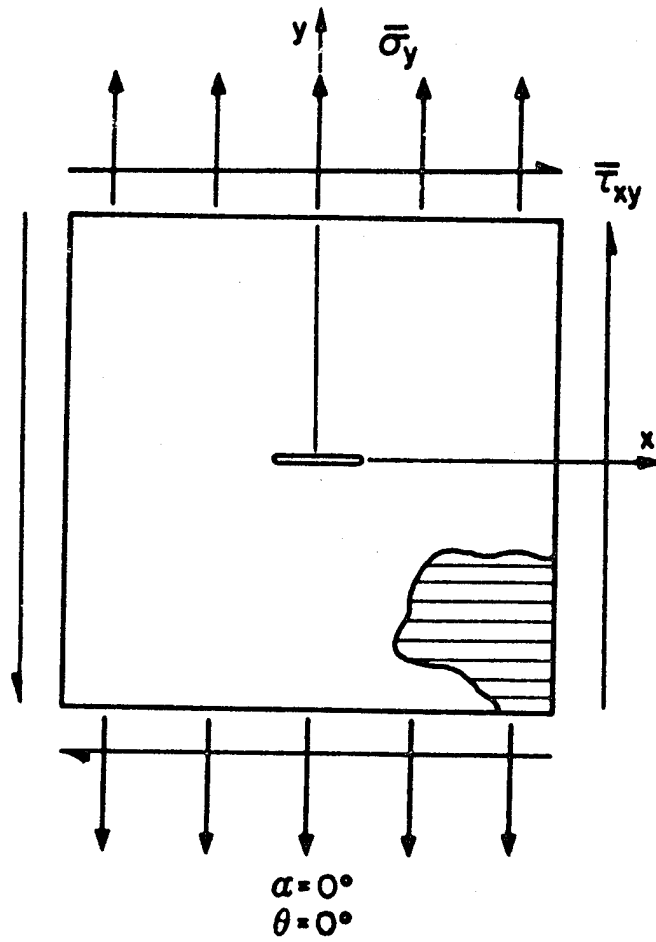


Fig. 4.9 Center Cracked Mixed-Mode Coupon.

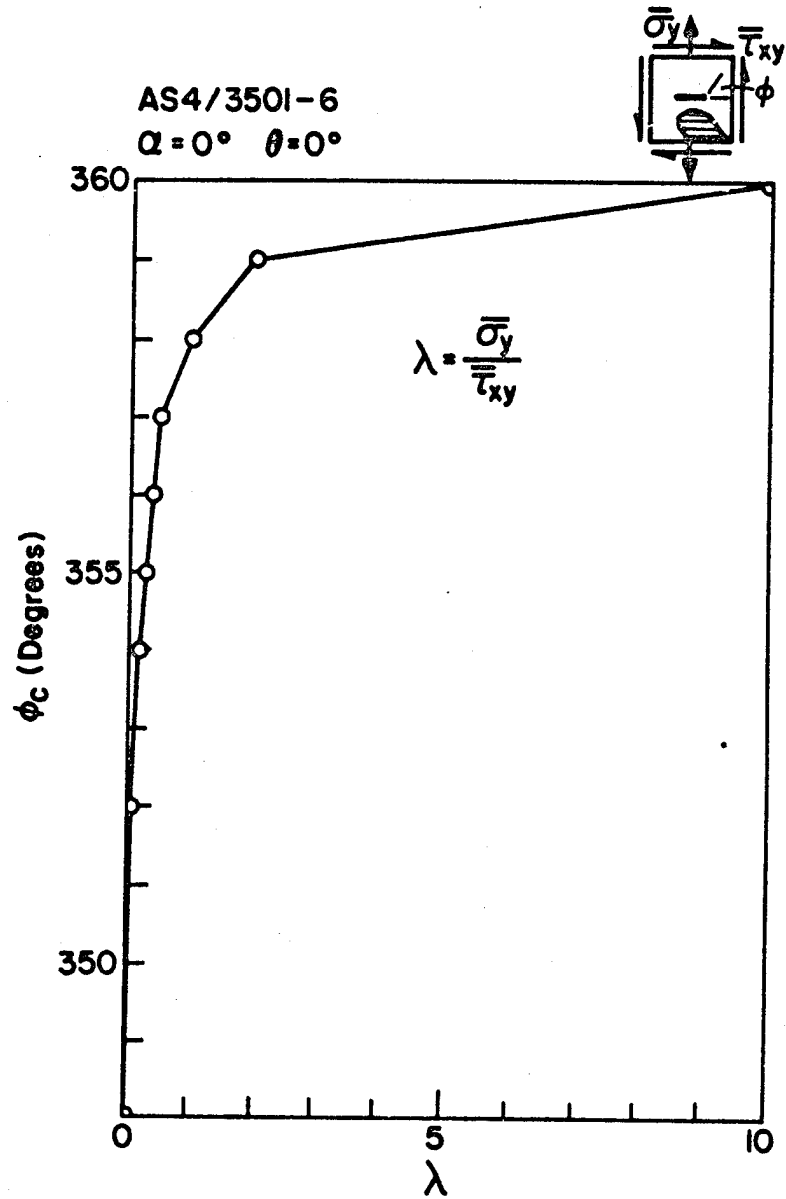


Fig. 4.10 Predicted Crack Growth Direction as a Function of Biaxial Load.

Chapter 5

CONCLUSIONS AND RECOMMENDATIONS

This study has been concerned with the development of models to predict the crack tip stress field in unidirectional composite materials, investigation of various crack growth direction criteria, and the effect of biaxial loading on the direction of crack extension.

For the cases analyzed, the Normal Stress Ratio has proven to be a consistent crack extension direction criteria. Two advantageous characteristics of the Normal Stress Ratio are, the presence of a strong peak in the direction of crack extension when plotted as a function of ϕ and the independence of ϕ_c on the choice of r_0 . Though the Normal Stress Ratio may not have the accuracy to predict the direction of crack extension to within one degree, when observed graphically, this criterion predicts the direction of crack extension exceptionally well. The independence of ϕ_c on the choice of r_0 allows the prediction of crack extension direction in unidirectional composites without prior knowledge of a proper r_0 value.

This study has confirmed the discrepancies found by Buczek and Herakovich [5] regarding the Tensor Polynomial and Strain Energy Density crack growth criteria. The inability of these theories to predict the correct direction of crack growth was not due to an inaccurate finite element stress analysis, but due to limitations in the theories.

Application of the anisotropic elasticity solution to the analysis of unidirectional composites containing cracks has been very advantageous. The speed and reduction in cost of analyses based on the anisotropic elasticity solution relative to finite element solutions is

phenomenal. This access to an inexpensive analytical solution allows the performance of detailed parametric studies. Through these parametric studies, critical tests can be determined to better verify and evaluate crack direction criteria.

It has been shown that singular isoparametric finite elements can also be used to approximate crack tip stresses in anisotropic materials. Though the problems treated in this study were heuristic in nature, they have proven that singular isoparametric finite elements can be used to solve anisotropic fracture problems. Finite element solutions are particularly valuable for problems that cannot be addressed by the anisotropic elasticity solution, i.e., problems with finite size or complex geometries.

Though this study has proven the potential usefulness of singular isoparametric finite elements in anisotropic fracture, additional research is required. Particular emphasis should be given to the development of guidelines which will assist the analyst in mesh building, i.e., proper h/a ratios and element concentrations.

Additional experimental research is required to further verify the Normal Stress Ratio Criterion. Particular consideration should be given to performing tests under mode II loading. The Normal Stress Ratio predicts fiber breakage for pure mode II loading of a unidirectional graphite/epoxy composite with fiber orientation and crack orientation of 0° . Correspondence between experimentally observed and analytically predicted values of ϕ_c for tests involving fiber breakage would add significant credibility to the Normal Stress Ratio Criterion.

Lastly, to fully verify the Normal Stress Ratio Criterion other material systems must be studied. So far, all applications of the Normal Stress Ratio Criterion have been with graphite/epoxy. Material systems representing various degrees of anisotropy from isotropic to graphite/epoxy need to be investigated.

REFERENCES

1. Herakovich, C. T., "Influence of Layer Thickness on the Strength of Angle-Ply Laminates," Journal of Composite Materials, Vol. 16, 1982, pp. 216-227.
2. Wu, E. M., "Strength and Fracture of Composites," Composite Materials, Vol. 5, edited by L. J. Broutman, Academic Press, New York, 1974, pp. 191-247.
3. Sih, G. C., Chen, E. P., Huang, S. L., and McQuillen, E. J., "Material Characterization on the Fracture of Filament-Reinforced Composites," Journal of Composite Materials, Vol. 9, April 1975, pp. 167-186.
4. Wu, E. M., "Some Unique Crack Propagation Phenomena in Unidirectional Composites and Their Mathematical Characterization," Structure, Solid Mechanics and Engineering Design, Proceedings of the Southampton 1969 Civil Engineering Materials Conference Part 2, edited by M. Te'eni, Wiley-Interscience, New York, 1969.
5. Wu, E. M., "Failure Criteria to Fracture Mode Analysis of Composite Laminates," Advisory Group for Aerospace Research and Development Conference Proceedings, AGARD-CP-163, North Atlantic Treaty Organization, 1974.
6. Lo, K. H., Wu, E. M., and Konishi, D. Y., "Failure Strength of Notched Composite Laminates," Journal of Composite Materials, Vol. 17, September 1983, pp. 384-398.
7. Sih, G. C., and Chen, E. P., Mechanics of Fracture, Vol. 6, Martinus Nijhoff Publishers, The Hague, 1981.
8. Goree, J. G., and Jones, W. F., "Fracture Behavior of Unidirectional Boron/Aluminum Composite Laminates," NASA Contractor Report 3753, December 1983.
9. Buczek, M. B., and Herakovich, C. T., "Finite Element Models for Predicting Crack Growth Characteristics in Composite Materials," VPI-E-82-29, College of Engineering, Virginia Polytechnic Institute and State University, Blacksburg, Virginia, 1982.
10. Buczek, M. B., and Herakovich, C. T., "Direction of Crack Growth in Fibrous Composites," Mechanics of Composite Materials 1983, AMD-Vol. 58, edited by G. J. Dvorak, American Society of Mechanical Engineers, New York, 1983.
11. Tsai, S. W., and Wu, E. M., "A General Theory of Strength for Anisotropic Materials," Journal of Composite Materials, Vol. 5, January 1971, pp. 58-80.

12. Sih, G. C., "A Special Theory of Crack Propagation," Method of Analysis and Solutions to Crack Problems, edited by G. C. Sih, Wolters-Noordhoff, 1972.
13. Lekhnitskii, S. G., Theory of Elasticity of an Anisotropic Elastic Body, English translation by Brandstatton, Holden-Day Inc., San Francisco, 1963.
14. Wu, E. M., "Fracture Mechanics of Anisotropic Plates," Composite Materials Workshop, edited by S. W. Tsai, J. C. Halpin and N. J. Pagano, Technomic Press, Stamford, Conn., 1968.
15. Savin, G. N., Stress Concentration Around Holes, Pergamon Press, New York, 1961.
16. Barsoum, R. S., "Triangular Quarter-Point Elements as Elastic and Perfectly-Plastic Crack Tip Elements," International Journal for Numerical Methods in Engineering, Vol. 11, 1977, pp. 85-98.
17. Freese, C. E., and Tracey, D. M., "The Natural Isoparametric Triangle Versus Collapsed Quadrilateral for Elastic Crack Analysis," International Journal of Fracture, Vol. 12, 1976, pp. 767-771.
18. Henshell, R. D., and Shaw, K. G., "Crack Tip Finite Elements are Unnecessary," International Journal for Numerical Methods in Engineering, Vol. 9, 1975, pp. 495-507.
19. Hilton, P. D., and Sih, G. C., Mechanics of Fracture, Vol. 1, edited by G. C. Sih, Noordhoff International Publishing, Leyden, The Netherlands, 1973, pp. 427-483.
20. Reddy, J. N., An Introduction to the Finite Element Method, McGraw-Hill Book Company, New York, 1984.
21. Bathe, K. J., Finite Element Procedures in Engineering Analysis, Prentice-Hall, Inc., Englewood Cliffs, NJ, 1982.
22. Cook, R. D., Concepts and Applications of Finite Element Analysis, Second Edition, John Wiley and Sons, New York, 1981.
23. Barsoum, R. S., "On the Use of Isoparametric Finite Elements in Linear Fracture," International Journal for Numerical Methods in Engineering, Vol. 10, 1976, pp. 25-37.
24. Hertzberg, R. W., Deformation and Fracture Mechanics of Engineering Materials, John Wiley and Sons, New York, 1976.
25. Smith, D. G., and Mullinix, B. R., "Fracture Mechanics Design Handbook for Composite Materials," U.S. Army Missile Command, Redstone Arsenal, Alabama, Technical Report T-78-6, September, 1977.
26. Herakovich, C. T., Gregory, M. A., and Beuth, J. L., Jr., "Crack Growth Direction in Unidirectional Off-Axis Graphite-Epoxy," European Mechanics Colloquium 182, "Mechanical Characterization of Load Bearing Fibre Composite Laminates," Brussels, August, 1984.

APPENDIX A

1-2 Coordinate System

$$f(\sigma_i) = F_1\sigma_1 + F_2\sigma_2 + F_{11}\sigma_1^2 + F_{22}\sigma_2^2 + 2F_{12}\sigma_1\sigma_2 + F_{66}\sigma_6^2$$

Mathematical Expressions for the Strength Tensor Terms as a

Function of Measured Strengths

$$F_1 = (1/S_T + 1/X_C)$$

$$F_2 = (1/Y_T + 1/Y_C)$$

$$F_{11} = -1/(X_T X_C)$$

$$F_{22} = -1/(Y_T Y_C)$$

$$F_{66} = 1/(S^2)$$

X-Y Coordinate System

$$f(\sigma_i) = F_x\sigma_x + F_y\sigma_y + F_S\tau_{xy} + F_{xx}\sigma_x^2 + F_{yy}\sigma_y^2 + F_{SS}\tau_{xy}^2 \\ + 2F_{xy}\sigma_x\sigma_y + 2F_{xS}\sigma_x\tau_{xy} + 2F_{yS}\sigma_y\tau_{xy}$$

Transformation of Strength Tensor Terms

$$F_x = m^2F_1 + n^2F_2$$

$$F_y = n^2F_1 + m^2F_2$$

$$F_S = 2mnF_1 - 2mnF_2$$

$$F_{xx} = (m^4F_{11} + n^4F_{22} + 2m^2n^2F_{12} + m^2n^2F_{66})$$

$$F_{yy} = (n^4F_{11} + m^4F_{22} + 2m^2n^2F_{12} + m^2n^2F_{66})$$

$$F_{SS} = (4m^2n^2F_{11} + 4m^2n^2F_{22} - 8m^2n^2F_{12} + (m^2 - n^2)^2F_{66})$$

$$F_{xy} = (m^2n^2F_{11} + m^2n^2F_{22} + (m^4 + n^4)F_{12} - m^2n^2F_{66})$$

$$F_{xS} = (2m^3nF_{11} - 2mn^3F_{22} + 2(mn^3 - m^3n)F_{12} + (mn^3 - m^3n)F_{66})$$

$$F_{yS} = (2mn^3F_{11} - 2m^3nF_{22} + 2(m^3n - mn^3)F_{12} + (m^3n - mn^3)F_{66})$$

where $m = \cos \theta$ and $n = \sin \theta$.

APPENDIX B

To provide a better understanding of singular isoparametric finite elements, the form of the singularity along the line 1-2 ($s = 0$) in Fig. B.1 will be calculated.

For a six noded isoparametric triangular element, the following relations hold:

$$x = \sum_{i=1}^n h_i(r,s) x_i \quad (1)$$

$$u = \sum_{i=1}^n h_i(r,s) u_i \quad (2)$$

where

h_i is the shape function for the i^{th} node

x_i is the x-coordinate of the i^{th} node

u_i is the x-direction displacement of the i^{th} node

x is the x-coordinate mapping function

u is the x-direction displacement interpolation function

Evaluation of the shape functions, along the line 1-2 ($s = 0$), considering nodes 1, 2 and 4 only yields:

$$h_1 = 1 - 3r + 2r^2$$

$$h_2 = -r + 2r^2$$

$$h_4 = 4r - 4r^2$$

Substitution of these shape functions into Eq. 1 yields:

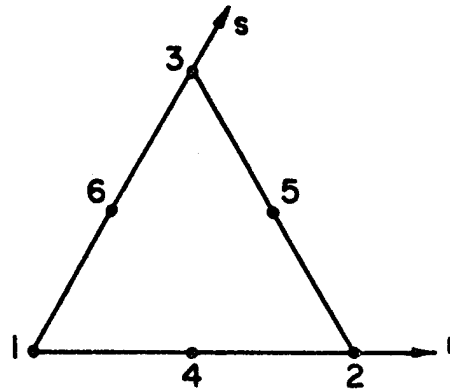
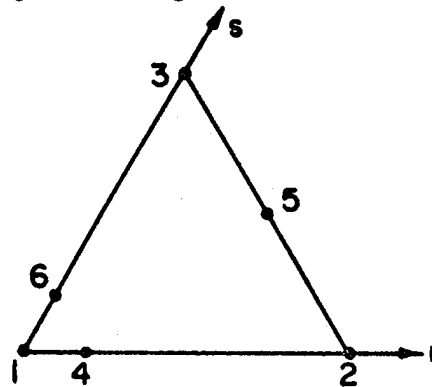
Conventional Triangular Element**Singular Triangular Element**

Fig. B.1 Node Locations in Conventional and Singular Isoparametric Triangular Elements.

$$x = (1-3r+2r^2)x_1 + (-r+2r^2)x_2 + (4r-4r^2)x_4 \quad (3)$$

Choosing for the singular configuration, $x_1 = 0$, $x_2 = L$ and $x_4 = L/4$ substitution into Eq. 3 yields:

$$x = (-r+2r^2)L + (4r-4r^2)\frac{L}{4} \quad (4)$$

simplifying,

$$x = r^2L$$

Rearranging Eq. 5, an expression for r in terms of x is obtained.

$$r = \sqrt{\frac{x}{L}} \quad (6)$$

An expression for u along the line 1-2 is:

$$u = (1-3r+2r^2)u_1 + (-r+2r^2)u_2 + (4r-4r^2)u_3 \quad (7)$$

Substitution of Eq. 6 into Eq. 7 yields:

$$u = (1-3\sqrt{\frac{x}{L}} + 2\frac{x}{L})u_1 + (-\sqrt{\frac{x}{L}} + 2\sqrt{\frac{x}{L}})u_2 + (4\sqrt{\frac{x}{L}} - 4\frac{x}{L})u_3 \quad (8)$$

The strain in the x -direction is then;

$$\epsilon_x = \frac{\partial u}{\partial x} = \left(\frac{2}{L} - \frac{3}{2\sqrt{xL}}\right)u_1 + \left(\frac{2}{L} - \frac{1}{2\sqrt{xL}}\right)u_2 + \left(\frac{2}{\sqrt{xL}} - \frac{4}{L}\right)u_3 \quad (9)$$

Analysis of Eq. 9 reveals that the strain singularity along the line 1-2 is of the order $\frac{1}{\sqrt{r}}$, which is the required singularity for fracture mechanics applications.

APPENDIX C

The following figures show the distribution in the stress components as a function of ϕ for the seven gauss points. This information is included to give a better understanding of the stress field distribution through the element. The problem under consideration is a center cracked AS4/3501-6 plate ($\theta = 90^\circ$, $2a = 0.5''$) subjected to a far field stress $\bar{\sigma}_y$ of 1.0 KSI.

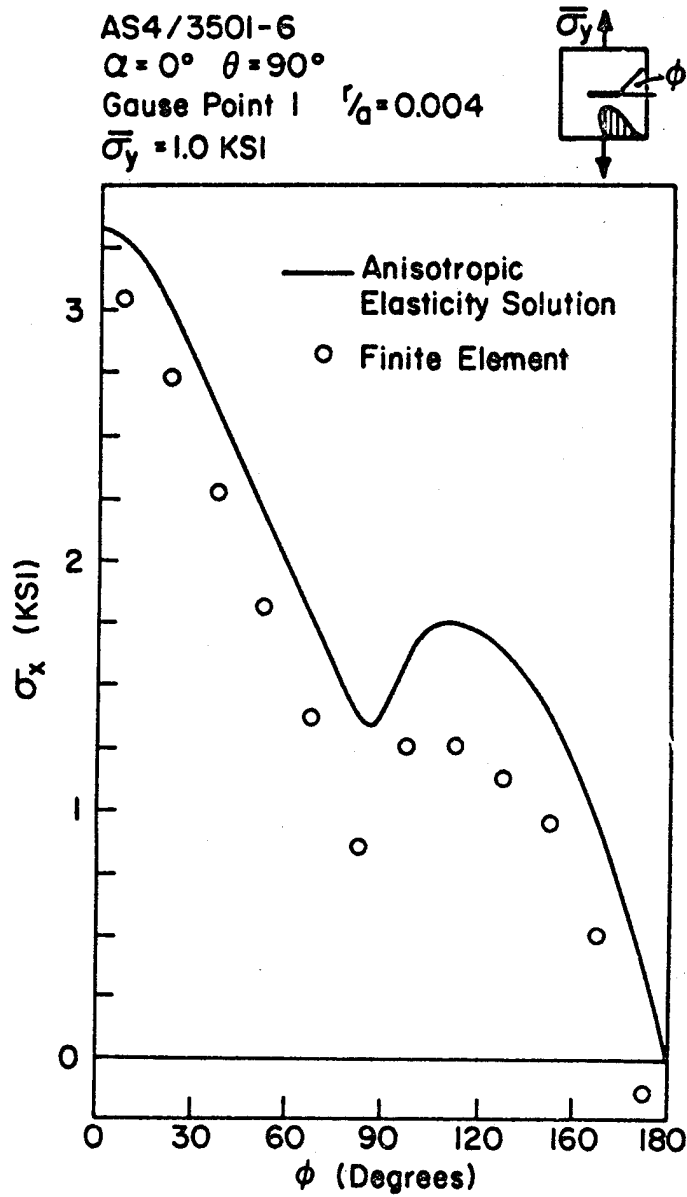


Fig. C.1 σ_x vs. ϕ at Gauss Point 1 for a Center Cracked Graphite/Epoxy Plate.

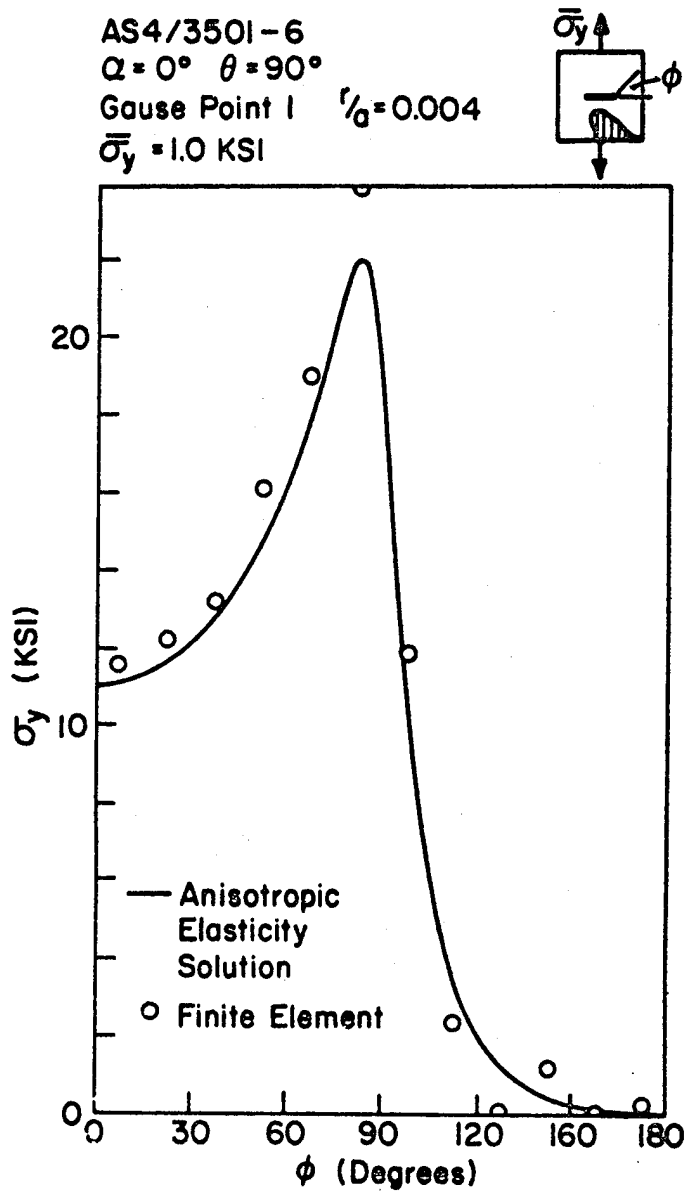


Fig. C.2 σ_y vs. ϕ at Gauss Point 1 for a Center Cracked Graphite/Epoxy Plate.

AS4/3501-6
 $\alpha = 0^\circ \quad \theta = 90^\circ$
 Gauss Point 1 $r/a = 0.004$
 $\bar{\sigma}_y = 1.0 \text{ KSI}$

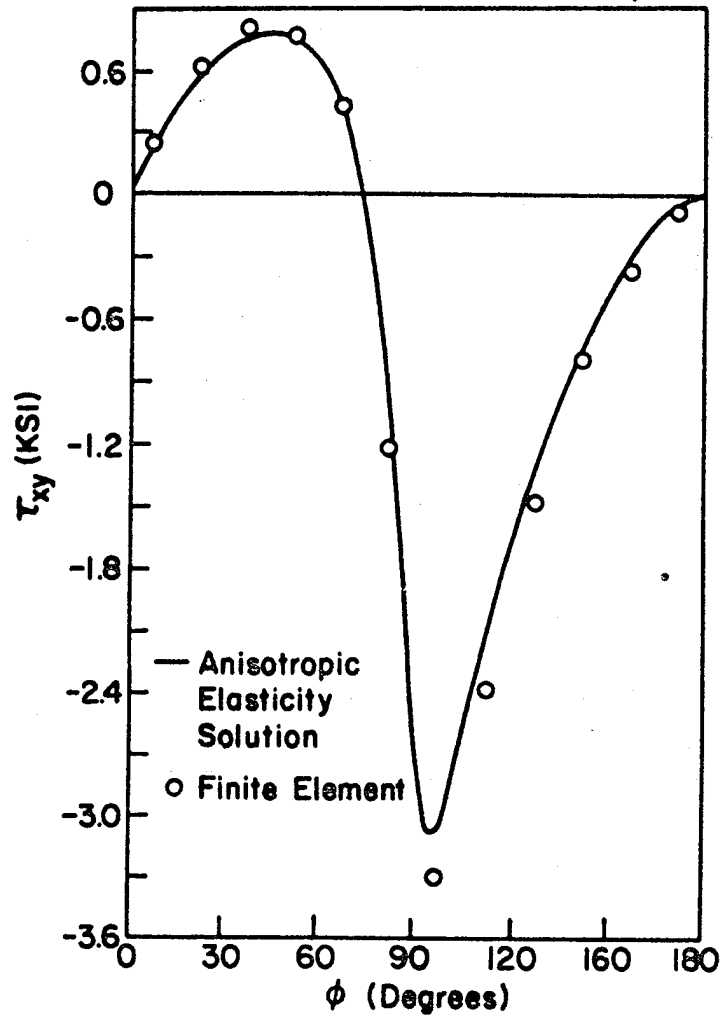
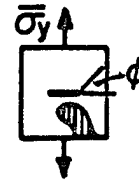


Fig. C.3 τ_{xy} vs. ϕ at Gauss Point 1 for a Center Cracked Graphite/Epoxy Plate.

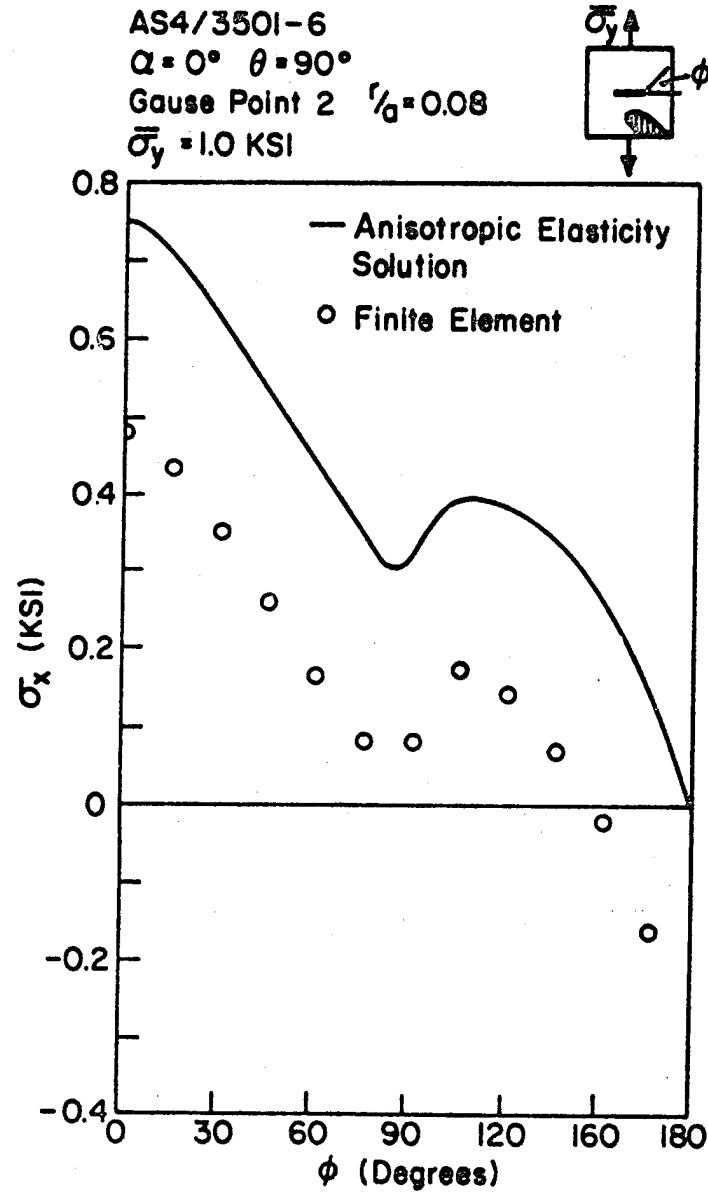


Fig. C.4 σ_x vs. ϕ at Gauss Point 2 for a Center Cracked Graphite/Epoxy Plate.

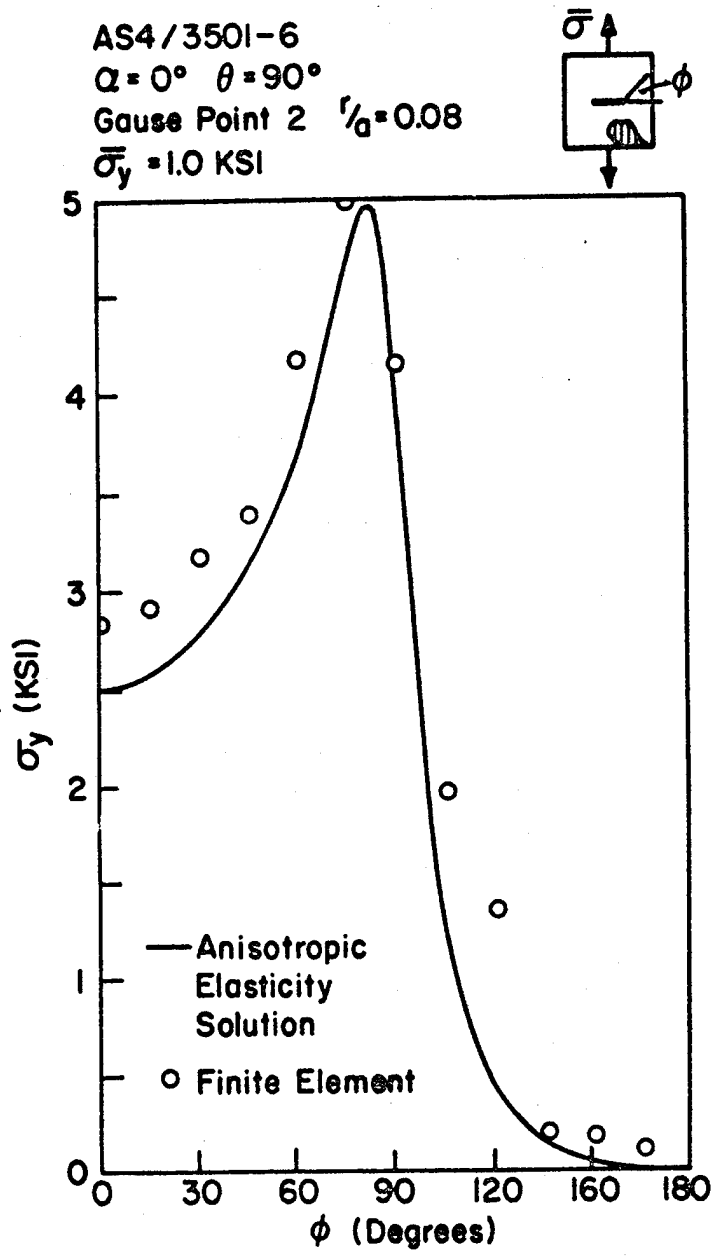


Fig. C.5 σ_y vs. ϕ at Gauss Point 2 for a Center Cracked Graphite/Epoxy Plate.

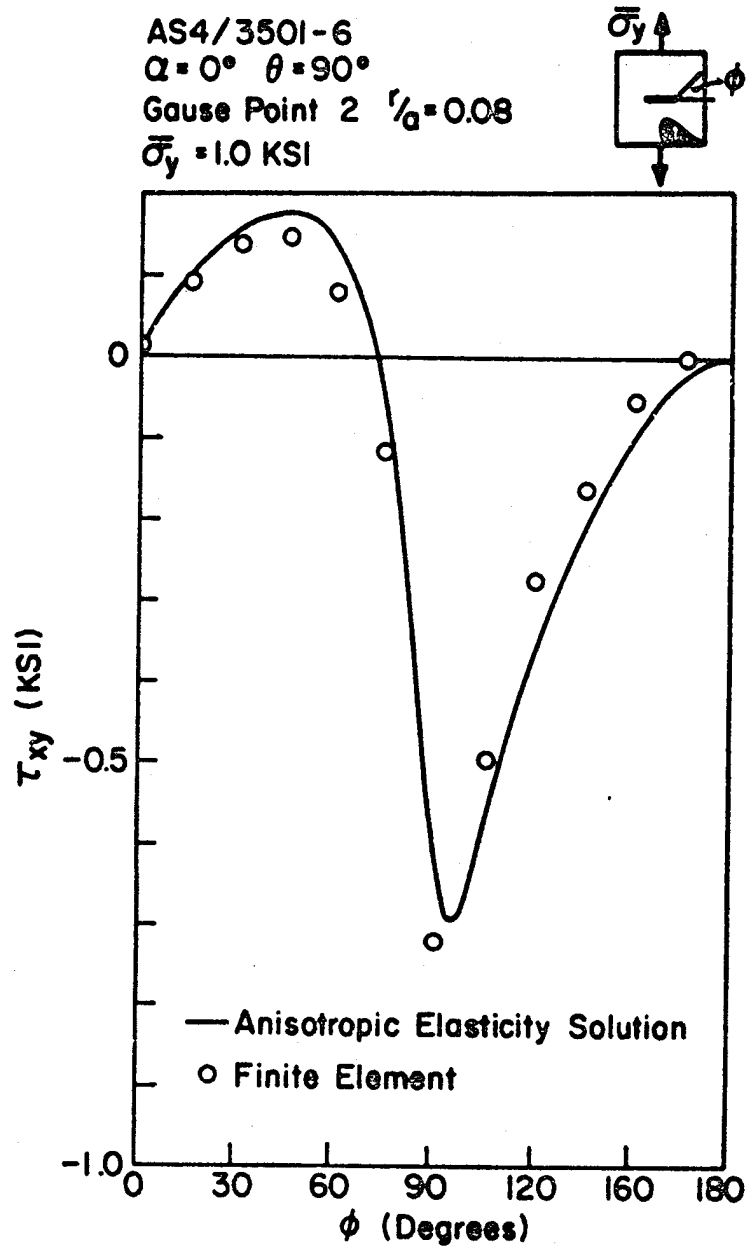


Fig. C.6 τ_{xy} vs. ϕ at Gauss Point 2 for a Center Cracked Graphite/Epoxy Plate.

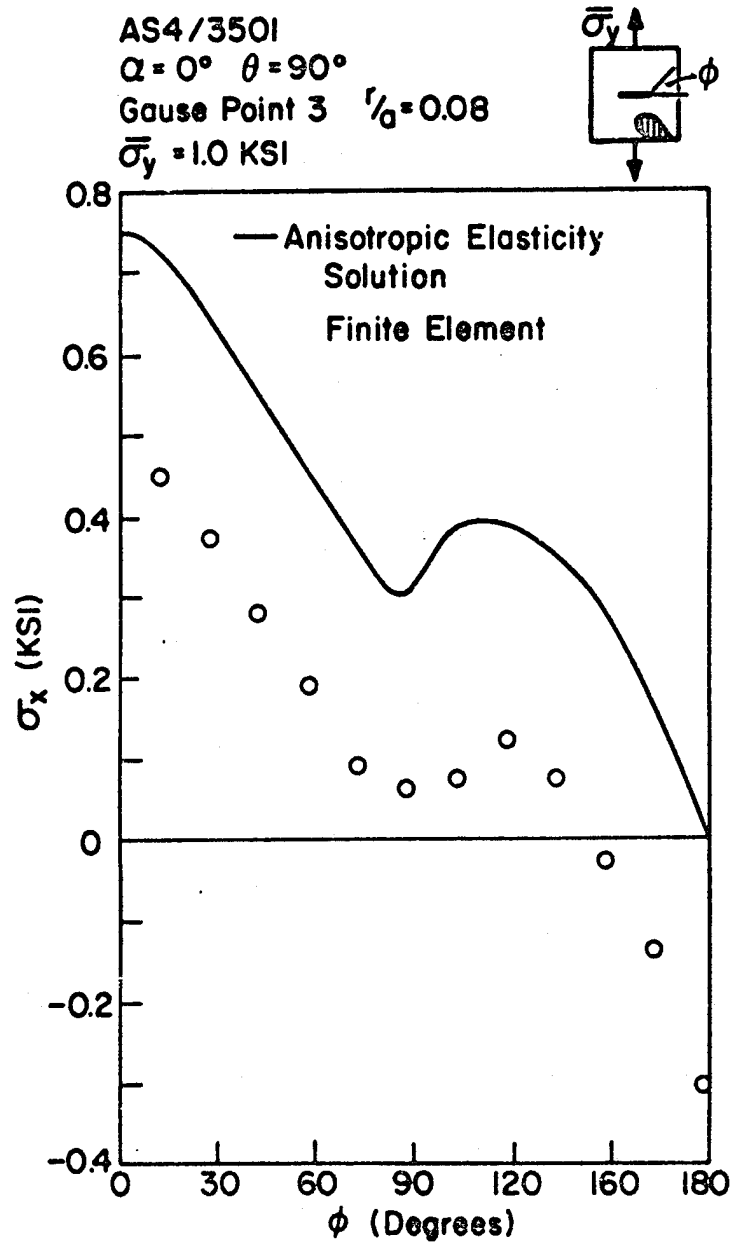


Fig. C.7 σ_x vs. ϕ at Gauss Point 3 for a Center Cracked Graphite/Epoxy Plate.

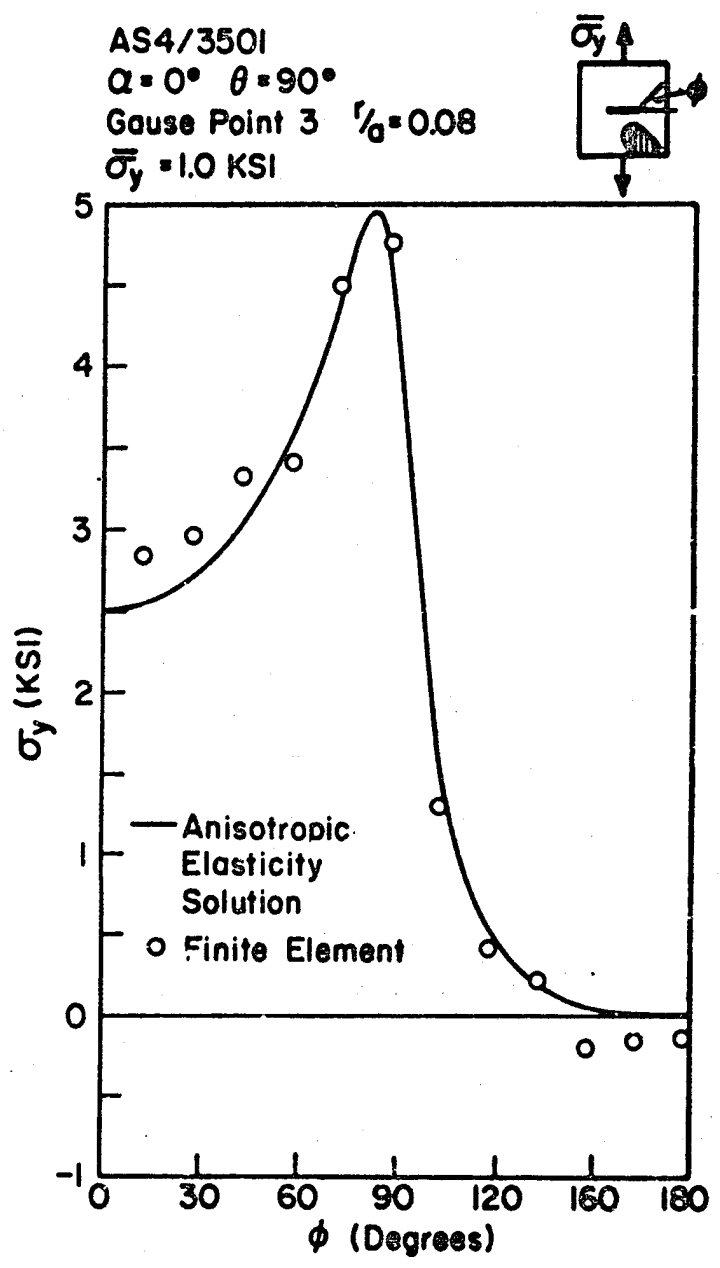


Fig. C.8 σ_y vs. ϕ at Gauss Point 3 for a Center Cracked Graphite/Epoxy Plate.

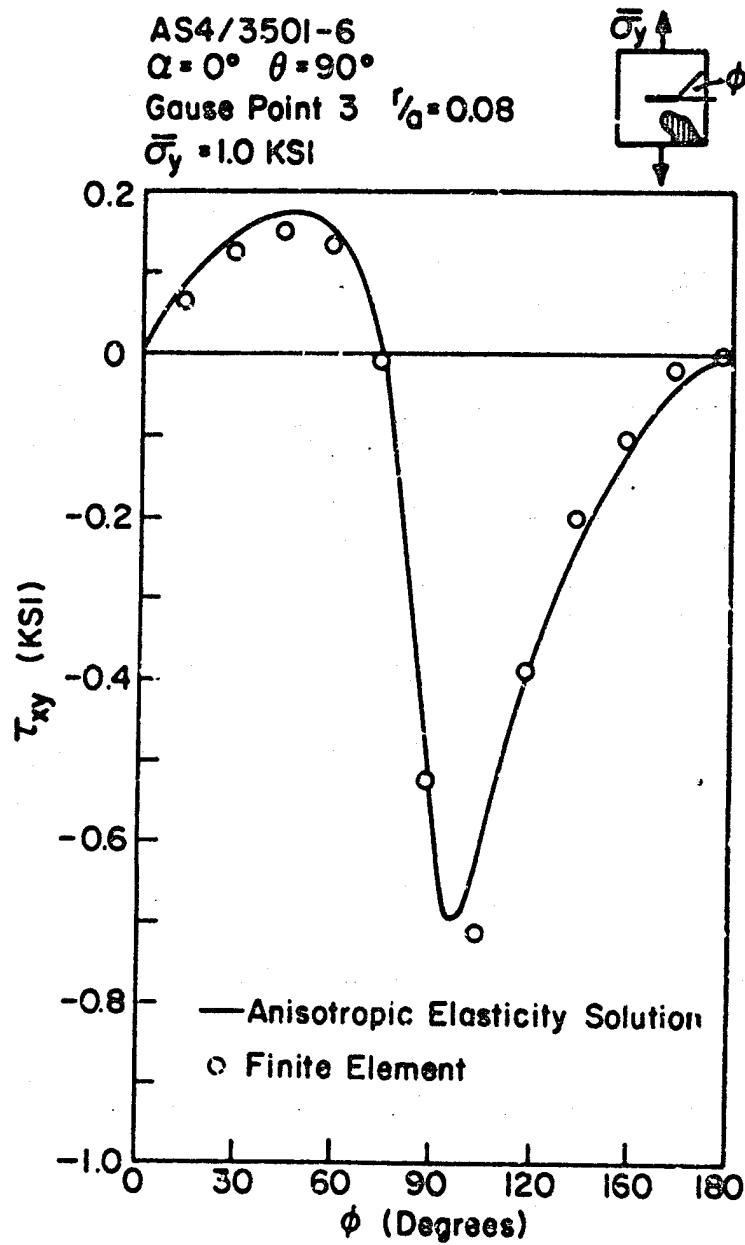


Fig. C.9 τ_{xy} vs. ϕ at Gauss Point 3 for a Center Cracked Graphite/Epoxy Plate.

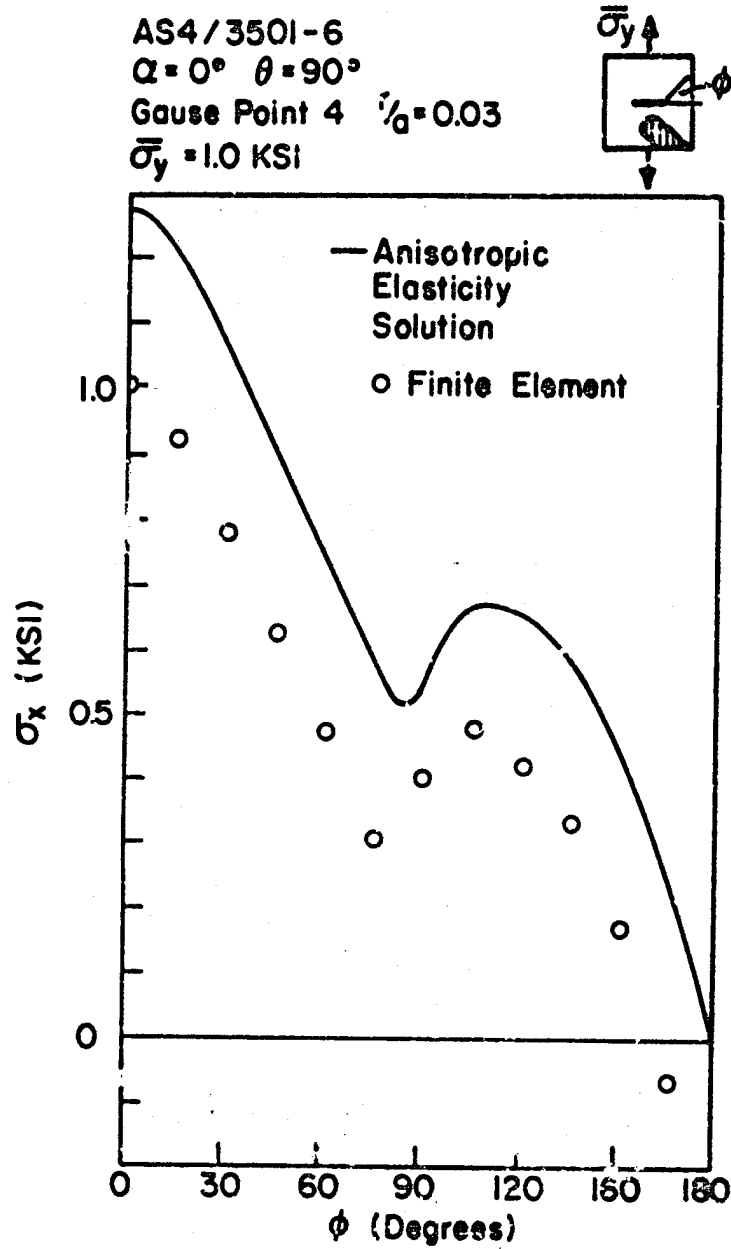


Fig. C.10 σ_x vs. ϕ at Gauss Point 4 for a Center Cracked Graphite/Epoxy Plate.

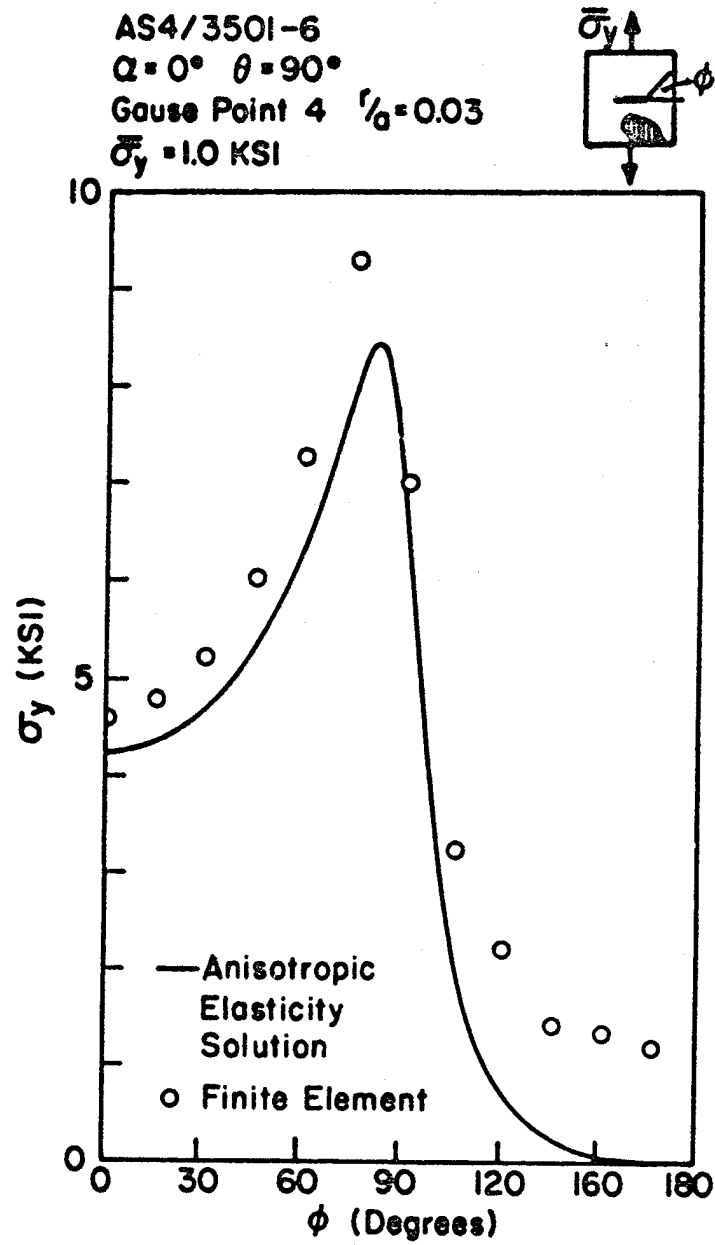


Fig. C.11 σ_y vs. ϕ at Gauss Point 4 for a Center Cracked Graphite/Epoxy Plate.

AS4/3501-6
 $\alpha = 0^\circ \quad \theta = 90^\circ$
 Gauss Point 4 $r/a = 0.03$
 $\bar{\sigma}_y = 1.0 \text{ KSI}$

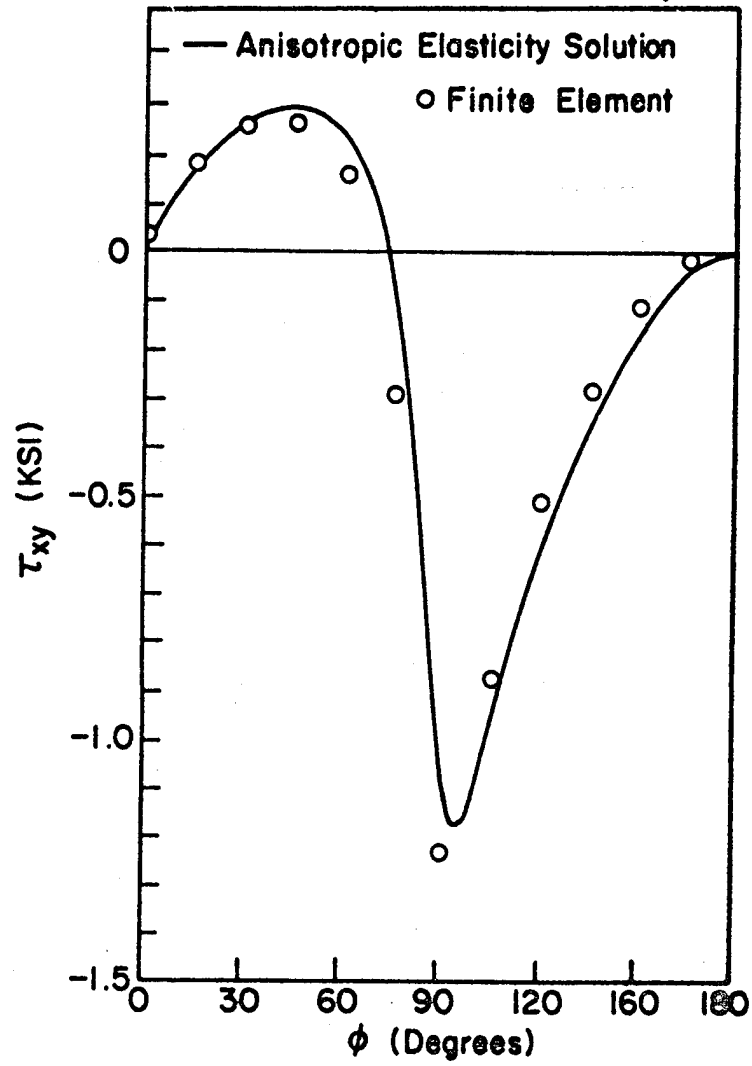
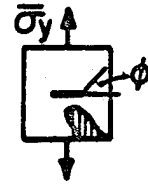


Fig. C.12 τ_{xy} vs. ϕ at Gauss Point 4 for a Center Cracked Graphite/Epoxy Plate.

AS4/3501-6
 $\alpha = 0^\circ \quad \theta = 90^\circ$
 Gause Point 5 $r/a = 0.09$
 $\bar{\sigma}_y = 1.0 \text{ KSI}$

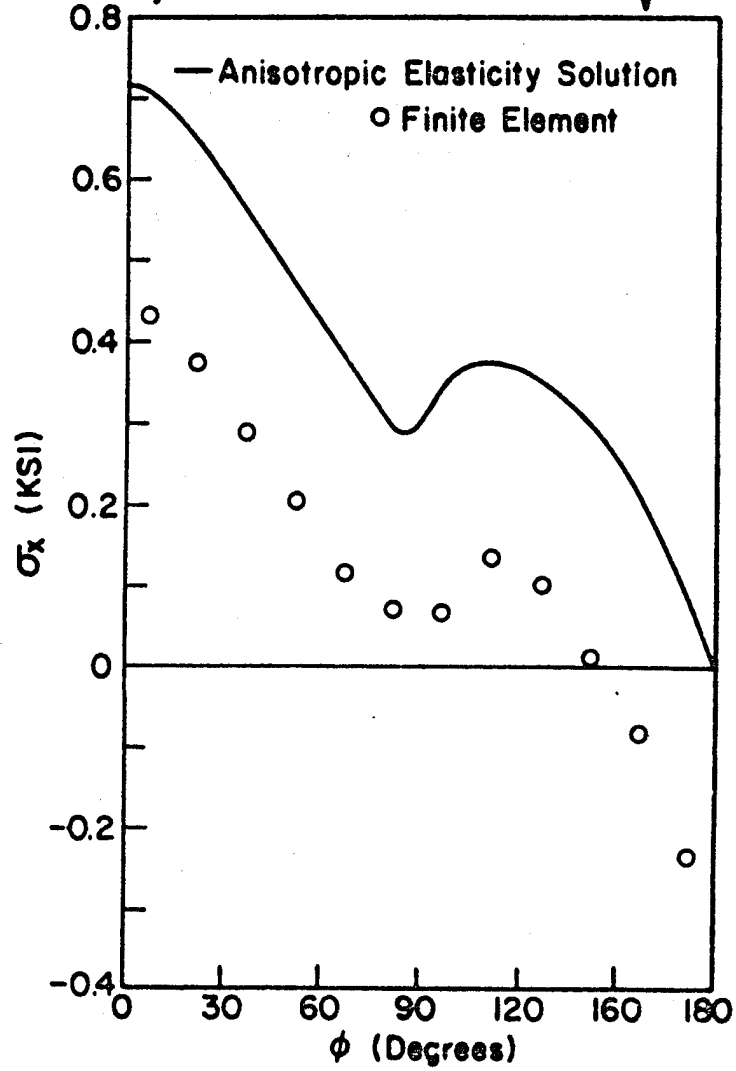
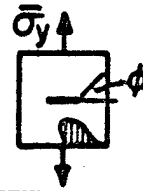


Fig. C.13 σ_x vs. ϕ at Gauss Point 5 for a Center Cracked Graphite/Epoxy Plate.

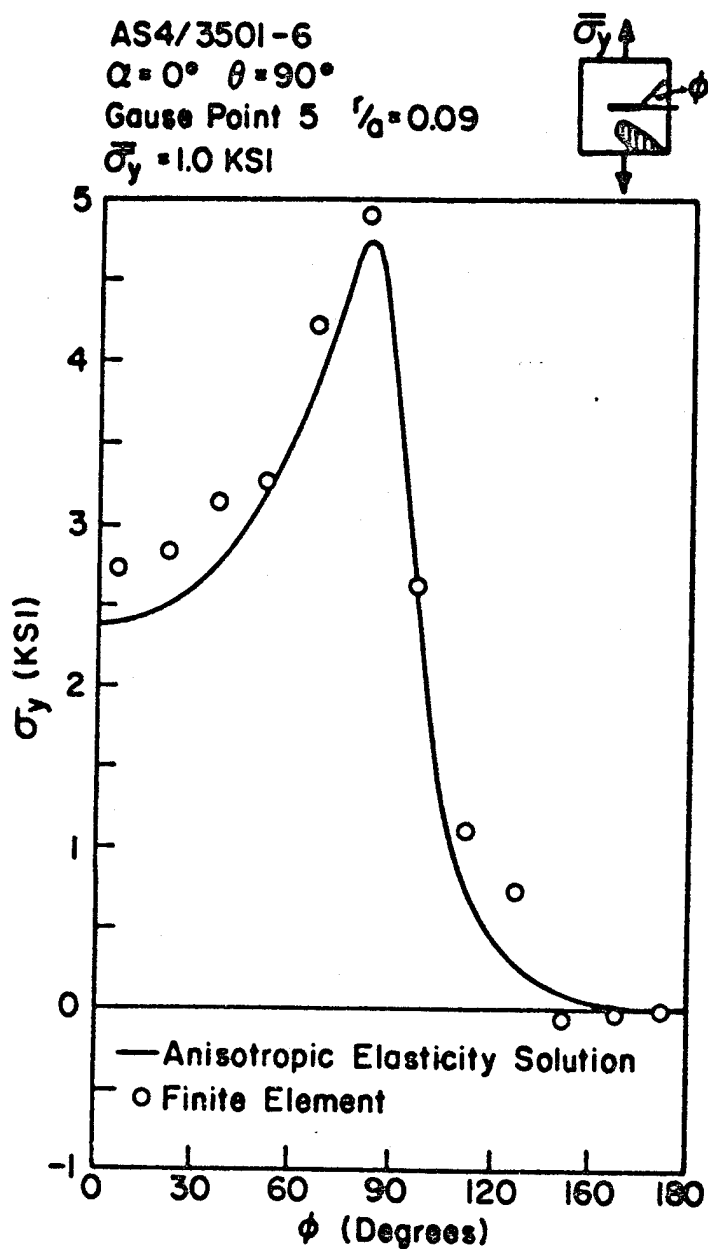


Fig. C.14 σ_y vs. ϕ at Gauss Point 5 for a Center Cracked Graphite/Epoxy Plate.

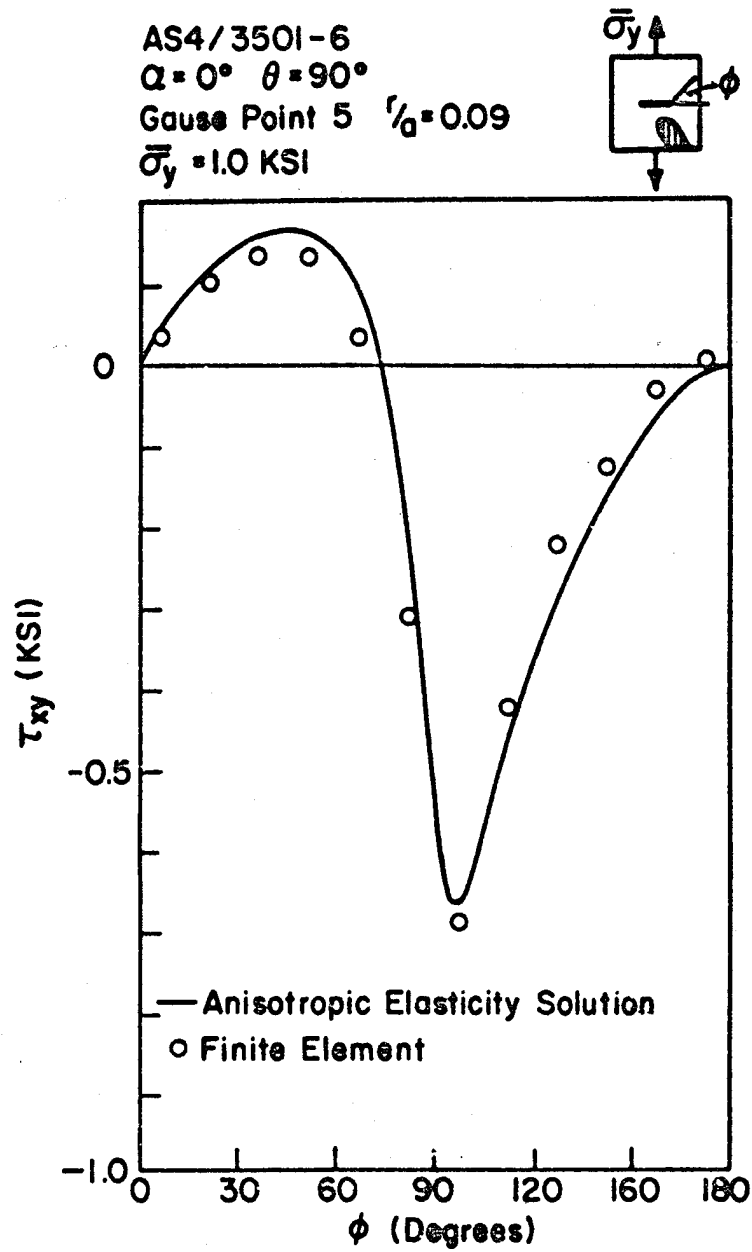


Fig. C.15 τ_{xy} vs. ϕ at Gauss Point 5 for a Center Cracked Graphite/Epoxy Plate.

AS4/3501-6
 $\alpha = 0^\circ \quad \beta = 90^\circ$
 Gauss Point 6 $r/a = 0.03$
 $\bar{\sigma}_y = 1.0 \text{ KSI}$

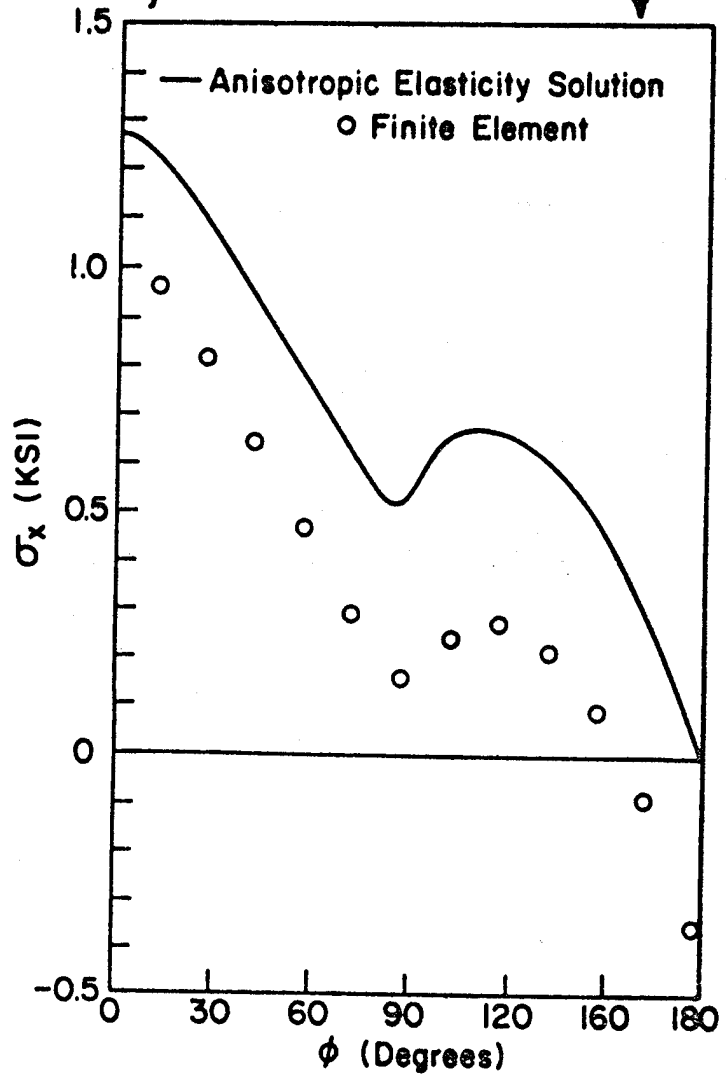
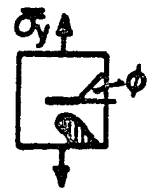


Fig. C.16 σ_x vs. ϕ at Gauss Point 6 for a Center Cracked Graphite/Epoxy Plate.

AS4/3501-6
 $Q = 0^\circ \quad \theta = 90^\circ$
 Gauss Point 6 $r/a = 0.03$
 $\bar{\sigma}_y = 1.0 \text{ KSI}$

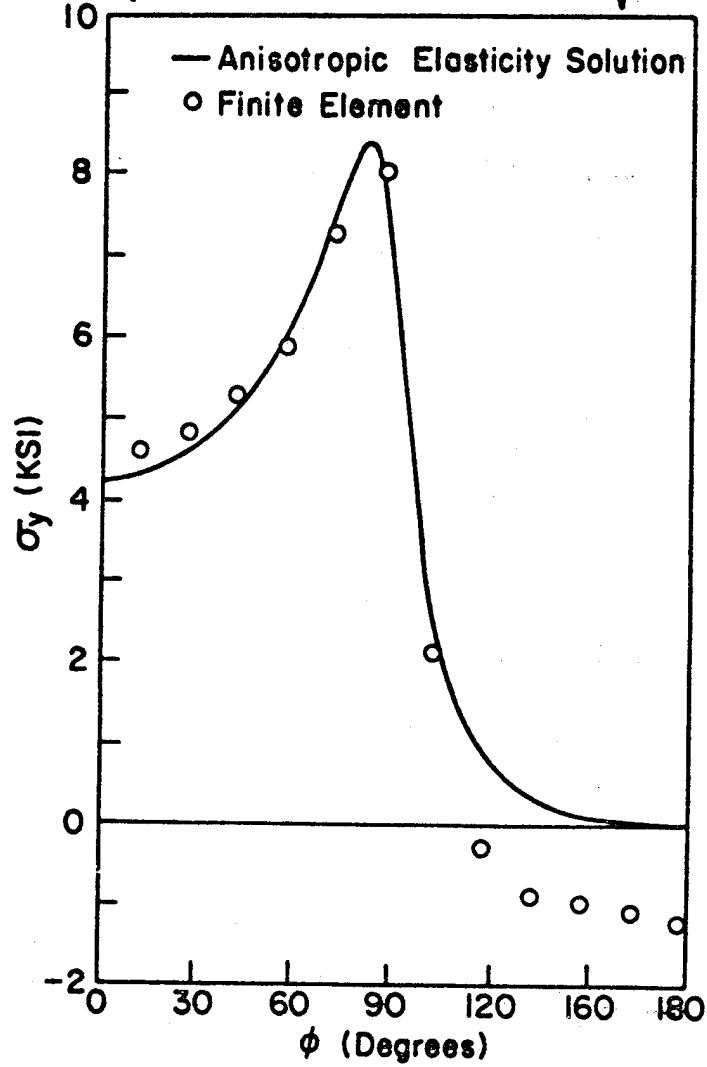
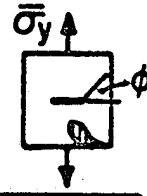


Fig. C.17 σ_y vs. ϕ at Gauss Point 6 for a Center Cracked Graphite/Epoxy Plate.

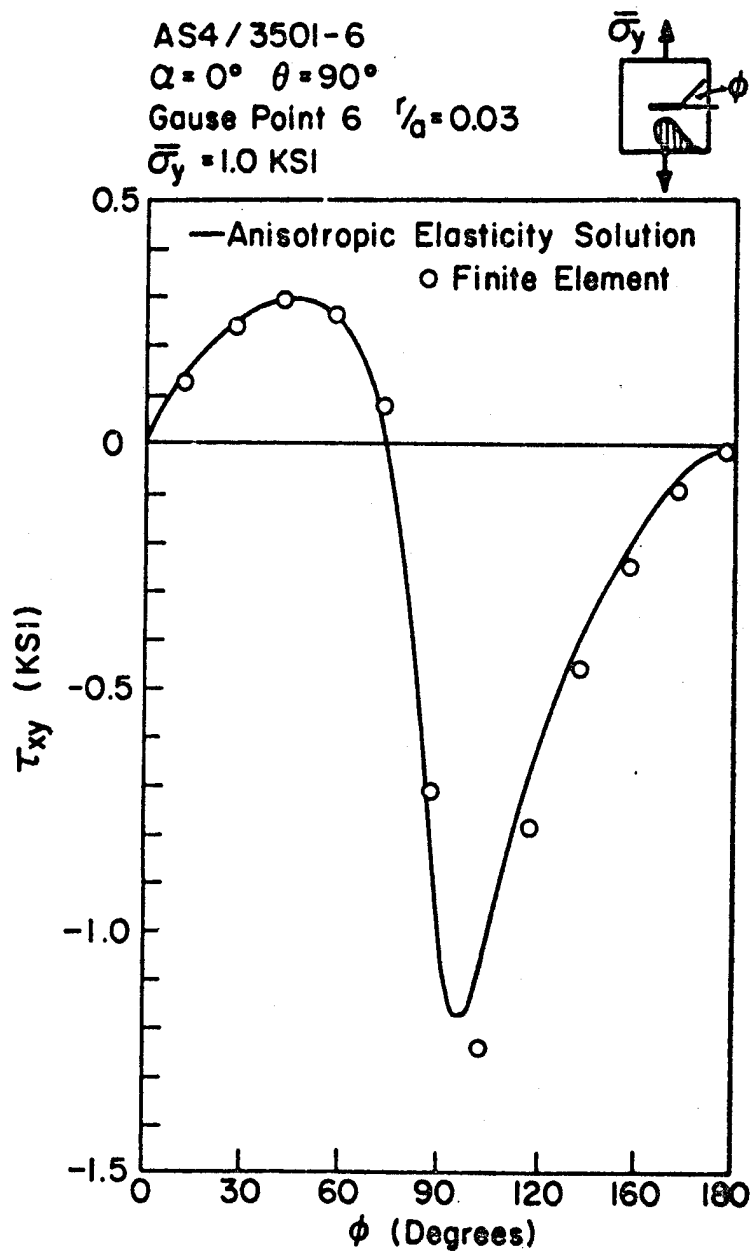


Fig. C.18 τ_{xy} vs. ϕ at Gauss Point 6 for a Center Cracked Graphite/Epoxy Plate.

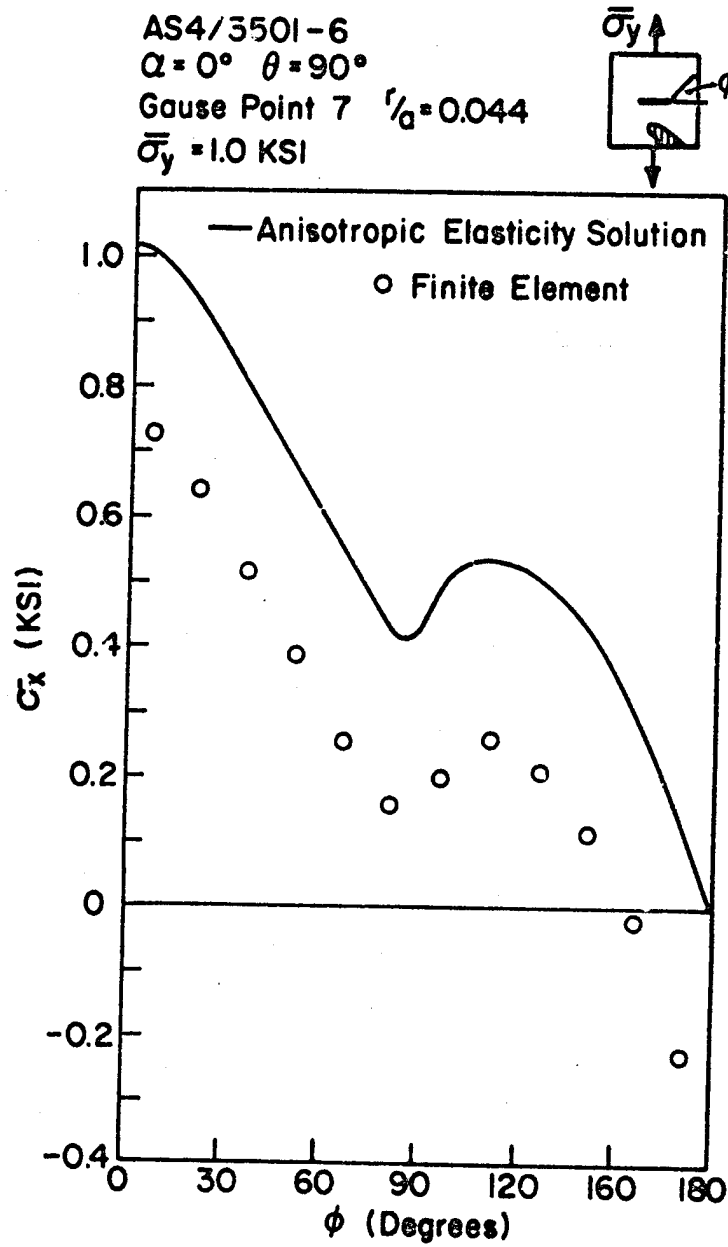
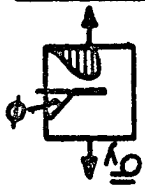
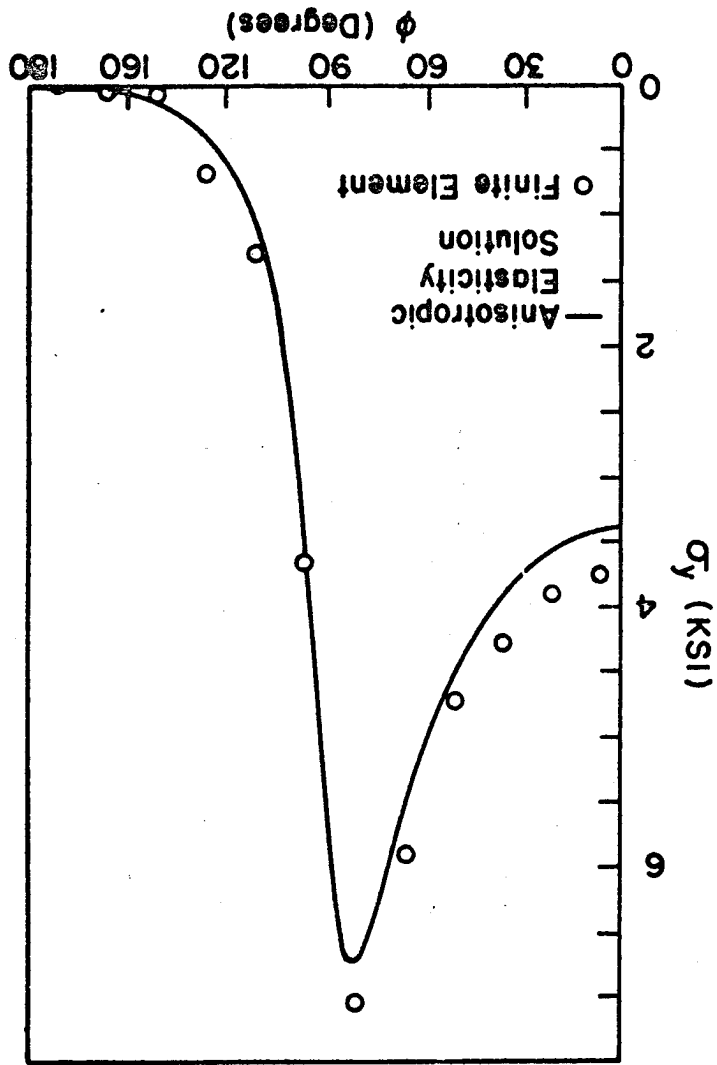


Fig. C.19 σ_x vs. ϕ at Gauss Point 7 for a Center Cracked Graphite/Epoxy Plate.

Fig. C.20 σ_y vs. ϕ at Gauss Point 7 for a Center Cracked Graphite/Epoxy Plate.



AS4/3501-6
 $\alpha = 0^\circ$ $\theta = 90^\circ$
 Gauss Point 7 $r/a = 0.044$
 $\bar{\sigma}_y = 1.0$ KSI

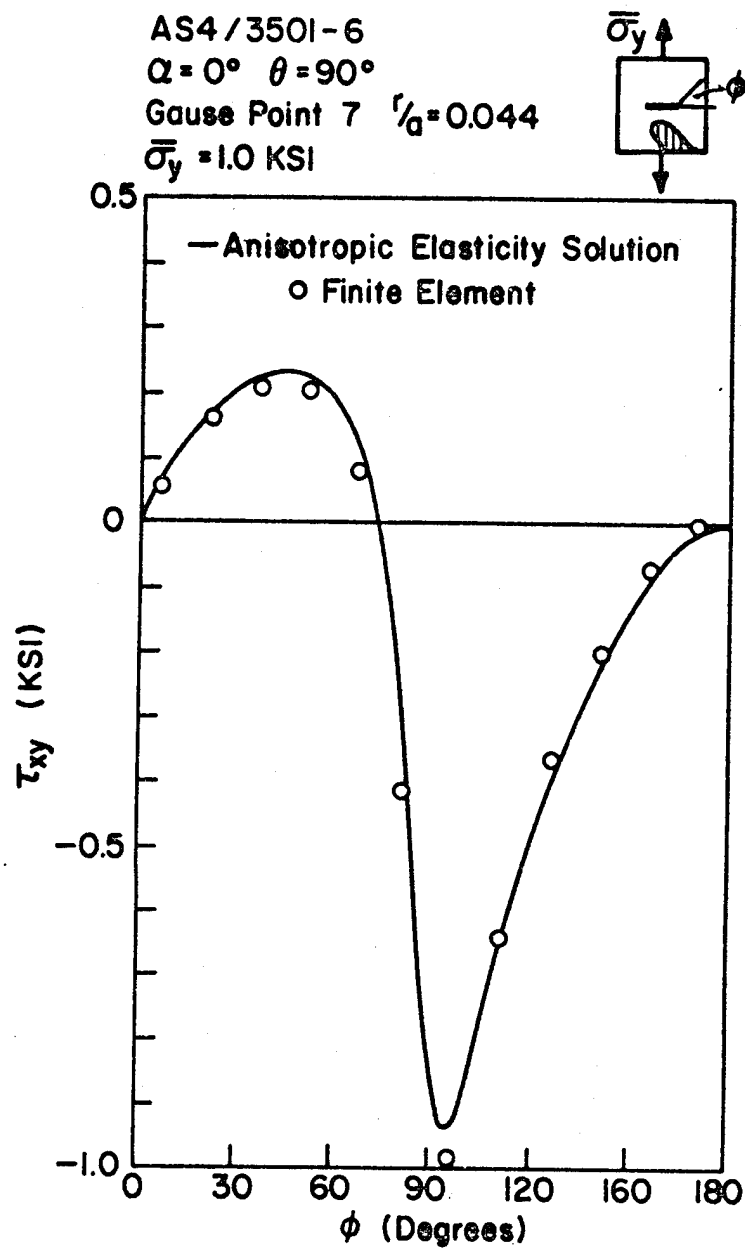


Fig. C.21 τ_{xy} vs. ϕ at Gauss Point 7 for a Center Cracked Graphite/Epoxy Plate.

APPENDIX D

This section is included to provide additional information concerning the prediction of crack extension in unidirectional composites. The figures presented, provide insight into the crack tip stress states and characteristics of the crack extension direction criteria.

T300/5208
 $\alpha = 0^\circ$ $\theta = 120^\circ$
 $r_0 = 0.002$ in
 $\bar{\sigma}_y = 1.0$ KSI

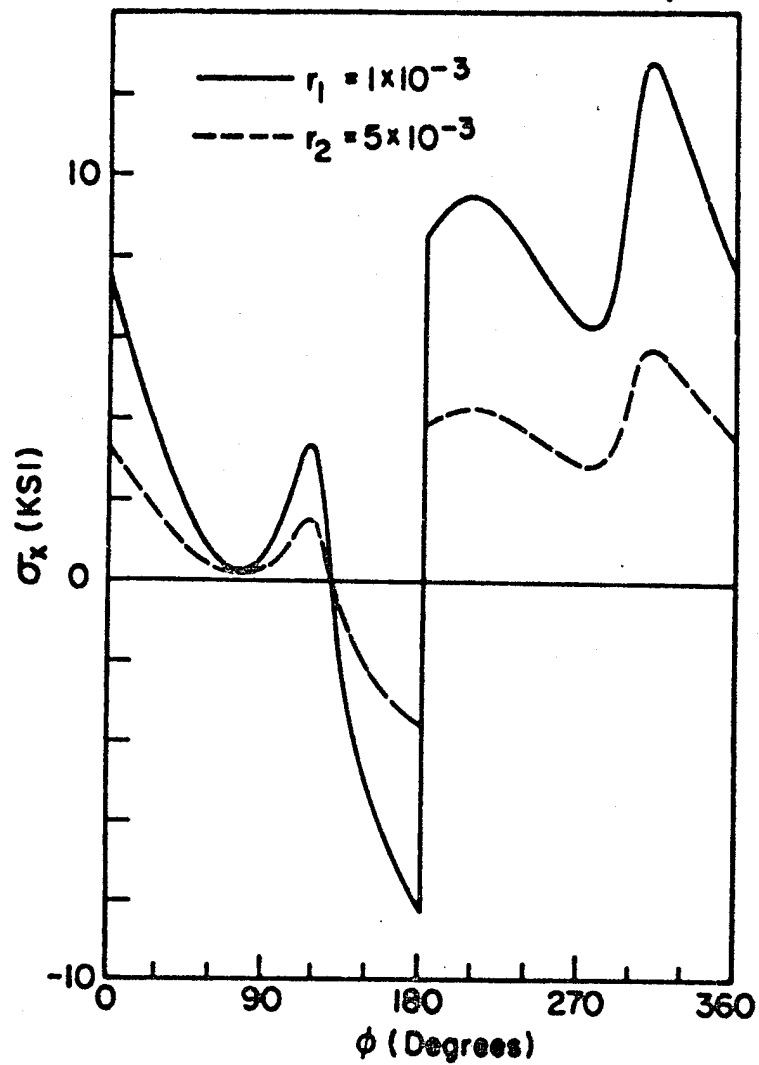


Fig. D.1 Influence of r_0 on the Distribution of σ_x in a Center Cracked Graphite/Epoxy Plate ($\theta = 120^\circ$).

T300/5208
 $\alpha = 0^\circ$ $\theta = 120^\circ$
 $r_0 = 0.002$ in
 $\bar{\sigma}_y = 1.0$ KSI

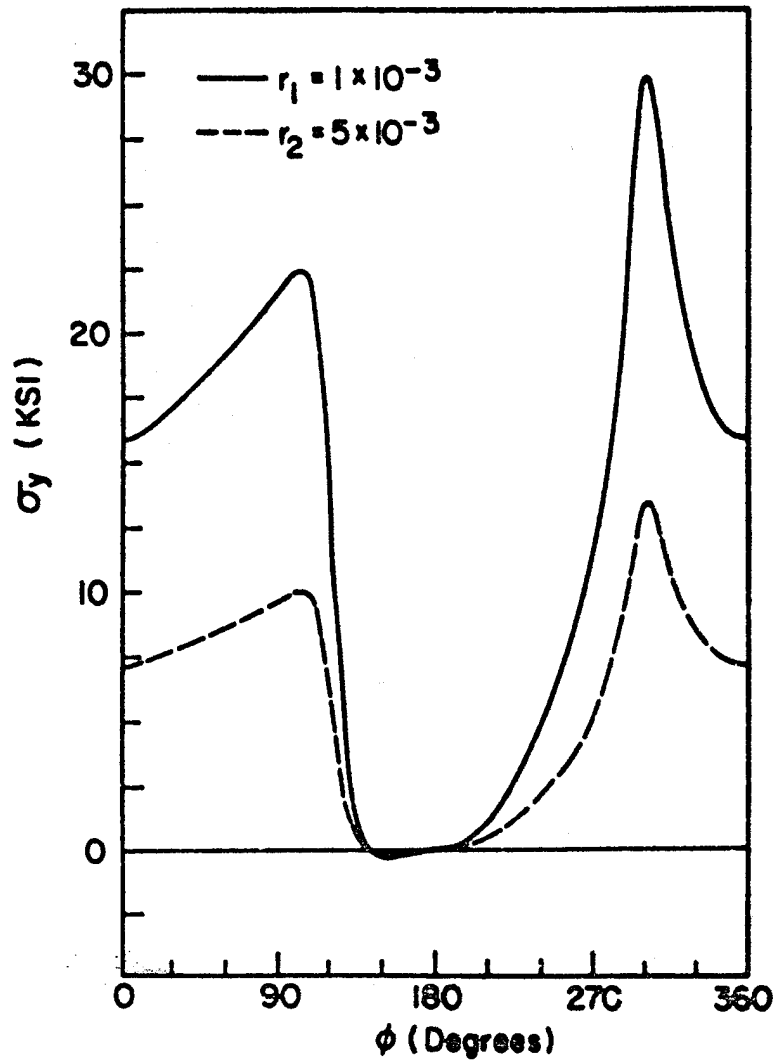


Fig. D.2 Influence of r_0 on the Distribution of σ_y in a Center Cracked Graphite/Epoxy Plate ($\theta = 120^\circ$).

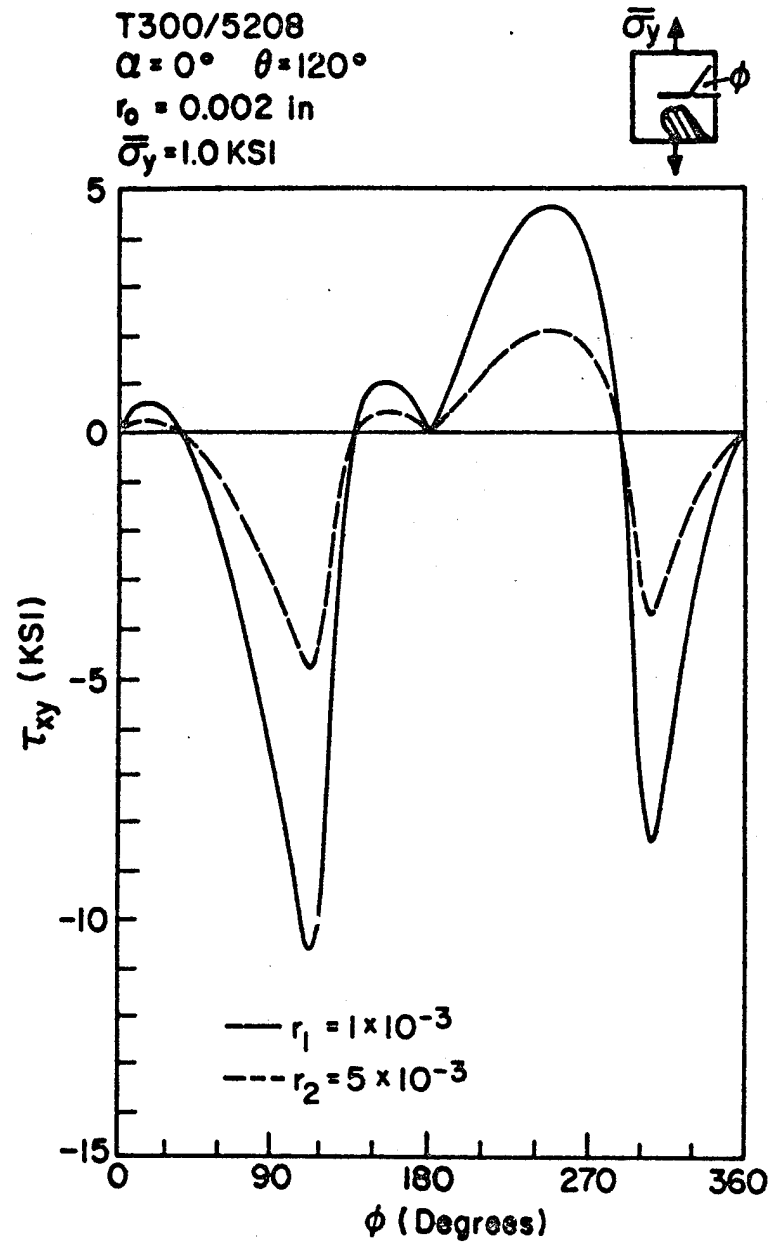


Fig. D.3 Influence of r_0 on the Distribution of τ_{xy} in a Center Cracked Graphite/Epoxy Plate ($\theta = 120^\circ$).

T300/5208
 $\alpha = 0^\circ \quad \theta = 120^\circ$
 $r_0 = 0.002 \text{ in}$
 $\bar{\sigma}_y = 1.0 \text{ KSI}$

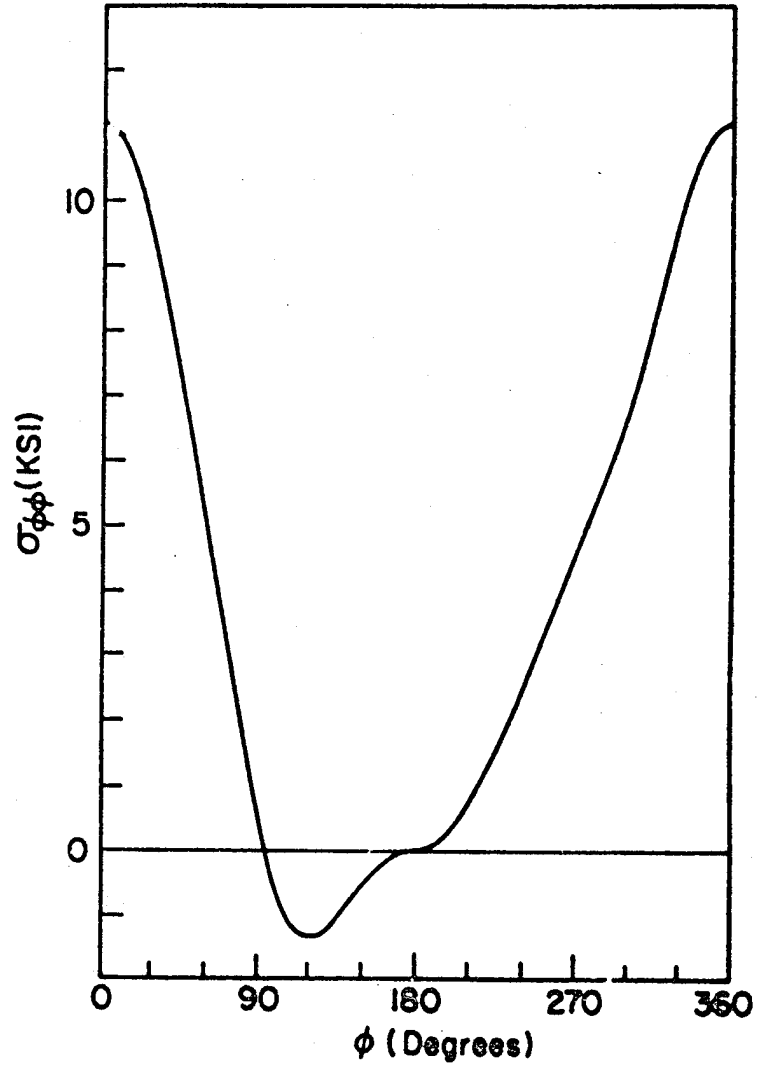
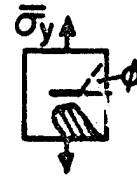


Fig. D.4 $\sigma_{\phi\phi}$ vs. ϕ for a Center Cracked 30° Graphite/Epoxy Plate.

T300/5208
 $\alpha = 0^\circ \quad \theta = 120^\circ$
 $r_0 = 0.002 \text{ in}$
 $\bar{\sigma}_y = 1.0 \text{ KSI}$

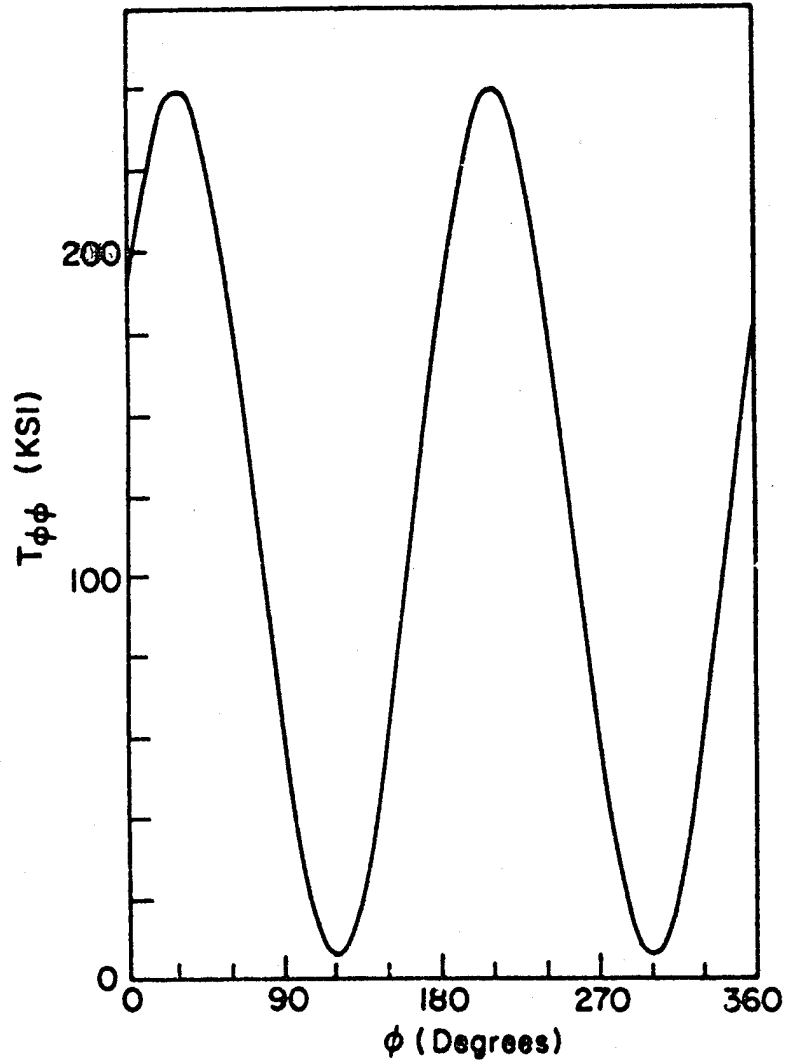
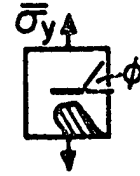


Fig. D.5 T_{ϕ} vs. ϕ for a Center Cracked 30° Graphite/Epoxy Plate.

T300/5208
 $\alpha = 0^\circ \quad \theta = 120^\circ$
 $r_0 = 0.002$ in
 $\bar{\tau}_{xy} = 1.0$ KSI

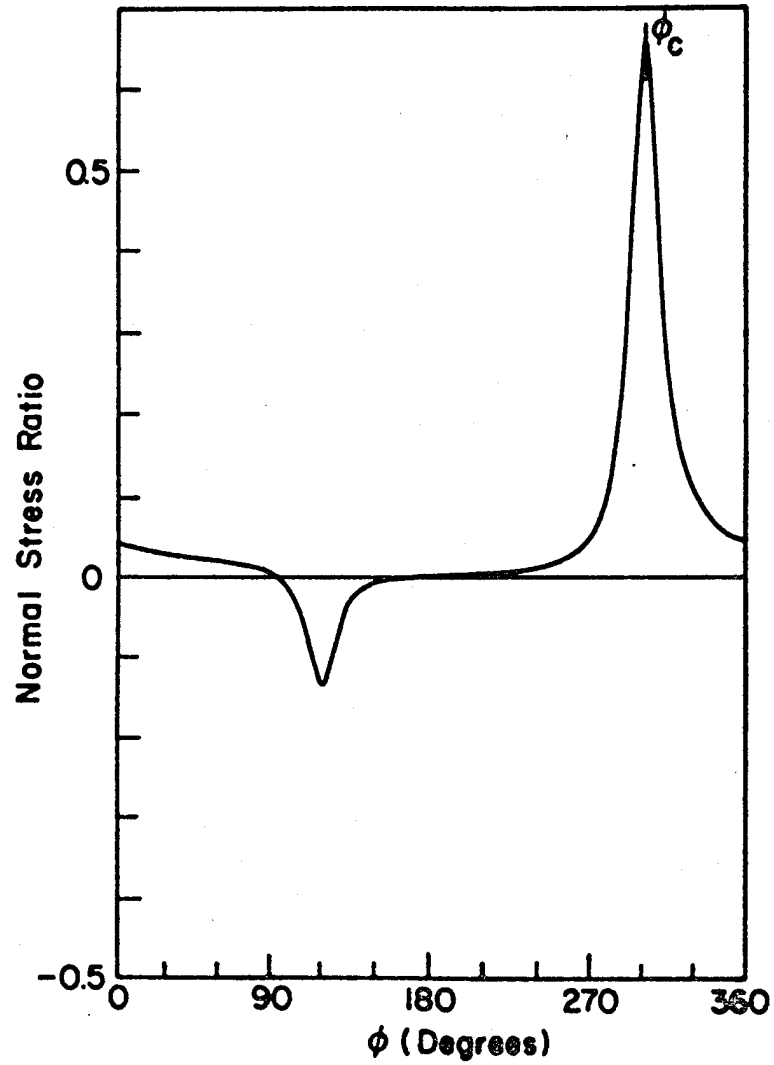


Fig. D.6 Normal Stress Ratio vs. ϕ for a Center Cracked 30° Graphite/Epoxy Plate Under Pure Shear.

T300/5208
 $\alpha = 0^\circ$ $\theta = 120^\circ$
 $r_0 = 0.002$ in
 $\bar{\tau}_{xy} = 1.0$ KSI

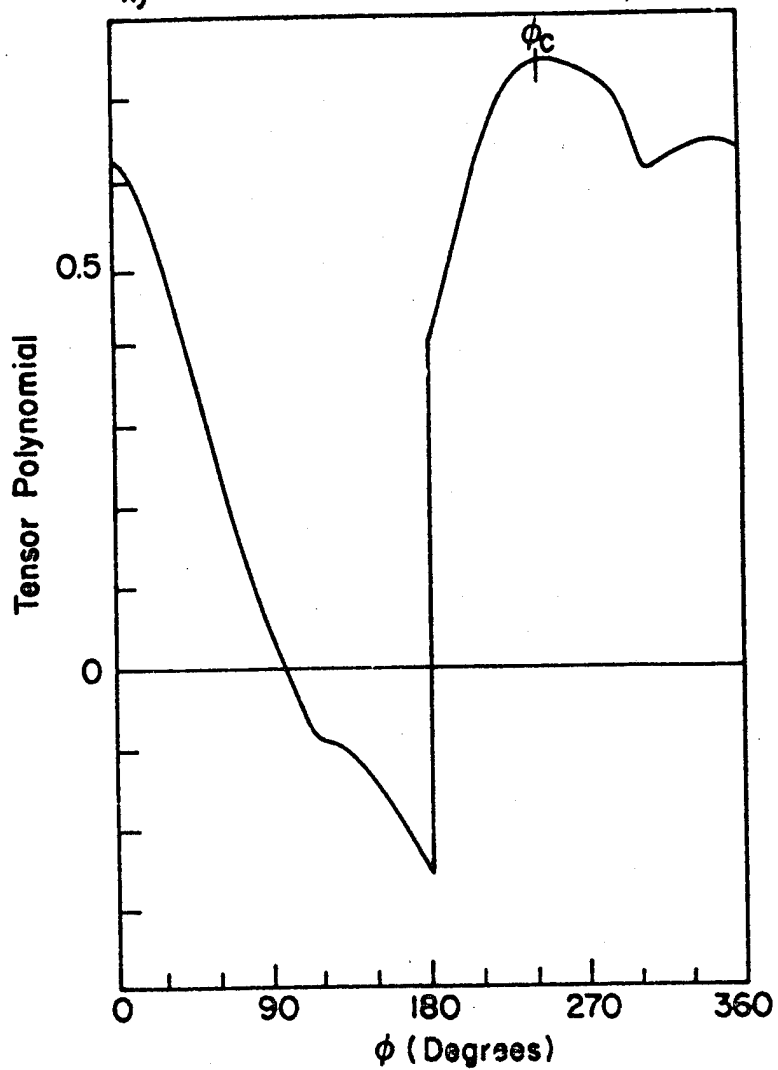


Fig. D.7 Tensor Polynomial vs. ϕ for a Center Cracked 30° Graphite/Epoxy Plate Under Pure Shear.

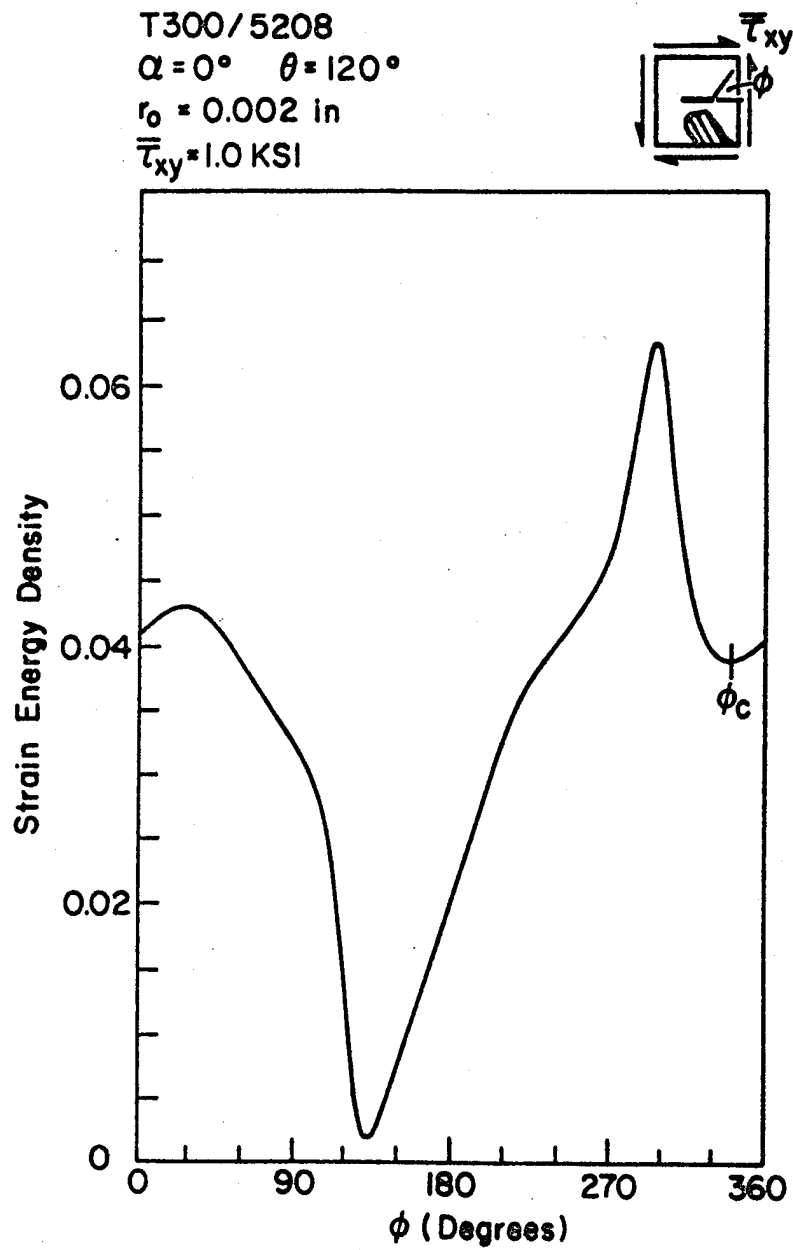


Fig. D.8 Strain Energy Density vs. ϕ for a Center Cracked 30° Graphite/Epoxy Plate Under Pure Shear.

AS4/3501-6
 $\alpha = 0^\circ \quad \theta = 105^\circ$
 $r_0 = 0.002 \text{ in}$
 $\bar{\sigma}_y = 1.0 \text{ KSI}$

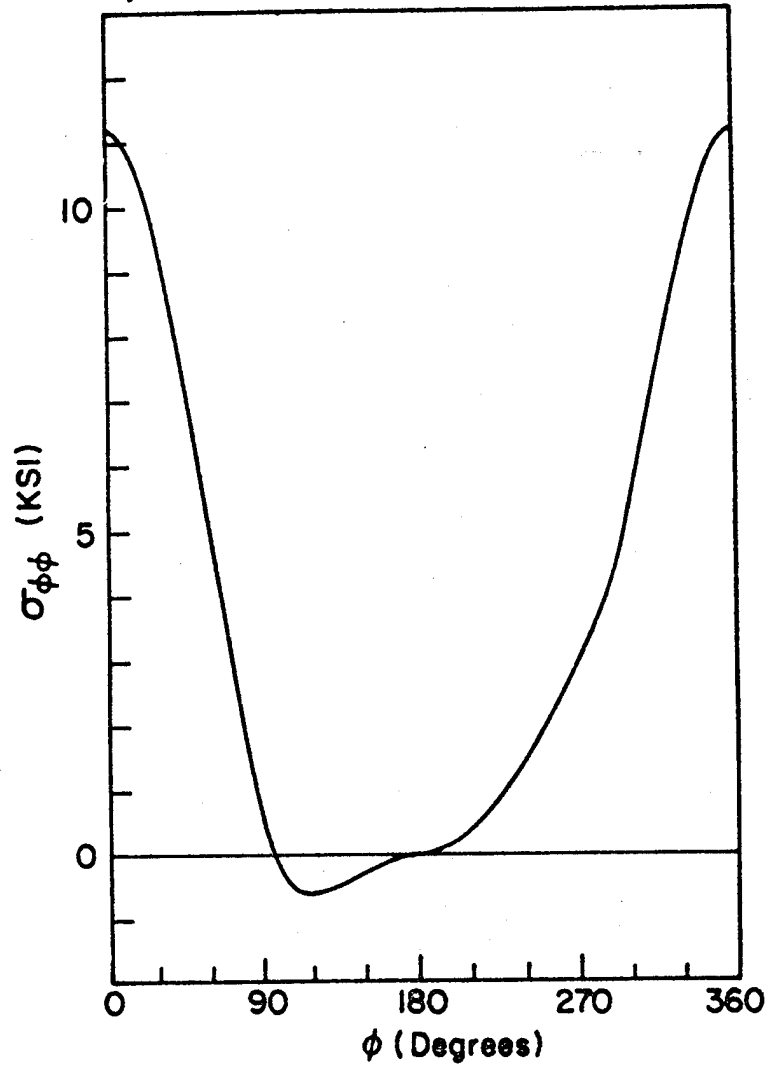
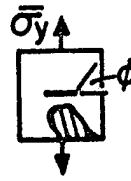


Fig. D.9 $\sigma_{\phi\phi}$ vs. ϕ for a Center Cracked 15° Graphite/Epoxy Plate.

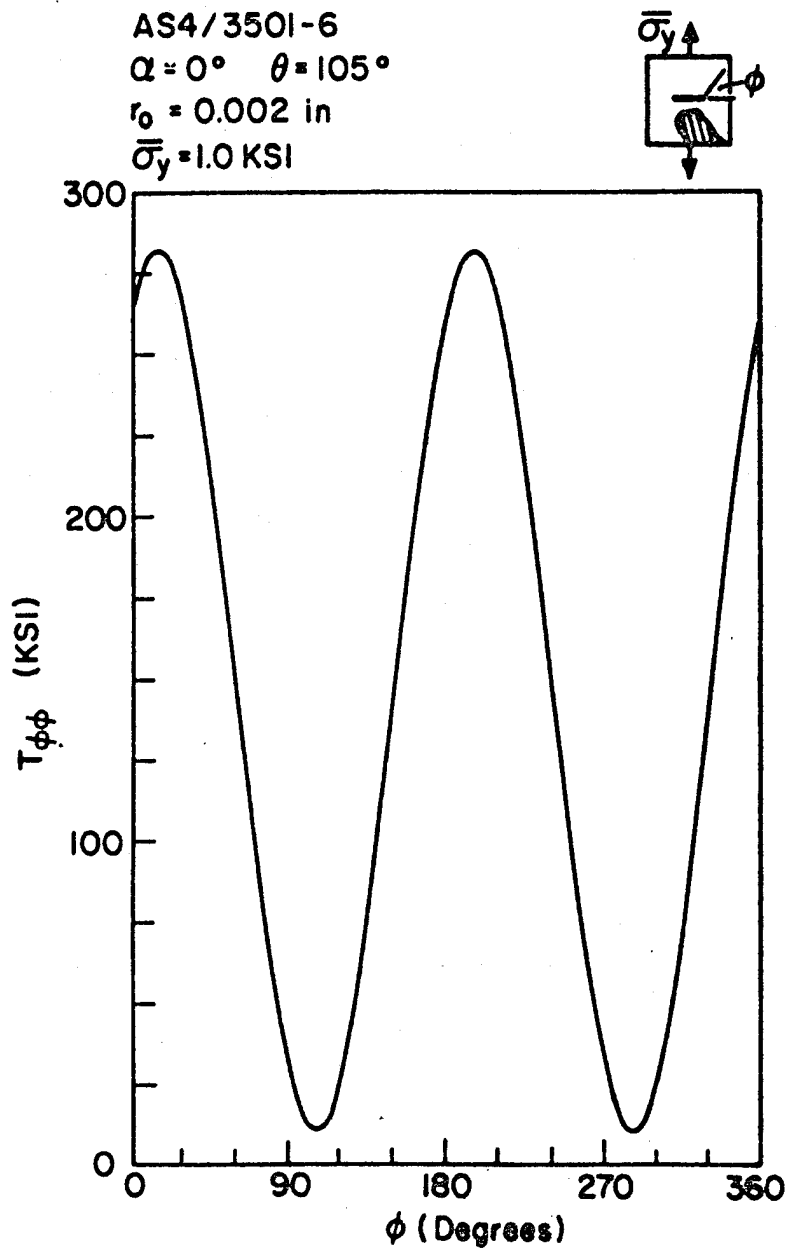


Fig. D.10 $T_{\phi\phi}$ vs. ϕ for a Center Cracked 15° Graphite/Epoxy Plate.

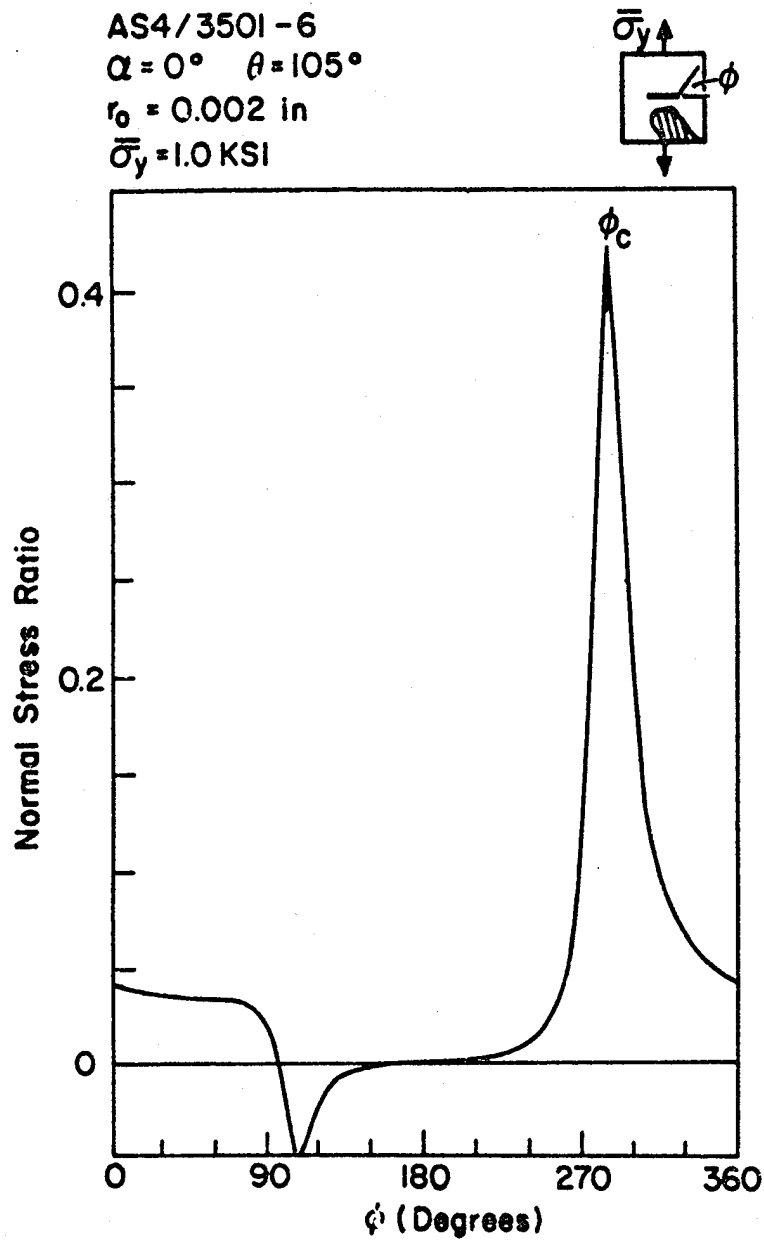


Fig. D.11 Normal Stress Ratio vs. ϕ for a Center Cracked 15° Graphite/Epoxy Plate.

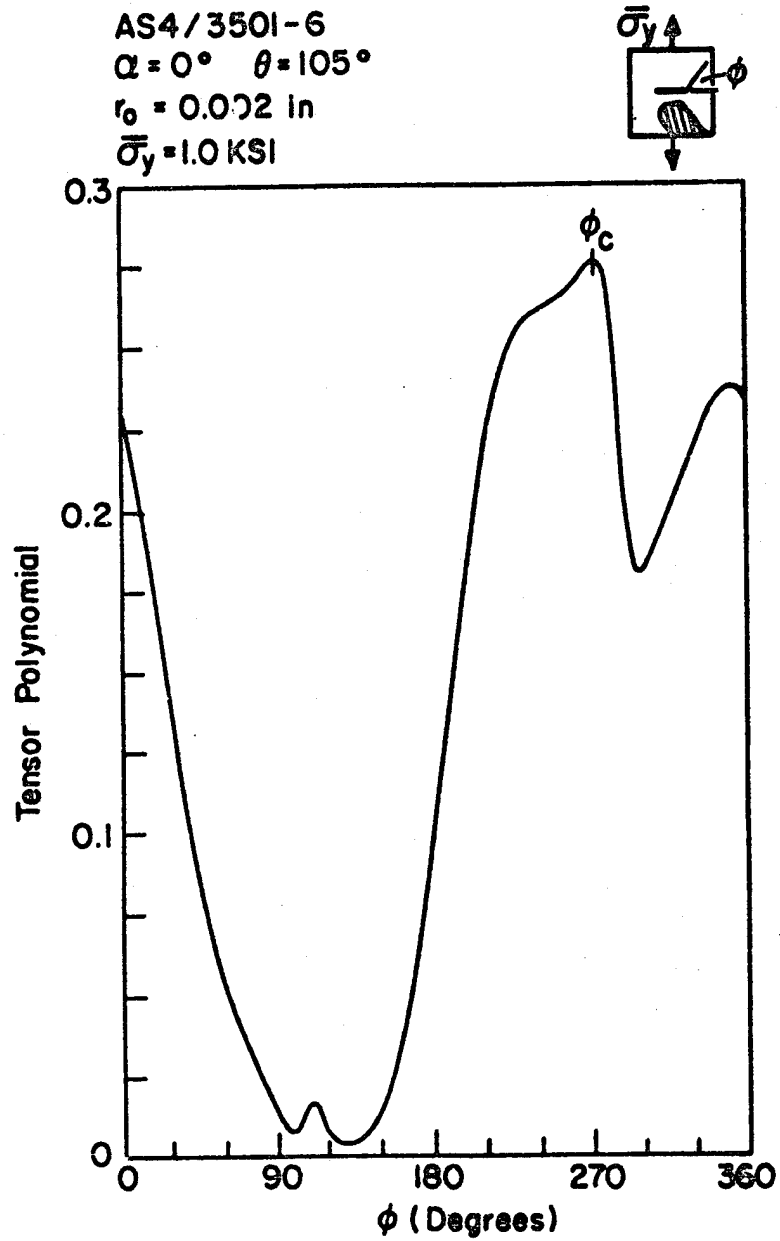


Fig. D.12 Tensor Polynomial vs. ϕ for a Center Cracked 15° Graphite/Epoxy Plate.

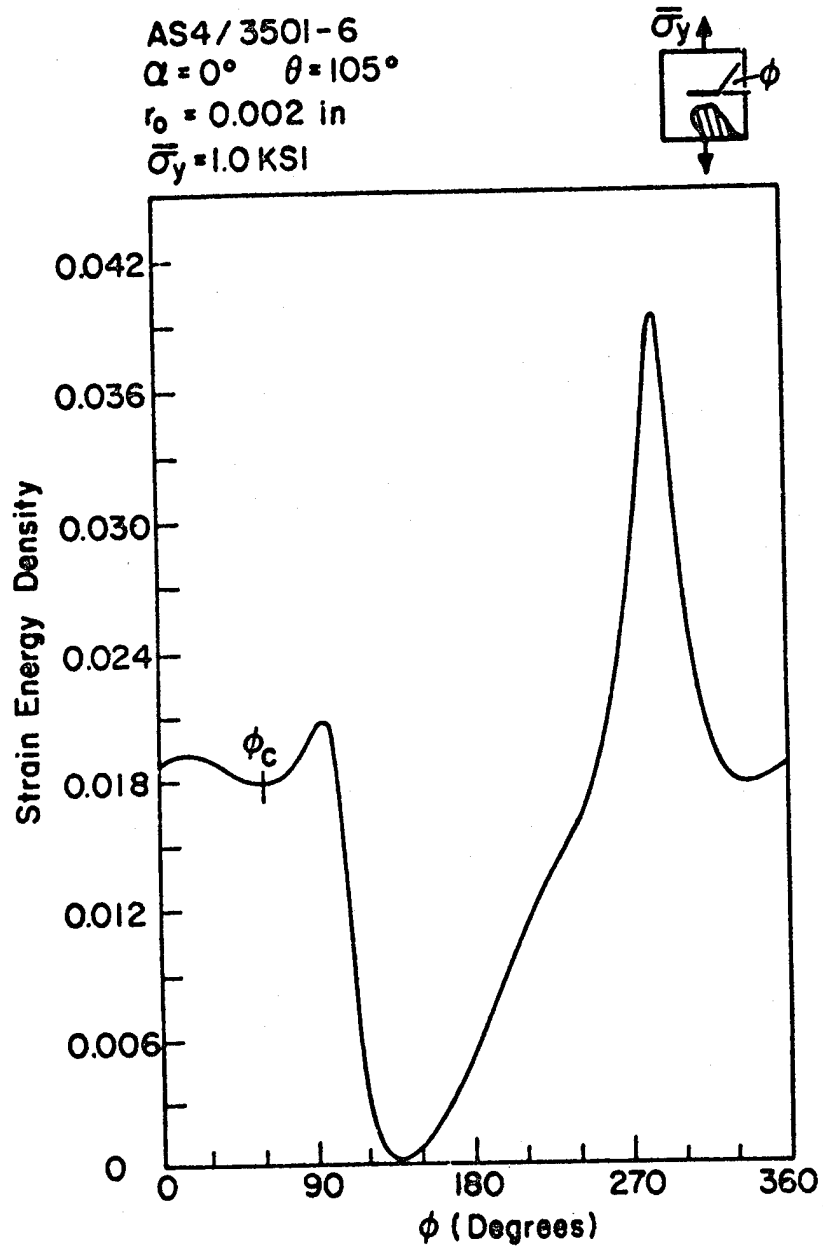


Fig. D.13 Strain Energy Density vs. ϕ for a Center Cracked 15° Graphite/Epoxy Plate.

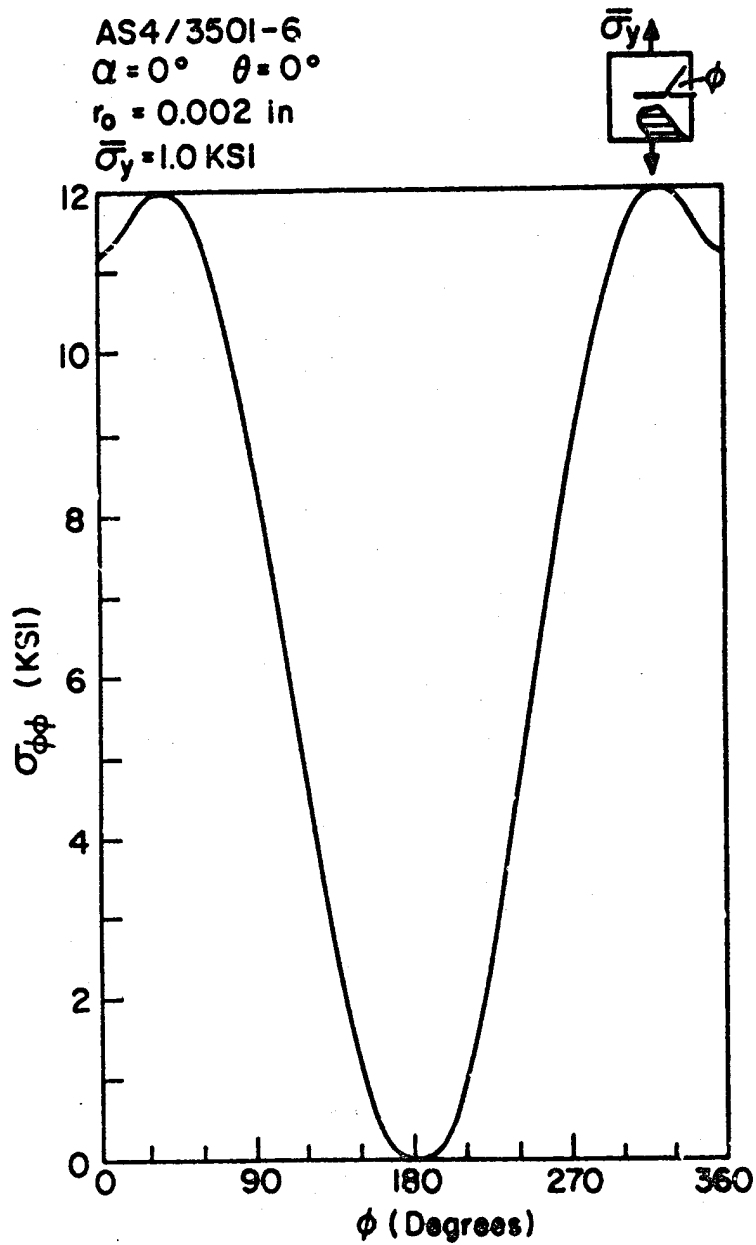


Fig. D.14 $\sigma_{\phi\phi}$ vs. ϕ for a Center Cracked Graphite/Epoxy Plate ($\alpha = 0^\circ$ and $\theta = 0^\circ$).

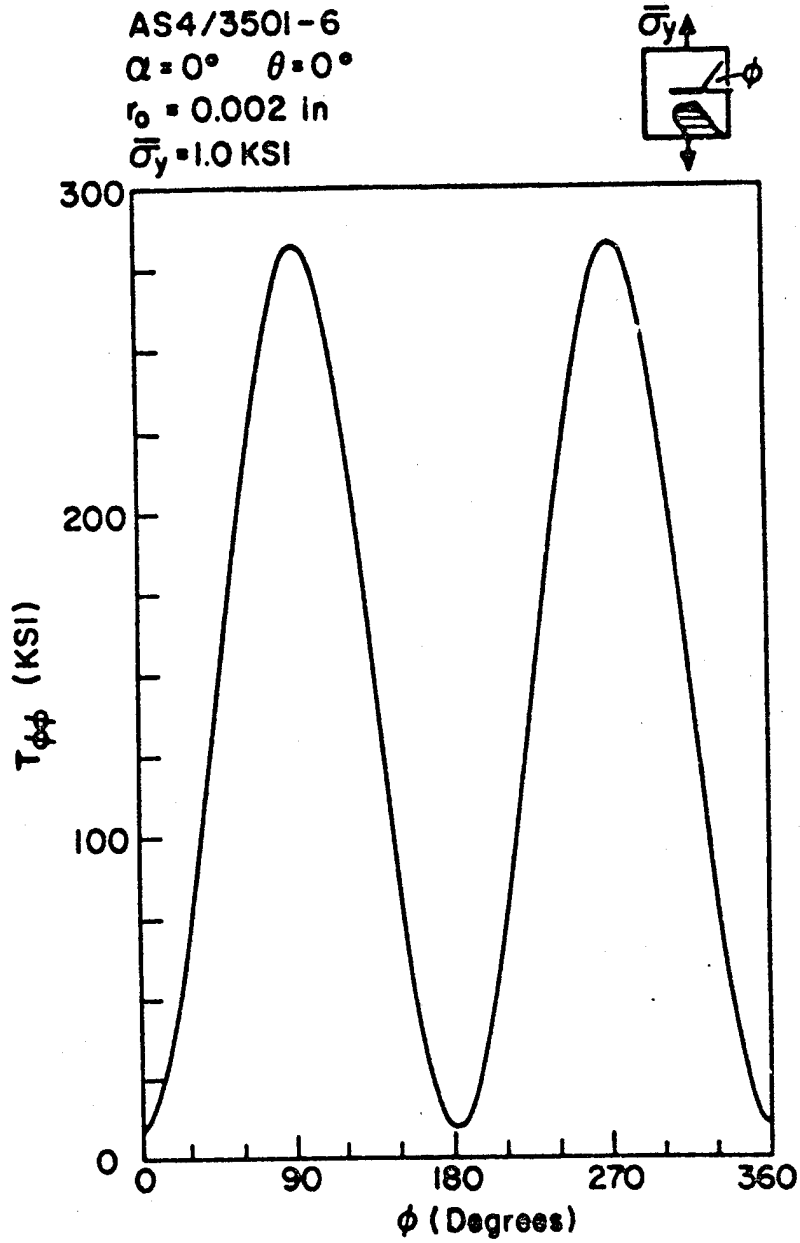


Fig. D.15 $T_{\phi\phi}$ vs. ϕ for a Center Cracked Graphite/Epoxy Plate ($\alpha = 0^\circ$ and $\theta = 0^\circ$).

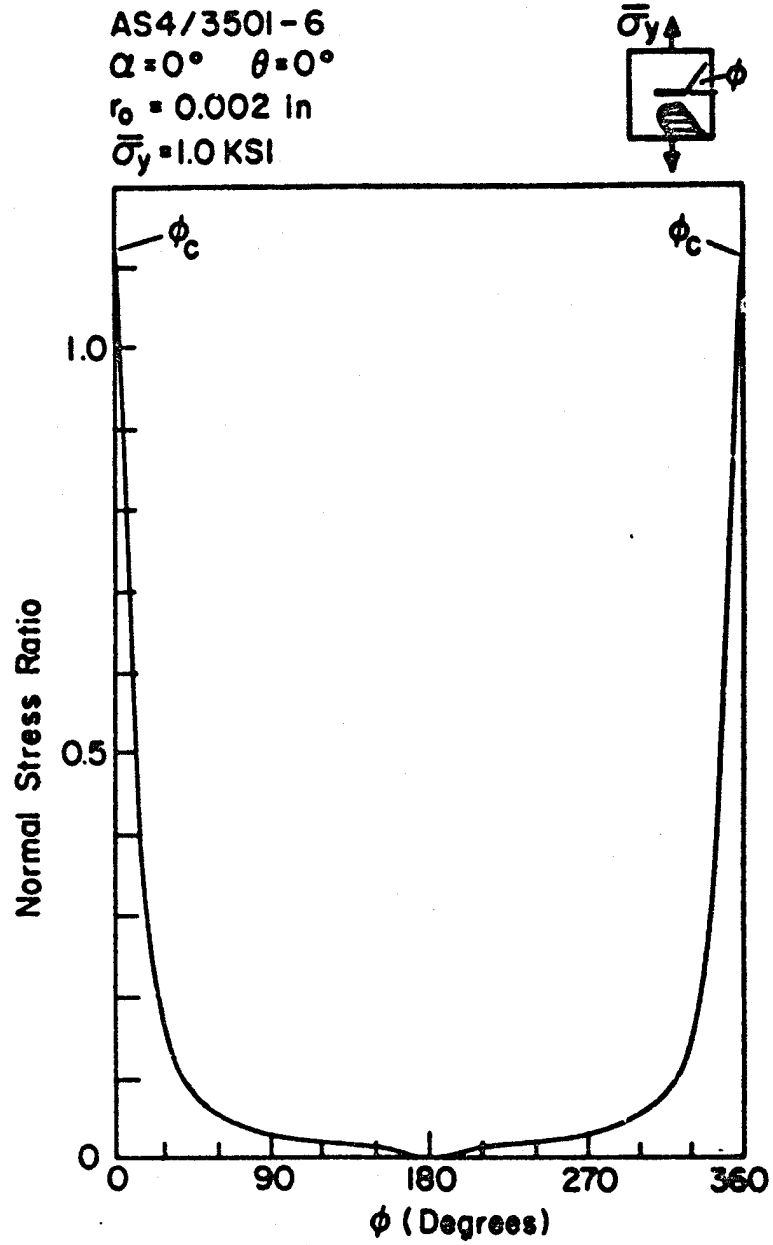


Fig. D.16 Normal Stress Ratio vs. ϕ for a Center Cracked Graphite/Epoxy Plate ($\alpha = 0^\circ$ and $\theta = 0^\circ$).

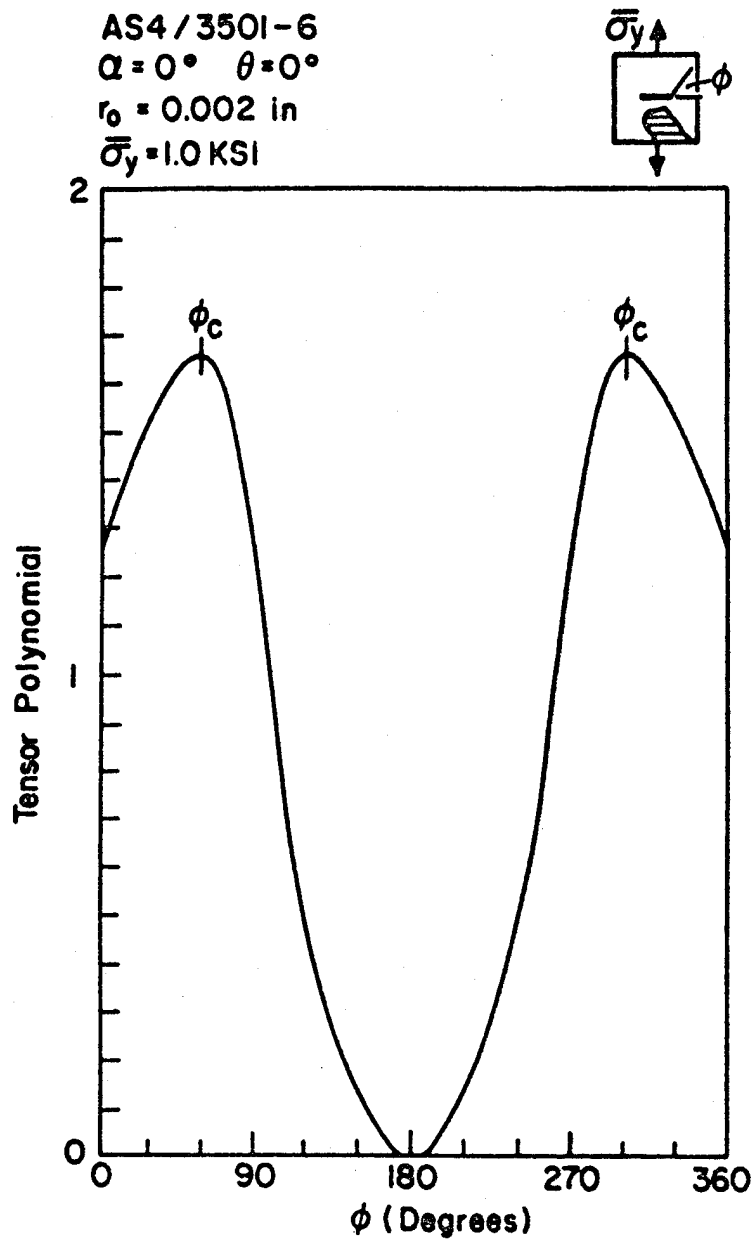


Fig. D.17 Tensor Polynomial vs. ϕ for a Center Cracked Graphite/Epoxy Plate ($\alpha = 0^\circ$ and $\theta = 0^\circ$).

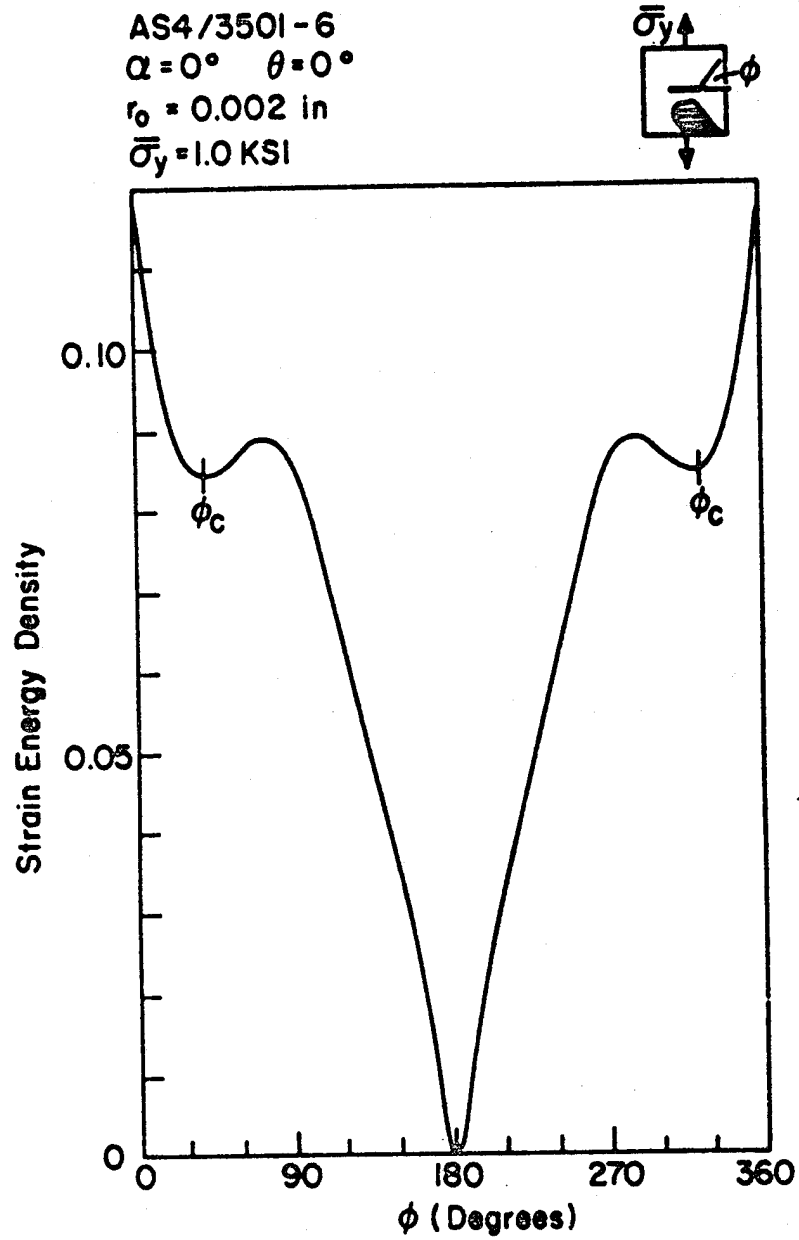


Fig. D.18 Strain Energy Density vs. ϕ for a Center Cracked Graphite/Epoxy Plate ($\alpha = 0^\circ$ and $\theta = 0^\circ$).

APPENDIX E

AS4/3501-6 Graphite/Epoxy

$$E_1 = 21.6 \text{ MSI}$$

$$E_2 = 1.96 \text{ MSI}$$

$$G_{12} = 0.83 \text{ MSI}$$

$$\nu_{12} = 0.28$$

$$\chi_T = 282 \text{ KSI}$$

$$Y_T = 10 \text{ KSI}$$

$$S = 14.2 \text{ KSI}$$

T300/5208 Graphite/Epoxy

$$E_1 = 10.2 \text{ MSI}$$

$$E_2 = 1.56 \text{ MSI}$$

$$G_{12} = 0.82 \text{ MSI}$$

$$\nu_{12} = 0.24$$

$$\chi_T = 219.5 \text{ KSI}$$

$$\chi_C = -246 \text{ KSI}$$

$$Y_T = 6.35 \text{ KSI}$$

$$Y_C = -23.8 \text{ KSI}$$

$$S = 12.6 \text{ KSI}$$

APPENDIX F

This section is included to provide additional information concerning the convergence of the singular finite element solution. Results presented are for the finite element mesh shown in Fig. F.1. For this mesh the l/a ratio is 1.0 and the $2a/w$ ratio is 0.1. The problem under consideration is a center cracked AS4/3501-6 plate ($\theta = 90^\circ$ and $\alpha = 0^\circ$) subjected to a far field stress $\bar{\sigma}_y = 1.0$ KSI.

Distributions of the stress components near the crack tip as a function of ϕ are given in Figs. F.2 to F.4. In these figures, the solid line represents results from the anisotropic elasticity solution and the finite element results for gauss point 1 are represented by circles. Analysis of the figures indicates the finite element solution adequately approximates the distribution of the stress components as a function of ϕ . However, there is a large discrepancy in the magnitude of the stresses predicted by the finite element solution and those predicted by the anisotropic elasticity solution.

Comparison of these results with the results of Chapter 3 shows the importance of the l/a ratio on the prediction of crack tip stresses. The finite element mesh used in Chapter 3 has a smaller l/a ratio ($l/a = 0.1$) and hence better approximates the crack tip stress field.

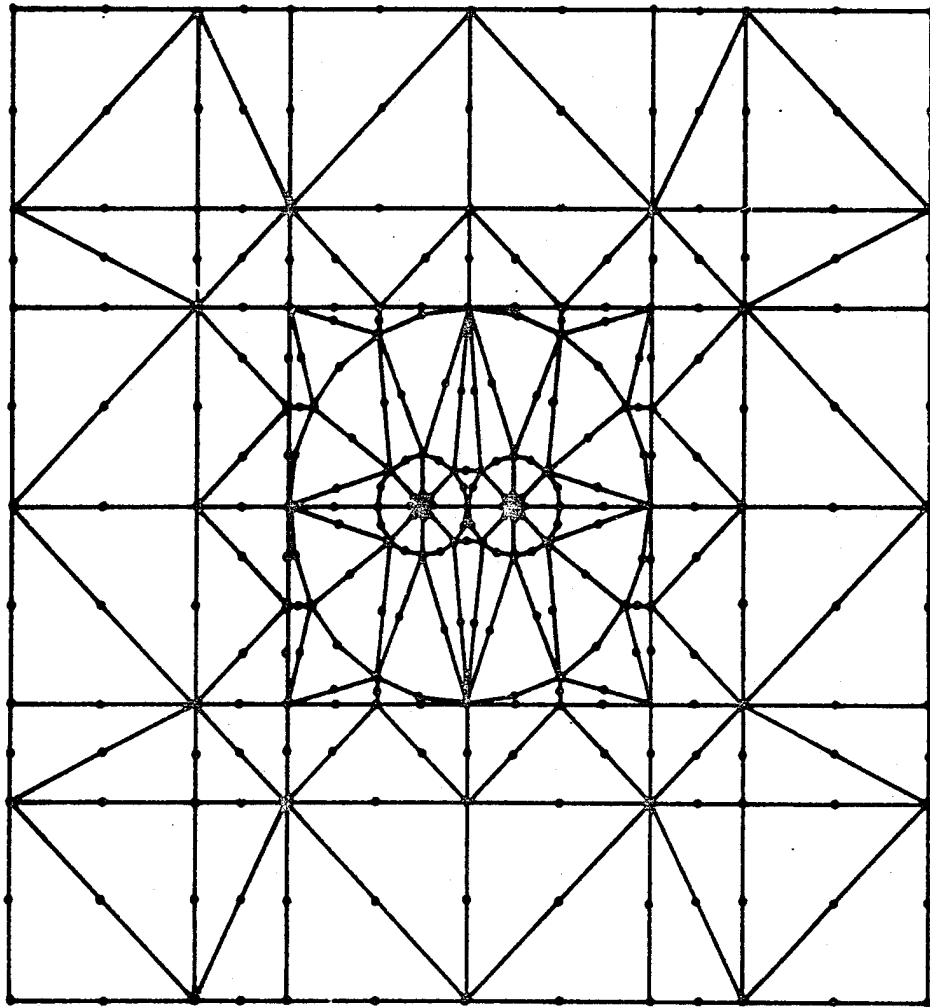


Fig. F.1 Finite Element Mesh of Center Cracked Plate (Full Plate).

AS4/3501-6
 $\alpha = 0^\circ$ $\theta = 0^\circ$
 Gauss Point 1 $r/a = 0.807$
 $\bar{\sigma} = 1.0$ KSI

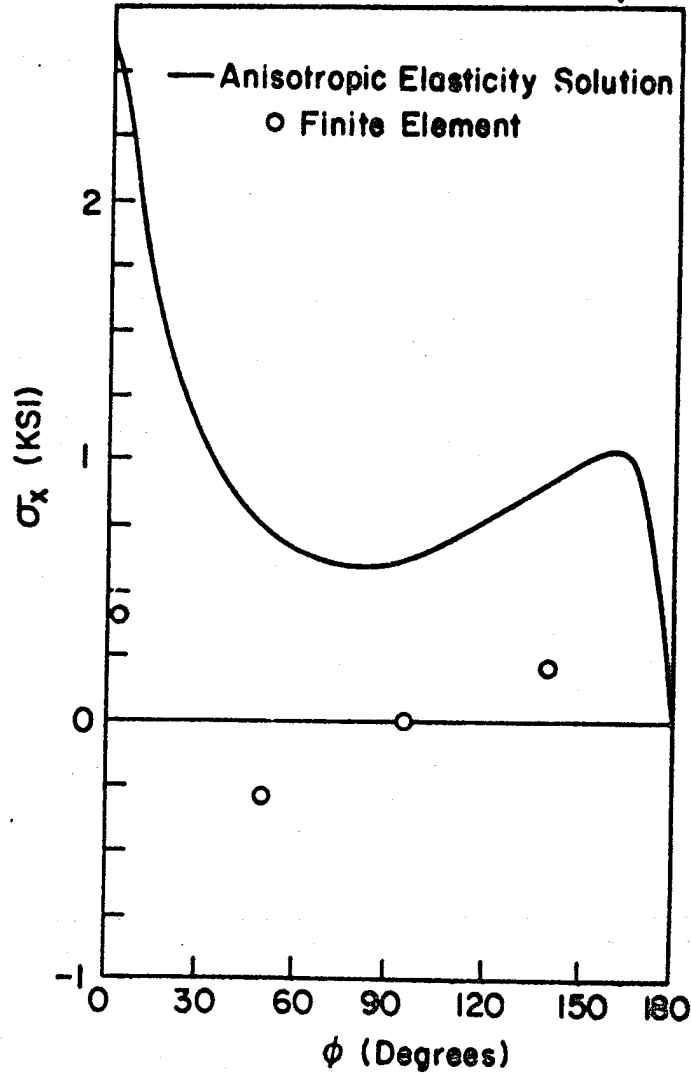
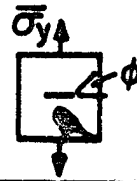


Fig. F.2 σ_x vs. ϕ at Gauss Point 1 for a Center Cracked Graphite/Epoxy Plate.

AS4/3501-6
 $\alpha = 0^\circ$ $\beta = 0^\circ$
 Gauss Point 1 $r/a = 0.807$
 $\bar{\sigma} = 1.0$ KSI

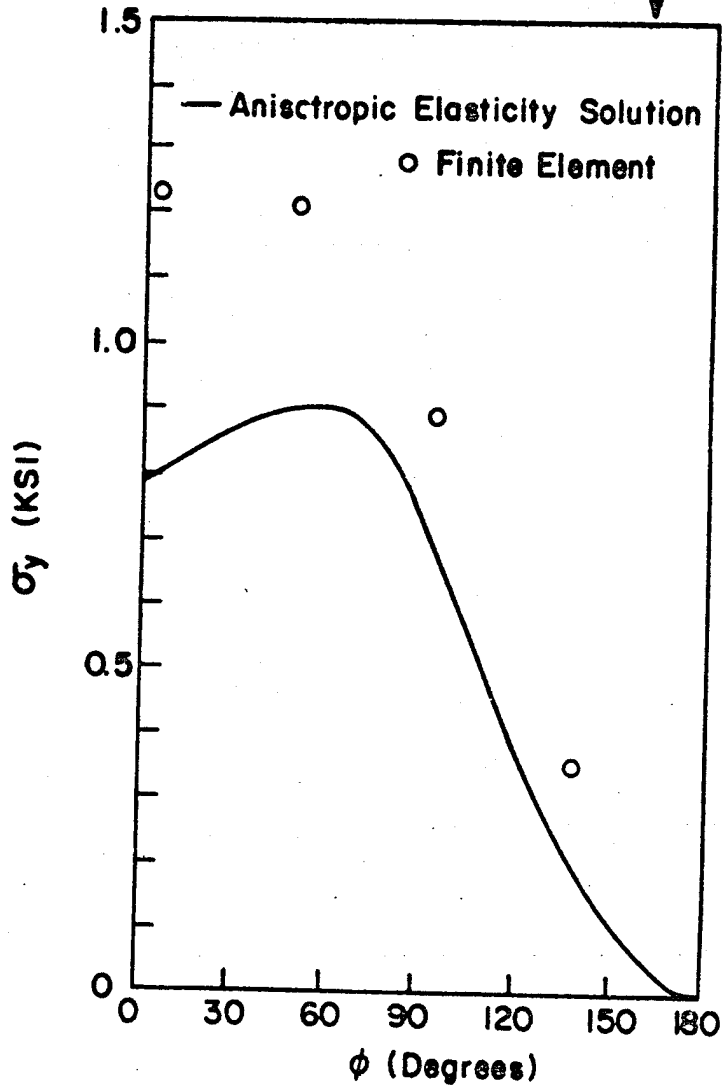
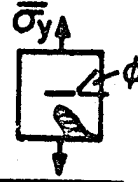


Fig. F.3 σ_y vs. ϕ at Gauss Point 1 for a Center Cracked Graphite/Epoxy Plate.

AS4/3501-6
 $\alpha = 0^\circ \quad \theta = 0^\circ$
 Gauss Point 1 $r/a = 0.807$
 $\bar{\sigma} = 1.0$ KSI

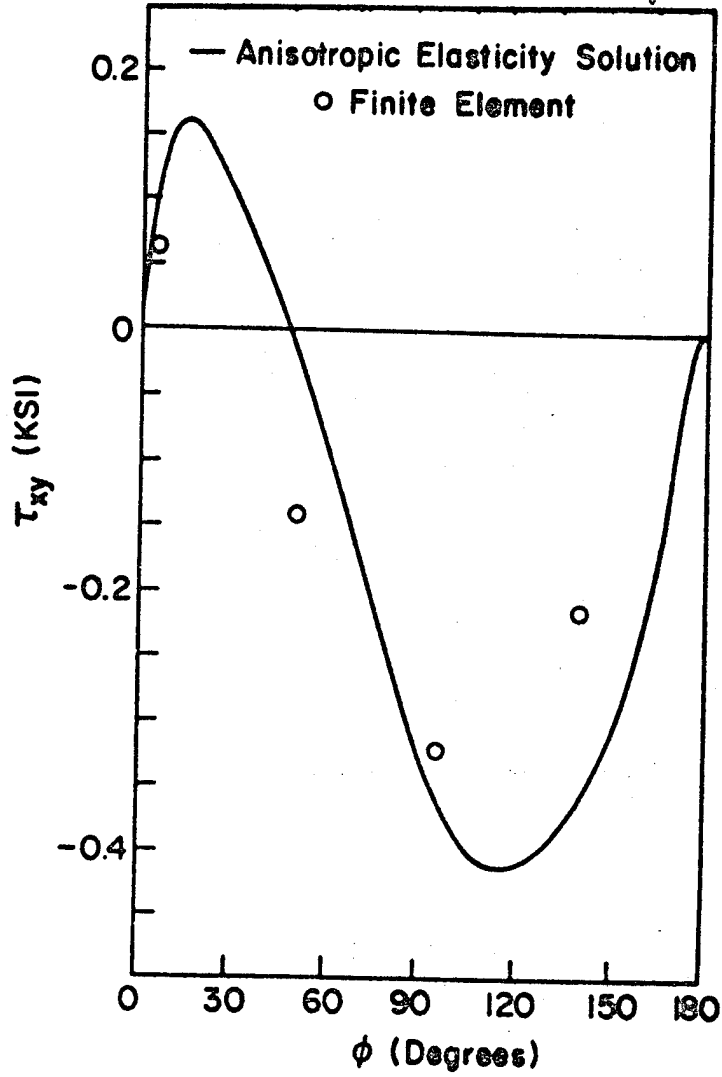


Fig. F.4 τ_{xy} vs. ϕ at Gauss Point 1 for a Center Cracked Graphite/Epoxy Plate.

VIRGINIA TECH CENTER FOR COMPOSITE MATERIALS AND STRUCTURES

The Center for Composite Materials and Structures is a coordinating organization for research and educational activity at Virginia Tech. The Center was formed in 1982 to encourage and promote continued advances in composite materials and composite structures. Those advances will be made from the base of individual accomplishments of the thirty-four founding members who represent ten different departments in two colleges.

The Center functions by means of an Administrative Board which is elected yearly. The general purposes of the Center include:

- collection and dissemination of information about composites activities at Virginia Tech,
- contact point for other organizations and individuals,
- mechanism for collective educational and research pursuits,
- forum and mechanism for internal interactions at Virginia Tech.

The Center for Composite Materials and Structures is supported by a vigorous program of activity at Virginia Tech that has developed since 1963. Research expenditures for investigations of composite materials and structures total well over five million dollars with yearly expenditures presently approaching two million dollars.

Research is conducted in a wide variety of areas including design and analysis of composite materials and composite structures, chemistry of materials and surfaces, characterization of material properties, development of new material systems, and relations between damage and response of composites. Extensive laboratories are available for mechanical testing, nondestructive testing and evaluation, stress analysis, polymer synthesis and characterization, material surface characterization, component fabrication and other specialties.

Educational activities include eight formal courses offered at the undergraduate and graduate levels dealing with the physics, chemistry, mechanics, and design of composite materials and structures. As of 1982, some 33 Doctoral and 37 Master's students have completed graduate programs and several hundred Bachelor-level students have been trained in various aspects of composite materials and structures. A significant number of graduates are now active in industry and government.

Various Center faculty are internationally recognized for their leadership in composite materials and composite structures through books, lectures, workshops, professional society activities, and research papers.

FOUNDING MEMBERS OF THE CENTER

Aerospace and Ocean Engineering
Raphael T. Haftka
William L. Hallauer, Jr.
Eric R. Johnson

Chemical Engineering
Donald G. Baird

Chemistry
James E. McGrath
Thomas C. Ward
James P. Wightman

Civil Engineering
Raymond H. Plaut

Electrical Engineering
Ioannis M. Besieris
Richard O. Claus

Engineering Science and Mechanics
Hal F. Brinson
John C. Duke, Jr.
Daniel Frederick
Robert A. Heller
Edmund G. Henneke, II
Carl T. Herakovich
Michael W. Hyer
Robert M. Jones
Manohar P. Kamat
Alfred C. Loos
Don H. Morris
Daniel Post
Jununthula N. Reddy
Kenneth L. Reifsnider
Wayne W. Stinchcomb

Industrial Engineering and Operations Research
Joel A. Nachlas

Materials Engineering
David W. Dwight
D. P. H. Hasselman
Charles R. Houska
M. R. Louthan, Jr.

Mathematics
Werner E. Kohler

Mechanical Engineering
Norman S. Eiss, Jr.
Charles E. Knight
S. W. Zewari

Inquiries should be directed to:

Center for Composite Materials & Structures
College of Engineering
Virginia Tech
Blacksburg, VA 24061
Phone: (703) 961-4969